

LEVEL ICE INTERACTION WITH SLOPING AND
CONICAL OFFSHORE STRUCTURES

JONATHON E.F. BRUCE

Level Ice Interaction with Sloping and Conical Offshore Structures

By

Jonathon E.F. Bruce, B.Eng.

A thesis submitted to the School of Graduate Studies
in partial fulfillment of the requirements for the degree of
Master of Engineering

Faculty of Engineering and Applied Science
Memorial University of Newfoundland
April 2009

St. John's Newfoundland Canada

Abstract

The use of sloping sided or conical structures is often a favorable design option for structures placed in ice covered waters. An understanding of the mechanics involved during level ice interaction with conical or sloping sided structures is necessary for safe structural design in environments where ice cover is present. This work provides a review of the failure mechanics involved during an ice interaction with a conical or sloping sided structure and the methods which have been developed to model these types of interactions.

The sensitivity of the ice loads, estimated by the Croasdale Model, to the variation in input parameters has been studied in this work. From this analysis, it was determined that if a rubble pile was present on the structure, the flexural strength of ice was not a significant factor affecting the ice load. There were however a number of scenarios which were outlined for which the flexural strength of ice was of significance. A ship ramming event is one such scenario for which the flexural strength of ice plays a significant role in limiting the maximum ice load. The maximum ice load occurs as a crushing failure on the bow of the ship, which is limited by flexural failure due to the weight of the vessel on the ice feature. Another scenario for which the flexural strength of the ice may dominate involves the use of conical structures in the Arctic. Here, designers are concerned with thick multiyear floes interacting with large conical structures. In this scenario, ride up is likely to occur with limited rubble formation due to

the dissipation of kinetic energy, thus making the flexural strength of the ice a critical component affecting the design load. Further to this, the scale of the interaction has been found in this work to be a critical component affecting the flexural strength of ice, which is due to the presence of a size effect.

The results presented in Chapter 3 show that the methodology used to predict the flexural strength of ice based on brine volume alone may well lead to an over estimation of the flexural strength of ice for full scale interactions. This is achieved by using full scale data from the icebreaker Oden during the International Arctic Ocean Expedition in 1991 where the icebreaker Oden was part of a three vessel expedition to the central Arctic Basin. The results of the work show a significant reduction in flexural strength when compared to the methodology which considers brine volume only. This result is due to the size effect present in the flexural strength of ice. The author recommends the use of the methodology presented by Williams and Parsons (1994), which includes the scale of the interaction, when calculating the flexural strength of ice for full scale ice structure interactions.

In Chapter 4 a probabilistic model was developed to determine extreme level ice loads acting on the conical Confederation Bridge piers in the Northumberland Strait. A Monte Carlo technique was utilized to simulate the ice environment and to derive the annual maximum ice loads on the structure. In order to achieve this, full scale data was obtained

from public sources and fitted with probability distributions to model the input parameters.

The model developed in this work simulates the total number of ice floes interacting with a bridge pier in the Northumberland Strait for a given season, as well as individual parameters for each ice floe. Each ice floe is assigned a diameter, an ice thickness, and an ice-structure friction coefficient. Each floe is then broken up into intervals which are individually assigned a flexural strength, along with a rubble height and the angle that the rubble pile makes with the horizontal axis. The Croasdale model is utilized to calculate the horizontal and vertical ice forces acting on the bridge pier for every interval in each floe. The maximum force acting on the bridge pier for each floe is stored and the annual maximum ice force is obtained from these. The model was then run for 4000 years worth of ice structure interactions, resulting in an estimated 100 year ice load of 10.7 MN and a 10,000 year ice load of 16.0 MN acting on a 52° conical bridge pier with a diameter of 14m at the waterline located in the Northumberland Strait.

In Chapter 5 the author has used data published by the Confederation Bridge Ice Monitoring Program and the National Research Council to validate the probabilistic model developed in Chapter 4. The model developed is believed to provide an appropriate representation of the level ice loads acting on the Confederation Bridge piers. The model which was developed in this work produced results which suggest that the 10

year ice load is 8.6MN, whilst the maximum load published by the Confederation Bridge Ice Monitoring Program is 8.4MN for the first 10 years of operation.

Acknowledgements

I would first like to thank my supervisor Dr. Ian Jordaan for giving me the opportunity to pursue this research. Working with Ian throughout this process has been an invaluable experience. Thank you for your support and encouragement along the way.

I would also like to thank Mark Fuglem for his many helpful suggestions, his continued interest in my work and his guidance along the way. Thank you to Paul Stuckey for his Matlab wizardry and his patience in sharing this with me. Thank you to Jim Bruce for taking the time to share some of his knowledge of the Northumberland Strait and the Confederation Bridge instrumentation. This process would have been much more difficult without the help of you all.

Lastly, I would like to thank my wife, Elyse and my family for always believing in me.

Table of Contents

1	INTRODUCTION	1
1.1	Scope of Research.....	2
1.2	Thesis Organization	3
2	LITERATURE REVIEW	5
2.1	Background.....	5
2.2	Flexural Failure Mechanics.....	7
2.3	Ice Induced Vibration of Structures.....	12
2.4	Deterministic Flexural Failure Models	16
2.4.1	Croasdale’s Ice Force Model	16
2.4.2	Nevel’s Ice Force Model.....	22
2.4.3	Määttänen and Hoikkanen’s Ice Force Model	24
2.4.4	Lau’s Ice Force Model.....	25
2.4.5	Mayne’s Ice Force Model	25
2.5	Design Load Methodology	27
2.6	Fracture During Ice-Structure Interaction.....	29
2.6.1	Non-Simultaneous Failure	31
2.6.2	Scale Effect in Flexural Strength	33
2.7	Probabilistic Design Methodology	34
2.7.1	Risk and Safety	34
2.7.2	Offshore Structure Safety Classes and Reliability.....	35
2.7.3	Uncertainty.....	36
2.7.4	Extreme Value Analysis	39
2.7.5	Monte Carlo Simulation.....	43
3	FRACTURE OF ICE: FLEXURAL FAILURE	47
3.1	Flexural Strength.....	47
3.2	Scale Effect in Flexural Strength – Review of Relevant Literature.....	50
3.3	Sensitivity of Ice Loads on Sloping Structures to Flexural Strength.....	57
3.4	Full Scale Ice – Ship Interaction.....	63

3.4.1	Ship Ramming Process Description.....	64
3.4.2	Case Study: The Icebreaker Oden.....	66
3.4.3	Simulation of Ice-Ship Interaction – Fmax Program.....	68
3.4.4	Simulation Results	70
3.5	Concluding Remarks.....	76
4	PROBABILISTIC MODELING OF ICE LOADS.....	77
4.1	Introduction.....	77
4.2	Case Study: The Confederation Bridge	77
4.3	Modeling the Ice Environment	80
4.3.1	Freezing Degree Days.....	80
4.3.2	Ice Thickness	87
4.3.3	Ice Thickness Growth	89
4.3.4	Season Length.....	93
4.3.5	Ice Floe Size.....	95
4.3.6	Number of Ice Floes per Year.....	99
4.3.7	Ice Velocity.....	104
4.3.8	Rubble Height	105
4.3.9	Rubble Pile Angle.....	109
4.3.10	Friction.....	112
4.3.11	Flexural Strength.....	114
4.4	Simulation Process.....	115
4.5	Concluding Remarks.....	123
5	VALIDATION OF THE PROBABILISTIC MODEL.....	124
5.1	Introduction.....	124
5.2	Monitoring Ice Loads Acting on the Confederation Bridge	125
5.3	Ice Observations at the Confederation Bridge	127
5.4	Recommendations for Future Work.....	133
5.5	Concluding Remarks.....	136
6	CONCLUSIONS AND RECOMMENDATIONS	137

7	REFERENCES	142
8	APPENDIX A.....	153
9	APPENDIX B.....	159

List of Figures

Figure 2-1 Kemi – I lighthouse with significant rubble formation.....	6
Figure 2-2 Confederation Bridge	7
Figure 2-3: Level ice interaction with a conical structure (front view).....	9
Figure 2-4: Level ice interaction with a conical structure (top view).....	10
Figure 2-5 Rubble height definition.....	11
Figure 2-6 Sample load trace showing peaks and troughs associated with ice failing by crushing against the Medof panels on the east face of the Molikpaq during its deployment at Amauligak I-65.	13
Figure 2-7 The breaking force, H_B is the horizontal force required to induce radial cracks followed by the formation of the circumferential crack.	20
Figure 2-8 H_p is the force required to push the advancing ice sheet through an existing rubble pile.	20
Figure 2-9 H_L is the horizontal force required to lift and shear the rubble pile above.	21
Figure 2-10 H_R is the horizontal force required to push the ice blocks up the slope of the structure through an existing rubble pile.	21
Figure 2-11 H_T is the horizontal force required to turn the ice blocks to a vertical orientation once they reach the top of the slope.	22
Figure 2-12 Free body diagram showing forces acting on the structure and rubble pile (Mayne, 2007).....	26
Figure 2-13 Global interaction area after Jordaan et al, 2005.....	28
Figure 2-14 Local design area after Jordaan et al., 2005.....	29
Figure 2-15 Showing radial cracking and circumferential cracking.....	30
Figure 2-16 Non-simultaneous failure illustration (Ashby et al., 1986).....	32
Figure 2-17 The effect of uncertainty in design problems.....	38

Figure 2-18: Best fit to the tail of local pressure data (Jordaan et al., 1993).....	40
Figure 2-19 The scale effect in alpha vs. area, after Jordaan et al. 2005.....	42
Figure 2-20 Effect of extremal analysis based on the parent distribution for 100 and 10,000 year return periods.	43
Figure 2-21 Sample flow chart showing Monte Carlo simulation (taken from Brown et al., 2001).	45
Figure 3-1(a) Three point loading setup. (b) Four point loading setup.	48
Figure 3-2 Shows arrangement for insitu cantilever beam testing.	49
Figure 3-3 Iceberg, sea, and freshwater ice flexural strength vs. volume after Parsons et al., 1992.....	51
Figure 3-4 Large beam sea ice flexural strength as a function of the square root of brine volume (Timco and O'Brien, 1994).....	53
Figure 3-5 Small beam sea ice flexural strength as a function of the square root of brine volume (Timco and O'Brien, 1994).....	53
Figure 3-6 A three dimensional plot of flexural strength versus brine volume and beam volume is shown with beam volume plotted on a log scale (Williams and Parsons, 1994).	56
Figure 3-7 Ice load as a function of flexural strength without ice rubble formation.	59
Figure 3-8 Illustrating the decreasing significance that flexural strength holds as a result of introducing a rubble pile. The top, middle and bottom plots have a rubble pile height of 0m, 3m and 6m respectively.....	61
Figure 3-9 The effect of varying rubble pile height whilst keeping the flexural strength constant at 500kPa. The breaking term becomes less significant with increasing rubble formation.....	62
Figure 3-10 The Ice Breaker Oden interacting with thick level ice.....	63
Figure 3-11 Schematic illustration of the phases involved during a ship ramming event (Jordaan et al., 2005).....	66
Figure 3-12 The Oden rounded landing craft hull design used for breaking ice in flexure. The local load instrumentation layout is also shown.	67

Figure 3-13 Histogram and exceedance probabilities of individual (parent) rams. This simulation utilized a flexural strength of 0.7MPa with a standard deviation of 0.2MPa.	73
Figure 3-14 Histogram and exceedance probabilities of individual (parent) rams. This simulation utilized a flexural strength of 0.4 MPa with a standard deviation of 0.2 MPa.	75
Figure 4-1 The ice environment surrounding the Confederation Bridge.	78
Figure 4-2 Geometry selected for design of the Confederation Bridge piers. Pier dimensions and locations of tiltmeters and accelerometers used for global load measurement are also shown.	79
Figure 4-3 Map showing the location of Summerside, Prince Edward Island in relation to the Confederation Bridge. Summerside is located approximately 20km from the North side of the bridge.	81
Figure 4-4 Freezing Degree Days for the month of December. Fit with a gamma distribution with $\alpha=3.49, \beta=37.3$.	82
Figure 4-5 Freezing Degree Days for the month of January. Fit with a gamma distribution with $\alpha=220.9, \beta=85.4$.	83
Figure 4-6 Freezing Degree Days for the month of February. Fit with a gamma distribution with $\alpha=194.3, \beta=72.3$.	84
Figure 4-7 Freezing Degree Days for the month of March. Fit with a gamma distribution with $\alpha=100.0, \beta=50.1$.	85
Figure 4-8 Freezing Degree Days for the month of April. Fit with a gamma distribution with $\alpha=0.80, \beta=12.3$.	86
Figure 4-9 thickness distribution for data provided by the Canadian Ice Services.	88
Figure 4-10 Shows the result of a power law best fit through the CIS data set in relation to the models described above.	90
Figure 4-11 Histogram showing the residuals for the ice growth curve shown above is normally distributed.	91
Figure 4-12 The result of 2000 simulated ice thickness values based on a distribution of freezing degree days. The ice thickness values are based on the curve $h = 1.36FDD^{0.52}$.	92

Figure 4-13 Season Length vs. FDD from ice clearing data obtained from the Northumberland Strait Bridge Crossing Project. A power law has been used to represent the data given by the equation: $Season\ Length = 4.25\ FDD^{0.50}$	95
Figure 4-14 Floe size distribution for the 1963-64 ice season – obtained from aerial photographs.....	96
Figure 4-15 Floe size distribution for the 1964-65 ice season – obtained from aerial photographs.....	97
Figure 4-16 Floe size distribution from the 1987-88 ice season – obtained from aerial sampling of digital X-band SAR imagery.	97
Figure 4-17 Floe size distribution obtained by combining all floe size data.	98
Figure 4-18 Simulated annual number of floes interacting with a bridge pier in the Northumberland Strait, fit with a normal distribution.	100
Figure 4-19 Cumulative distribution function showing the proportion of floes with a floe size less than the critical floe size (14m).	101
Figure 4-20 The annual number of critical floes per year resulting from considering only floes greater than or equal to the diameter of the confederation bridge piers (14m).....	103
Figure 4-21 Level ice thickness effect on the rubble pile height (Mayne and Brown, 2000)	106
Figure 4-22 A Weibull distribution is fit to the ratio of the observed rubble height to the upper limit rubble height predicted by the curve $h_R = 7.59h^{0.64}$ for a given ice thickness.	107
Figure 4-23 Sample results from the rubble model discussed above. Results are obtained by using 1000 randomly sampled ice thickness values from a uniform distribution between 0 and 1.5m.	109
Figure 4-24 The effect of varying the ice rubble pile angle acting on a conical structure as predicted by the Croasdale model.....	110
Figure 4-25 Simulated rubble pile angle using a mean of 40° and a standard deviation of 4°. The simulated rubble angles are limited such that they do not exceed 52°.....	111
Figure 4-26 The effect of varying the dynamic friction coefficient, between sea ice and a conical structure, on the horizontal load predicted by the Croasdale model.	112

Figure 4-27 Simulated dynamic ice-structure friction coefficient between sea ice and concrete.	114
Figure 4-28 Annual maximum horizontal ice forces for level ice interaction with the Confederation Bridge.....	120
Figure 4-29 The contributing input variables which give rise to the maximum annual horizontal ice loads. (a) rubble height, (b) rubble pile angle, (c) ice thickness, and (d) ice – structure friction coefficient.....	122
Figure 5-1: CCGS Terry Fox performing full scale pull test (Mayne, 2007).....	126
Figure 5-2: Annual maximum horizontal ice load measured by tiltmeters located on pier 31 of the Confederation Bridge using the 17 second average tilt data (Brown 2007)....	129
Figure 5-3: Simulated 10 year (10^{-1}) annual maximum horizontal force acting on a bridge pier using the probabilistic model developed in Chapter 4.....	132
Figure 5-4: Ridge keel depth vs. ice loads acting on the Confederation Bridge (Lemee, 2002). This result shows little correlation between ice load and keel depth.	135

List of Tables

Table 3-1 The constant values used for considering the sensitivity of flexural strength on ice loads.	58
Table 4-1 Table displaying the date of when the last ice was observed in the Northumberland Strait along with its Julian date.	93
Table 5-1: Freezing degree day values for the first 10 years of operation of the Confederation Bridge.....	131

1 INTRODUCTION

Mariners have known of the existence and perils of sea ice since vessels first ventured into northern regions. The numerous polar expeditions over the centuries have brought some understanding of the types and variability of conditions affecting these vast ocean areas. It is the steady increase in the consumer demand for oil and gas and the discovery of economically viable mineral reserves in various arctic and sub arctic locations that are the primary driving forces behind ice engineering today.

Whether a structure is intended Offshore structures built in arctic and sub-arctic locations must be designed and built to withstand large forces exerted by the ice environment. The structures built in these environments can be stationary like fixed oil platforms, bridge piers, and lighthouses, or mobile structures such as icebreakers, floating production, storage and offloading vessels (FPSO), and vessels intended for transporting goods. Depending on the location, these structures may be designed for interaction with level ice, multiyear ice floes, ice ridges and icebergs.

When ice interacts with a structure, there are several modes in which the ice may fail including compressive failure, flexural failure, shearing failure, buckling of the sheet, rafting of the ice, ridging of the ice, or any combination of those stated. The predominant mode of failure is a function of both the geometry of the structure and the mechanical properties of the ice.

For many applications involving level ice interaction with offshore structures, conical or slope sided structures are often favorable over vertical sided structures. Sloping or conical structures change the failure mechanism of the ice to flexural failure, often resulting in lower peak loads and a reduced risk of vibration in the structure, which can be induced by the crushing of ice on a vertically sided structure.

1.1 Scope of Research

The research developed in this work involves the study of flexural failure of ice during interaction with sloping and conical offshore structures. The focus of the research conducted in this work has been divided into three main contributions. The first contribution involved studying the effect of the scale of the interaction on the flexural strength of ice. The second major section involved the development of a probabilistic model to determine extreme ice loads on conical structures. For this work, the Confederation Bridge was used as a case study. This work is ultimately intended to contribute to the practical design of sloping and conical offshore structures for interaction with level ice features. Finally, in the third contribution the results obtained from the probabilistic model will be validated with actual measurements of ice loads acting on the Confederation Bridge which have been recorded and published.

1.2 Thesis Organization

This thesis is separated into 6 Chapters. The first chapter introduces the subject matter and discusses the organization of the thesis. Chapter 2, the literature review, will introduce the reader to the mechanics of flexural failure as have been observed by researchers on full scale structures, a review of various deterministic ice load models which have been developed in the past, a review of the fracture mechanics involved for sloping structures during an ice-structure interaction, followed by a discussion of the probabilistic design methodology.

Chapter 3 studies the effect of the scale of the interaction on the flexural strength of the ice sheet. The sensitivity of ice loads to variations in flexural strength is discussed for various loading conditions. The size effect in flexural strength is studied using full scale data from the International Arctic Ocean Expedition in 1991 where the icebreaker Oden was part of a three vessel expedition to the central Arctic Basin.

Chapter 4 presents a probabilistic model developed to estimate extreme level ice loads on the Confederation Bridge in the Northumberland Strait. Environmental data from the Northumberland Strait is used where available to develop the model using Monte Carlo simulation.

Chapter 5 provides a validation of the probabilistic model developed in Chapter 4. Published data by the Confederation Bridge Ice Monitoring Program and the National Research Council – Canadian Hydraulics Centre have been used.

Finally, Chapter 6 presents the conclusions and recommendations for future work. It provides a summary of the results developed in the thesis and discusses some recommendations for further work to strengthen the results obtained in this work.

2 LITERATURE REVIEW

2.1 Background

Conical and sloping structures have been in use in harsh offshore ice environments since the 1970's. The use of sloping structures is primarily intended to minimize the horizontal component of the force caused by the approaching ice floe. The reduction in force is achieved by changing the failure mechanism from crushing failure, typically observed on vertical sided structures, to flexural failure. During a flexural failure, the structure lifts the ice sheet out of plane causing it to bend and break under its self weight, whilst a crushing failure involves the formation of high pressure zones in the highly confined ice-structure interface leading to larger design loads. A detailed description of the mechanics involved in compressive crushing failure can be found in Jordaan (2001) among others.

Sloping and conical structures have been used with success in a number of full scale applications. The Kemi – I structure (Figure 2-1) in the Gulf of Bothnia is a 10m wide instrumented conical structure at the waterline which has a 55° slope. The Kemi -I structure was constructed in 1983. The structure experienced loading events from level ice, rafted ice and ice pressure ridges. A significant improvement in both peak loads and dynamics was achieved compared to vertical structures in the same region.



Figure 2-1 Kemi – I lighthouse with significant rubble formation

The Confederation Bridge (Figure 2-2) spanning 13 kilometers across the Northumberland Strait, connecting Prince Edward Island with New Brunswick, is another example of a successful application of conical structural design. Each pier is 14m in diameter at the waterline with a 52° slope. Two piers have been instrumented with tiltmeters, accelerometers, load panels and video cameras. Northumberland Strait is ice covered for 4 months every winter. Ice initially forms in late December or early January and is present until late April, although in extreme years ice has been present in the strait until late May. Floe sizes can reach 3 to 4 km in diameter, although the larger floes are typically of the order of several hundred meters. Level ice thickness can reach 1m although throughout the winter there is wide range of thicknesses present at any given time (Brown et al., 2001). The ice-structure interactions on the bridge piers are driven by

tidal currents, in addition to the effects of wind and the natural circulation current in the strait. Accordingly the bridge “sees” approximately 3000km of ice each winter (Kubat and Frederking, 2001). Level ice interaction with the Confederation Bridge will be part of the main focus of this work. It will be discussed in greater detail in Chapter 4.



Figure 2-2 Confederation Bridge

2.2 Flexural Failure Mechanics

A typical ice interaction with a sloping or conical structure is described below, as observed in the field by Määttänen (1986), Hoikkanen (1985), Croasdale (1980), Brown & Mayne (2000) among others.

During a flexural failure event, level ice interacts with the sloping structure where it then begins to ride up the structure. As the ice sheet is lifted out of plane, it flexes and breaks under its own weight. The concept of flexural failure has been postulated by theoretical models which are based on experimental scale model tests in ice test basins and field measurements (Croasdale 1980, Määttänen and Hoikkanen 1990, Nevel 1992, Lau 1999, and Mayne 2007 among others). These models will be discussed in greater detail in later sections.

The general components of a flexural failure model have been identified as: the breaking of the ice sheet in flexure, the ride up of the broken pieces along the face of the cone, and the collection of the broken pieces of ice rubble in front of the cone, supported by the approaching ice sheet and the structure. This is a simplification of a very dynamic process, but allows for easier analysis.

The breaking term in most models is based on Hetenyi's semi-infinite elastic beam on an elastic foundation analysis (Hetenyi, 1965). Here the floe is considered infinite in one direction and displacement due to uplift from the cone, or weight of the rubble pile on the approaching sheet is elastically resisted by the buoyancy of the ice floating on water. The foundation modulus of the floating ice sheet is equal to the unit weight of the water. The reaction forces along the beam are assumed to be proportionate to the deformation at

every point and these deformations are independent of deflections elsewhere in the beam (Hetenyi, 1965).

If we consider first the 2D case of the ride up term, we have the plane surface of the ice that is in full contact if they are resting on a constant slope. However, when we consider the 3D case of a cone shaped structure, the motion is allowed to deviate from the axis of loading around the sides of the cone.

When a level ice sheet interacts with a conical structure, bending failure will typically occur with some localized crushing on the underside of the ice sheet. Cracks radiating away from the structure at approximately 60° angle intervals initiate the failure of the ice sheet. The peak load in the breaking of the ice sheet typically occurs with the formation of a circumferential crack which breaks the wedges off. Figure 2-3 and Figure 2-4 below, illustrate this process.

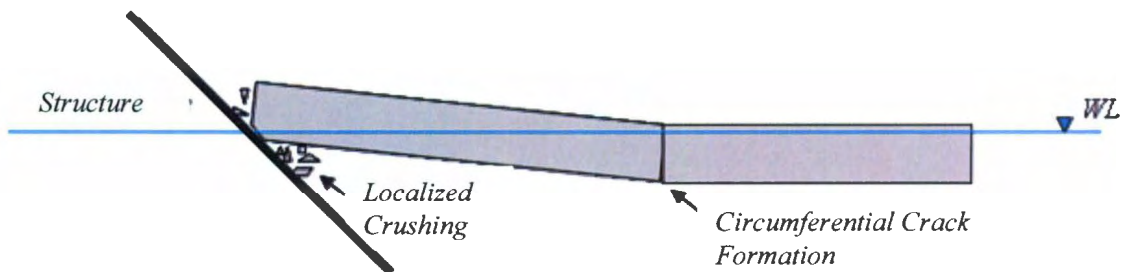


Figure 2-3: Level ice interaction with a conical structure (front view).

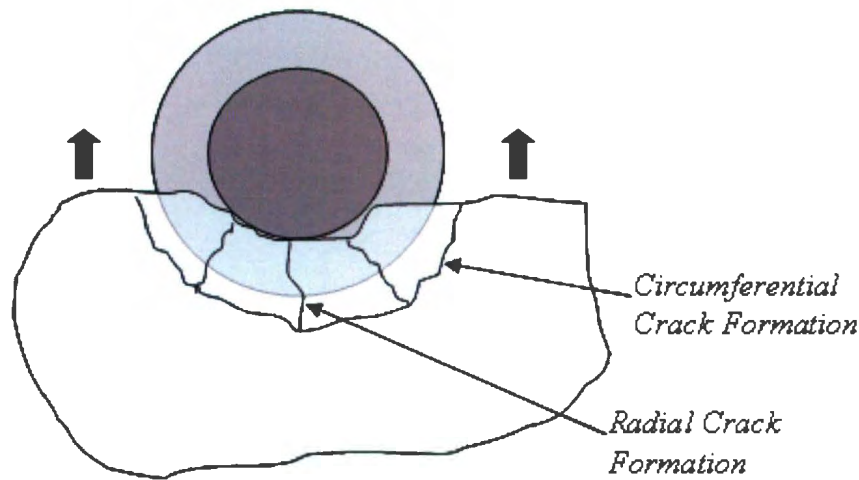


Figure 2-4: Level ice interaction with a conical structure (top view).

It has been found that depending on the size of the cone and the ice floe geometry, the decisive factor in ice load is the clearing ability of the structure, rather than the ice breaking component (Maattanan and Hoikkanen, 1990). When ice blocks fall back onto an approaching ice sheet, a rubble pile forms in front of the structure, which is initially supported by the advancing sheet. A rubble pile is defined as an accumulation of pieces of ice that have been derived directly from ice-structure interaction. It is generally accepted within the ice community that the accumulation height of the rubble pile must exceed at least two thicknesses of the parent ice sheet or floe to be considered rubble.

The height of the rubble pile is measured from the top of the level ice sheet, and extends to the location of maximum height of distinct fragments of rubble (Figure 2-5). The measurement is taken from the ice sheet rather than the waterline since when considering conical structures the ice sheet is often inclined with respect to the water level.

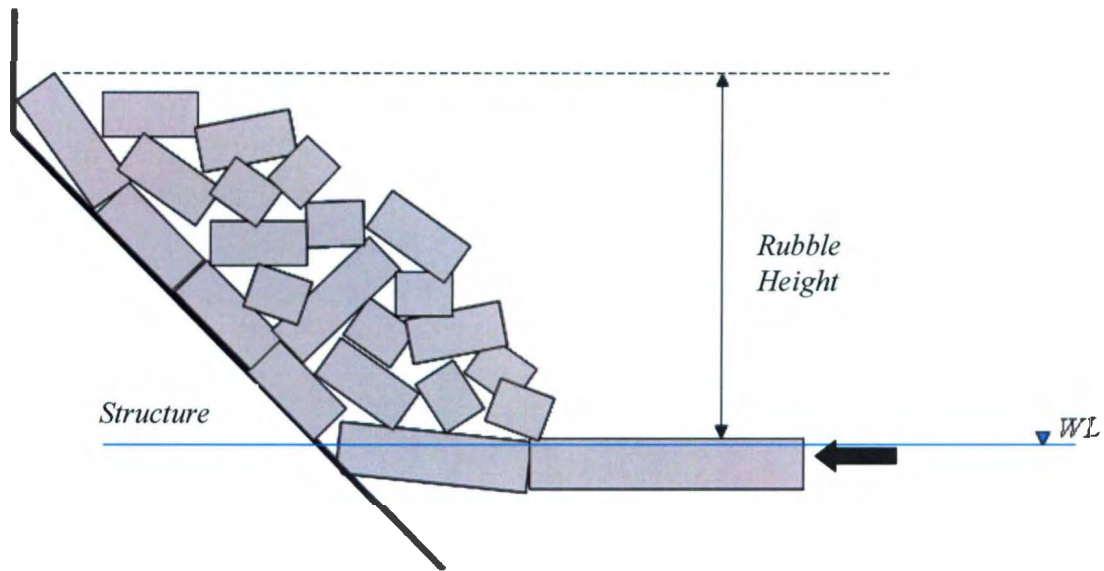


Figure 2-5 Rubble height measured from top of level ice sheet

For simplicity, ice rubble pieces are often depicted as rectangular in shape in order to emphasize that they are the product of the parent level ice sheet, as shown in Figure 2-5 (Cammaert et al, 1993). It should be noted however that piece size is often well graded decreasing the porosity of the rubble pile and consequently increasing the density and load on the structure.

The advancing ice can continue to be pushed through the rubble surcharge to fail against the slope of the structure, or it can become plugged. Eventually, the rubble surcharge will break the advancing ice sheet due to its own weight and the sequence is then repeated. It should also be noted that the ice sheet must have sufficient driving force in order for this process to continue. Smaller ice sheets with less inertia may be stopped, or

for the case of the Northumberland Strait, the tide can affect the driving force of the level ice cover.

The presence of a rubble pile also changes the way an ice sheet interacts with the structure. Mayne and Brown (2000) have observed that if there is no rubble pile present, the radial distance to the circumferential crack increases as it moves around the pier from the axis of loading. With the rubble pile present, the radial distance to the crack tends to decrease as it moves away from the axis of loading and is often not visible beyond the rubble pile boundary.

2.3 Ice Induced Vibration of Structures

Changing the ice-structure interaction to flexural failure decreases the ice loads which are associated with crushing failure on vertically sided structures. Flexural failure is also desirable as it provides designers with an alternative to dealing with the vibrations which can be associated with compressive or crushing failure against vertical sided structures. Arctic engineering experience has shown that interactions of ice features with vertical sided offshore structures are often accompanied by regular structural vibrations.

Regardless of the size or shape of a marine structure, the potential for dynamic ice forces exists. These dynamic loading events can be most significant when structures have vertical sided construction exposed to ice. Vertical sided structures can induce a crushing

failure mode which is characterized by a series of peaks and troughs in the pressure trace shown below (Figure 2-6) as spalls are formed and crushed ice is extruded. When the approaching ice sheet reaches a critical speed there is potential for phase locking between the ice failure frequency and the natural frequency of the structure. This type of ice structure interaction can be very dangerous for offshore structures.

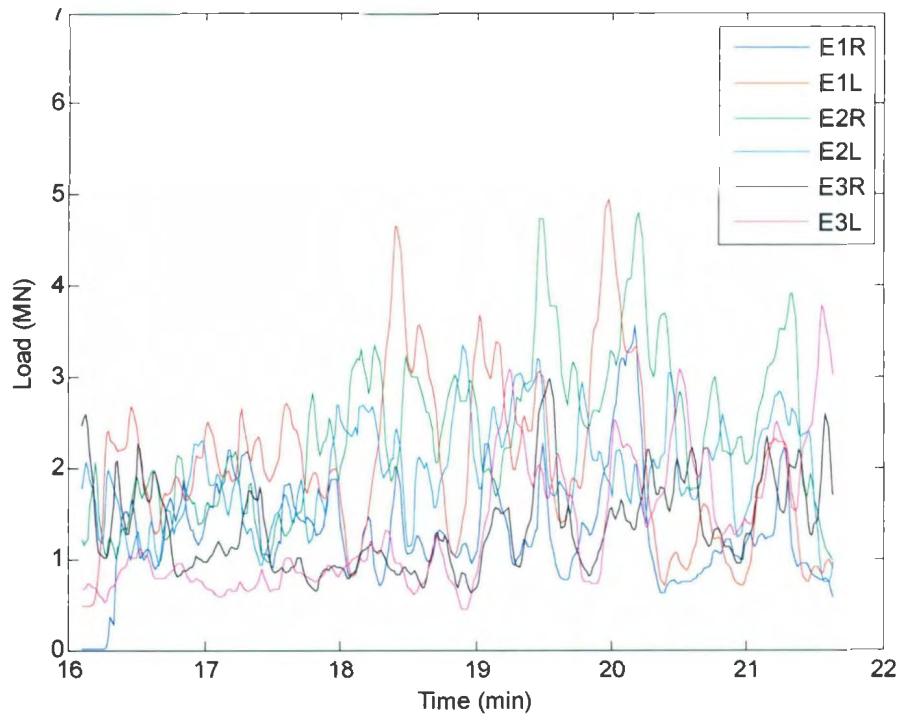


Figure 2-6 Sample load trace showing peaks and troughs associated with ice failing by crushing against the Medof panels on the east face of the Molikpaq during its deployment at Amauligak I-65.

Arctic engineering experience has shown that interactions of ice features with offshore structures are often accompanied by regular structural vibrations. In the past, this ice induced vibration was not considered a threat to overall structural stability. The actual extent and effects of full scale ice-induced vibrations were clearly demonstrated in

practice in 1986, when the Molikpaq experienced severe vibrations during the impact of a large ice floe. Crushing failure against the near-vertical sides of the Molikpaq created an extended period of severe vibrations which caused a portion of the sand core of the Molikpaq to liquefy – compromising both structural stability and the lateral strength of the structure. This event was first described by Jefferies and Wright (1988) and was later the topic of much debate regarding the magnitude of the load seen by the structure (Hewitt, 1994, Hewitt, Kennedy & Fitzpatrick, 1994, Timco & Johnson, 2003, among others). This incident illustrated the importance of dynamic loading and is a testimony to the fact that an understanding of ice-structure interaction is needed for the establishment of adequate design criteria.

In the Gulf of Bothnia and adjacent regions of the northern Baltic Sea, there are numerous offshore Swedish lighthouses with vertical sided construction which have been exposed to ice interaction. As a result of limited field data during the design stage, several of them were built with insufficient design load specifications, and as a result have since collapsed or have been severely damaged.

The response of most vertical sided lighthouses to ice action is highly dynamic, since they are in general compliant, non-rigid structures. Experiments by Määttänen (1983) on model lighthouse structures indicate that the standard deviation of dynamic peaks about the average load level may typically be about 50% of the average load level. This implies that peak loads can be approximately 2.5 times the average load on narrow

structures. This represents a very high level of structural response, and failure of the Swedish lighthouses described above is likely due to this excessive dynamic response. In an effort to reduce the effects of ice induced vibration Määttänen (1975) developed a strategy for utilizing vibration isolation for the overwater structures, arguing that it was a more economical solution than stiffening the vertical underwater structures. It was later determined that the use of conical structures for load and vibration reduction was more effective.

The use of sloping or conical geometries decrease the peak forces substantially and the flexural failure decreases the likelihood of ice induced vibration. The cyclic ice failure in flexure is seldom of high enough frequency to excite the natural frequency of the structure. Laboratory experiments conducted by Spencer et al. (1993) assessed the potential for dynamic loading of a 60° conical bridge pier. It was determined that the pier size was approximately 3.5 times the ice thickness leading to a characteristic frequency of failure given by the expression $f = \frac{V}{3h}$, where V is velocity and h is the level ice thickness. This continuous breaking of the ice sheet produces a dynamic loading characterized by numerous peaks and troughs. The characteristic frequency of the interaction was measured to be in the order of 0.13 Hz with more extreme events leading to frequencies of 0.34 Hz (Spencer et al., 1993). The natural frequency of the conical structure was determined to be 0.825 Hz, making the conical design very attractive when compared with a vertical cylindrical pier design. The vertical cylindrical structure tested with a diameter equal to the neck diameter of the cone produced average

peak loadings ten times higher for equivalent ice conditions. In addition a characteristic ice failure frequency of 1.3 Hz made ice induced vibration a serious design concern.

2.4 Deterministic Flexural Failure Models

One of the first attempts to analyze the ice forces on a conical structure was done by Kim and Kotras (1973). This work considered the forces due to initial cracking of a semi-infinite ice sheet followed by the simultaneous breaking of a number of ice wedges. Since then there has been a number of models developed to analyze the interaction of ice with sloping and conical structures. The focus here is on models which have been used in industry for design, as well as some newer models.

2.4.1 Croasdale's Ice Force Model

The Croasdale model was first developed in 1980 (Croasdale, 1980) for wide sloping structures and later modified in 1993 (Croasdale et al., 1993) to account for 3D effects during ice interaction with conical structures. It has been the most widely used model by industry for design of sloping and conical structures, and is also the model chosen for use in the probabilistic modeling developed in this work. For this reason it is discussed in the greatest detail here.

The Croasdale model treats the ice sheet as a semi-infinite elastic beam on an elastic foundation. The total horizontal load on the structure is the summation of five components of loading given by the equation below:

$$H = H_B + H_P + H_L + H_R + H_T \quad \text{Equation 2-1}$$

The breaking force (H_B) is the horizontal force required to induce radial cracks followed by the formation of the circumferential crack (Figure 2-7). The circumferential crack formation allows for forward progression of the ice sheet. The equation for H_B is given below:

$$H_B = \varepsilon_1 \sigma_f D \left(\frac{\rho_w g h^5}{E} \right)^{0.25} \left[D + (\pi^2 / 4) l_c \right] / D \quad \text{Equation 2-2}$$

Where σ_f is the flexural strength of the ice, D is the diameter of the structure at the waterline, ρ_w is the density of the water, g is the acceleration due to gravity, h is the thickness of the ice sheet, h_f is the maximum ride up height, E is the elastic modulus of the ice, ε_1 is a function of the cone angle and the friction coefficient, and l_c is the characteristic length. The characteristic length is given by the equation below:

$$l_c = \left(\frac{Eh^3}{12\rho_w g(1 - \nu^2)} \right)^{0.25} \quad \text{Equation 2-3}$$

Where ρ_w is the density of the water and ν is the Poisson's ratio.

H_p is the force required to push the advancing ice sheet through an existing rubble pile (Figure 2-8). The ice sheet must overcome the frictional resistance of the rubble pile before it interacts with the slope of the structure. H_p is given by the equation below:

$$H_p = Dh_r \mu_i \rho_i g (1 - \gamma) \left(1 - \frac{\tan \theta}{\tan \alpha} \right)^2 \left(\frac{1}{2 \tan \theta} \right) \quad \text{Equation 2-4}$$

Where h_r is the height of the rubble pile, μ_i is the ice-to-ice friction coefficient, γ is the porosity of the rubble pile, θ is the angle the rubble pile makes with the horizontal axis, and α is the angle the slope of the structure makes with the horizontal.

When the ice makes contact with the conical structure, H_L is the horizontal force required to lift and shear the rubble pile above (Figure 2-9). This is necessary to allow the ice sheet to begin to ride up the slope of the structure. H_L is given by the equation below:

$$H_L = 0.5Dh_r^2 \rho_i g (1 - \gamma) \epsilon \left(\frac{1}{\tan \theta} - \frac{1}{\tan \alpha} \right) \left(1 - \frac{\tan \theta}{\tan \alpha} \right) + 0.5Dh_r^2 \rho_i g (1 - \gamma) \epsilon \tan \phi \left(1 - \frac{\tan \theta}{\tan \alpha} \right)^2 + \epsilon c Dh_r \left(1 - \frac{\tan \theta}{\tan \alpha} \right) \quad \text{Equation 2-5}$$

Where c is the cohesive strength of the rubble pile and ϕ is the friction angle of the rubble.

H_R is the horizontal force required to push the ice blocks up the slope of the structure through an existing rubble pile (Figure 2-10). The ice sheet must overcome the friction between the ice sheet and the structure, as well as the friction between the ice sheet and the rubble pile above. H_R is given by the equation below:

$$H_R = PD \left(\frac{1}{\cos \alpha - \mu_s \sin \alpha} \right) \quad \text{Equation 2-6}$$

Where μ_s is the ice-structure friction coefficient and P is given by the equation below:

$$P = \frac{1}{2} \mu_i (\mu_i + \mu_s) \rho_i g (1 - \gamma) h_r^2 \sin \alpha \left(\frac{1}{\tan \theta} - \frac{1}{\tan \alpha} \right) \left(1 - \frac{\tan \theta}{\tan \alpha} \right) \\ + \frac{1}{2} (\mu_i + \mu_s) \rho_i g (1 - \gamma) h_r^2 \cos \alpha \left(\frac{1}{\tan \alpha} \right) \left(1 - \frac{\tan \theta}{\tan \alpha} \right) \\ + h_r h \rho_i g \left(\frac{\sin \alpha + \mu_s \cos \alpha}{\sin \alpha} \right) \quad \text{Equation 2-7}$$

Finally, H_T is the horizontal force required to turn the ice blocks to a vertical orientation once they reach the top of the slope (Figure 2-11). This is an optional term, as some structures will not have a vertical superstructure at the top of the slope. H_T is given by the following equation:

$$H_T = 1.5 h^2 \rho_i g D \left(\frac{\cos \phi}{\sin \phi - \mu_s \cos \phi} \right) \quad \text{Equation 2-8}$$

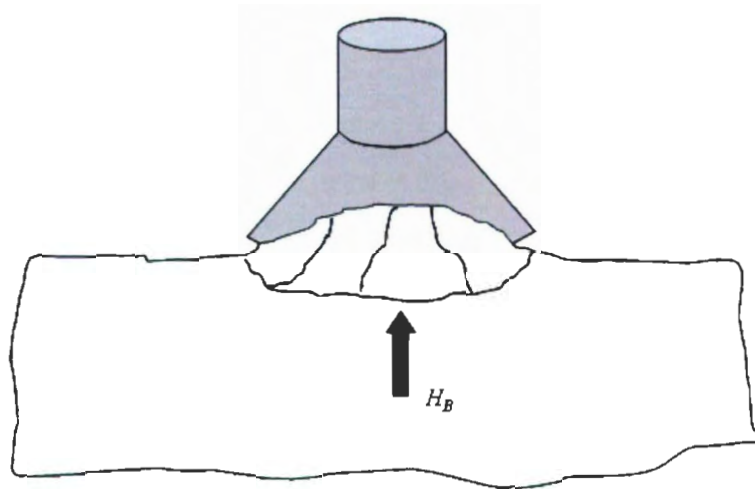


Figure 2-7 The breaking force, H_B is the horizontal force required to induce radial cracks followed by the formation of the circumferential crack.

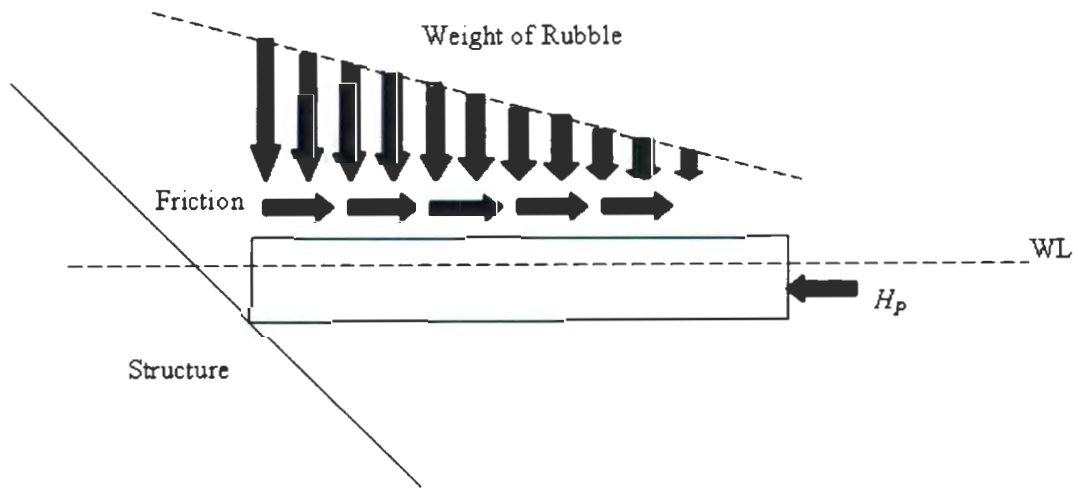


Figure 2-8 H_p is the force required to push the advancing ice sheet through an existing rubble pile.

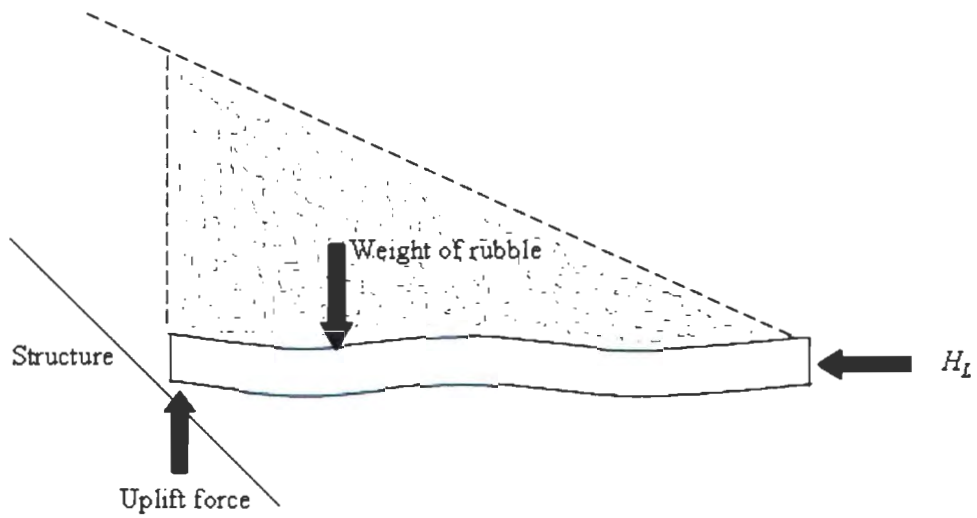


Figure 2-9 H_L is the horizontal force required to lift and shear the rubble pile above.

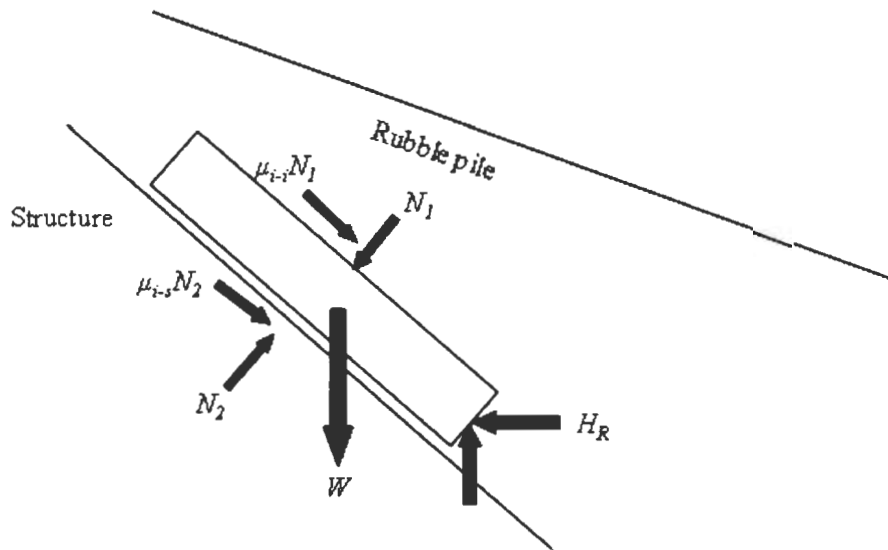


Figure 2-10 H_R is the horizontal force required to push the ice blocks up the slope of the structure through an existing rubble pile.

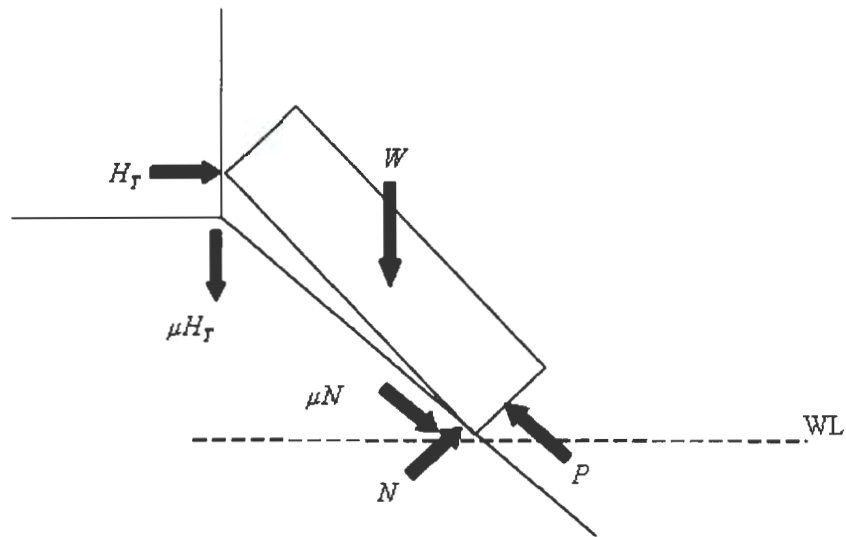


Figure 2-11 H_T is the horizontal force required to turn the ice blocks to a vertical orientation once they reach the top of the slope.

2.4.2 Nevel's Ice Force Model

Nevel's ice force model (1992) was developed for conical structures which built on previous work (Nevel 1980) where he studied a wedge on an elastic foundation subjected to an in plane force and an edge moment. The equations derived in Nevel (1992) are complex and have not been included in this work. A general description of Nevel's ice force model is given below.

The analysis begins when the ice sheet moves against the structure and begins to slide up the cone. The ice sheet undergoes radial cracking when the bending tensile stresses act

along the top portion of the ice sheet, forming truncated wedges. As the ice sheet proceeds forward, the truncated wedges break due to a bending tensile stress along the bottom portion of the wedge. The model considers the possibility of the ice wedges breaking simultaneously or sequentially, starting from the center wedge and proceeding to the outer wedges. Nevel's model assumes that the maximum load comes from the breaking of the center wedge.

A distinction is made between active ice action and passive ice action. Active ice action occurs when the broken ice pieces on the surface of the cone slide into the above section. Passive ice action occurs when broken ice pieces do not slide into the above section. For each wedge segment on the cone, the ride up forces are calculated proceeding from the smallest section near the neck to the largest section at the waterline. For each broken ice piece, the forces are determined which act on the cone and those which are transmitted to the broken ice piece below it. The analysis starts from the center wedge and proceeds to the outer wedge segments.

It is noted that Nevel (1992) does not consider the forces on a structure incurred by the presence of a rubble pile. Observations by Määttänen (1986) and Hoikkanen (1985) in the Bay of Bothnia as well as observations by Mayne and Brown (2000) in the Northumberland Strait suggest that rubble pile formation on conical structures occurs quite often. For this reason, some consideration for the presence of rubble should be added to this model.

2.4.3 Määttänen and Hoikkanen's Ice Force Model

Määttänen and Hoikkanen (1990) build on the work done by Määttänen (1986) to develop a new ice force calculation based on an elastic wedge on an elastic foundation. The bending moments caused by the an edge loading as well as distributed loads due to rubble pile formations are calculated using a finite element analysis.

Full scale tests with a conical structure by Määttänen and Mustamäki (1985) as well as Hoikkanen (1985), indicated that a rubble pile forms regularly in front of a conical structure. This model was the first to consider the effects of rubble. Määttänen and Hoikkanen determined that the edge loading and a single ride up should be limited to the initial phase of ice failure against an inclined wall as rubble formation would often produce the maximum loads seen by the structure.

Määttänen and Hoikkanen developed a curve which indicates the maximum height of a rubble pile as a function of ice thickness. The curve was obtained by observing full scale and laboratory scale model tests. A curve was presented for a “fully developed pile-up” where the end of the ice sheet was supported by the structure, as well as a curve for a “floating pile-up”, developed based on the maximum ice mass that the ice wedges can bear without support from the cone.

2.4.4 Lau's Ice Force Model

Lau's ice force model (Lau et al., 1999) is a method proposed which adapts Croasdale's 2D model to a 3D case. The model is intended to improve upon the representation of the 3D nature of the ice loading on a conical structure developed by Croasdale et al. (1994). Lau's ice force model considers the direction of ice force distribution around the cone surface, and gives a new method for determining the weight of the ride-up ice and the length of the circumferential crack. The model computes and integrates the distributed ice forces along the front perimeter of the cone to give the net vertical loads, from there it calculates the net horizontal force by using a resolution factor, which is essentially a function of the cone angle and the friction coefficient.

2.4.5 Mayne's Ice Force Model

Mayne's model (Mayne, 2007) was developed based on observations (Brown & Mayne, 2000) of rubble piles with bilinear profiles. Mayne's objective was to provide a more accurate representation of the loads seen by conical structures due to rubble pile formation. To achieve this, the method of slices is used. The method of slices was first developed for geotechnical applications by Morgenstern and Price (1965) to determine

loads on structures and slope stability. The figure below (Figure 2-12) shows a typical representation of a bilinear rubble profile as well as the forces on individual slices.

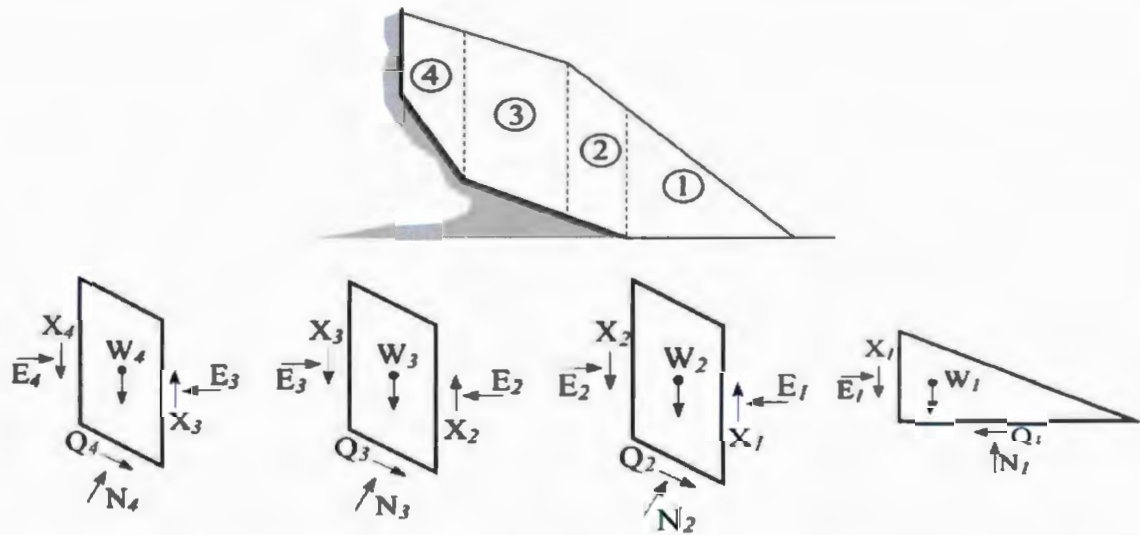


Figure 2-12 Free body diagram showing forces acting on the structure and rubble pile (Mayne, 2007).

In this approach, the rubble is assumed to be stationary on the cone and thus internal movement of ice within the pile is not accounted for. The slices can be chosen to fit the appropriate rubble geometry along with the known cone geometry. It is noted that this model is capable of analyzing cones with multiple angles as was the case with the confederation bridge cone construction, illustrated in the figure above (Figure 2-12). Analysis of each slice allows for determination of the ice rubble forces on the structure as well as the ice sheet. This resulting force on the structure is combined with a breaking term to determine the global load on the structure.

2.5 Design Load Methodology

When designing an offshore structure for ice loads, it is necessary to consider both global ice pressure and local ice pressure on the structure. To determine these, the global interaction area and local design area must both be considered carefully. Jordaan et al. (2005) presents a rational basis for defining local and global ice forces as well as the physical areas of concern in the interaction of ice masses with offshore structures.

Global ice forces represent the total force applied to the structure, whereas **local ice forces** consider the loading on a particular area of interest within the global structure. These areas of interest are typically of structural importance such as the plate between frames or other assemblies considered critical for design safety.

The **global interaction area** (also termed the **nominal interaction area**) is the area determined by the projection of the structure onto the original shape of the ice feature, without any reduction of the area for spalls and fractures that take place during the interaction. Within this area, there will be areas that carry little or no pressure, as well as zones of high pressure. Figure 2-13 below illustrates the concept of the global interaction area. During the interaction, large areas may spall from the ice feature (as indicated in the figure). The design issues related to global interaction areas are that of foundation stability (in shear) and overturning moments.

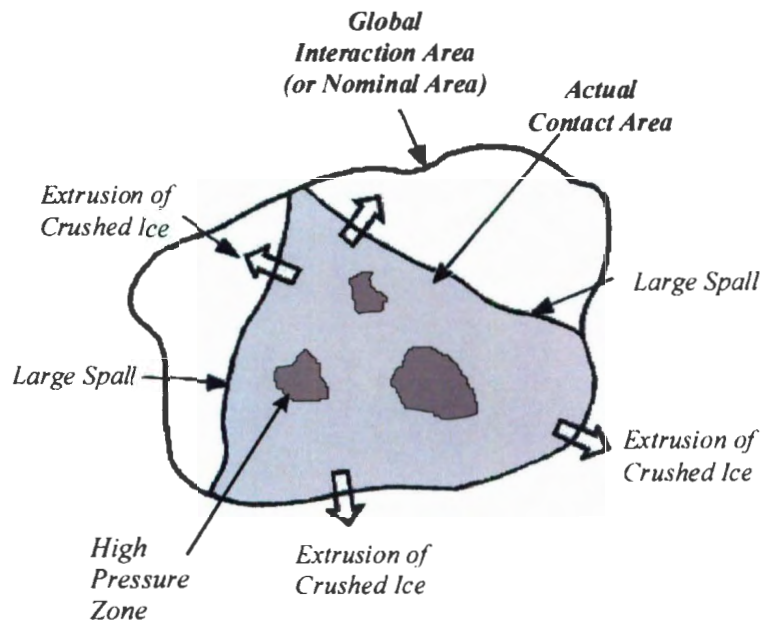


Figure 2-13 Global interaction area after Jordaan et al, 2005

As mentioned previously, for design purposes one needs to consider the **local design area**, which is typically the area of a plate between frames or a panel or substructure that is considered in design. Within the nominal interaction area, small areas of high pressure exist called high pressure zones. The local pressures present during an interaction can be many times greater than the global pressure which acts on the entire structure. The figure below (Figure 2-14) illustrates the concept of the local design area. The design issues typical of local design areas are plate or shell punching as well as shearing.

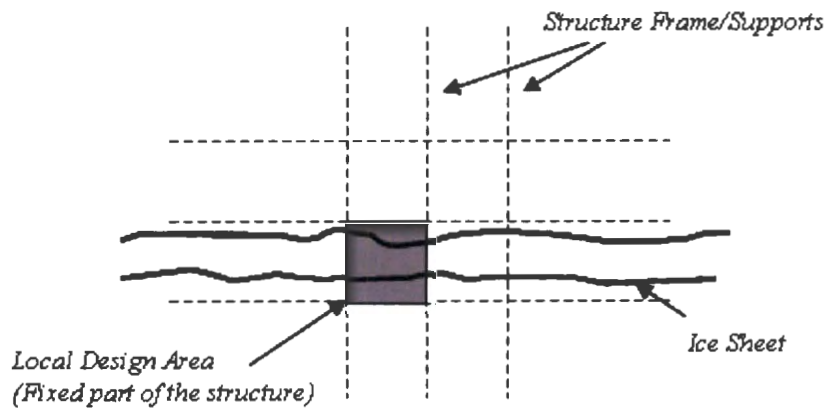
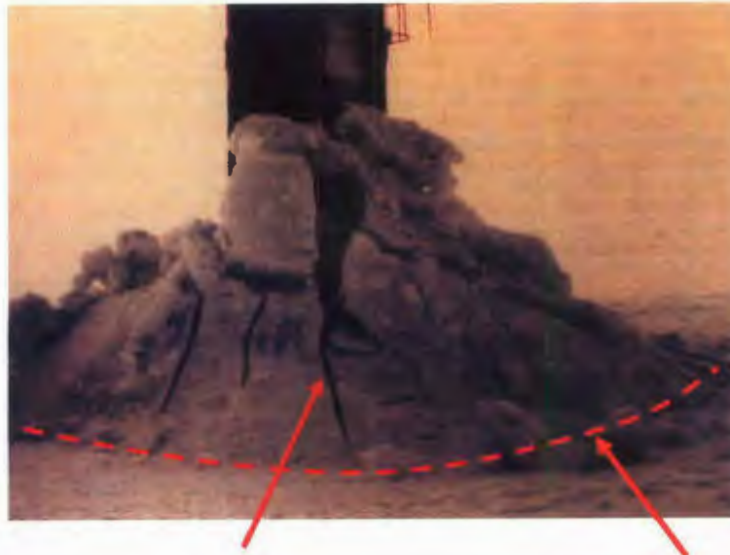


Figure 2-14 Local design area after Jordaan et al., 2005.

2.6 Fracture During Ice-Structure Interaction

Fracture is a process which involves the permanent deformation of an ice sheet, causing two or more regions of ice to separate, thus reducing the load carrying capability of the ice sheet. During ice interaction with a conical structure, the two predominant fracture modes are radial cracking followed by circumferential cracking (Figure 2-15). Palmer et al. (1982) provides a description of these fracture processes. Radial cracking involves the growth of vertical cracks directed radially away from the contact region and running through the whole thickness. Circumferential cracks form as a result of lifting the ice sheet out of plane acting in conjunction with radial cracks to fail the ice sheet in flexure. The combined effect of radial and circumferential cracking produces the characteristic triangular or trapezoidal fragments observed in the field (Määttänen, 1986). It is noted

that the contact region on the underside of the ice sheet often undergoes local crushing while radial and circumferential cracks form and fail the ice sheet.



Radial Cracking

Circumferential Cracking

Figure 2-15 Showing radial cracking and circumferential cracking (Määttänen and Hoikkanen, 1990)

The analysis of fracture in medium and full scale tests exhibits a considerable scale effect, characterized by a decreasing nominal pressure with an increasing contact area. A very reasonable explanation of this effect is the occurrence of spalls and fractures. Fracture events during the process of ice-structure interaction reduce the contact area between the structure and the ice mass, thus reducing the load applied. This process has the effect of reducing the global pressure as area increases.

2.6.1 Non-Simultaneous Failure

When fracture takes place during ice-structure interaction the leading edge of the ice sheet is highly irregular. This irregular contact plane is continuously changing as more fractures occur during interaction. The irregular contact and following fracture leads to a phenomenon called non-simultaneous failure. Failure will occur in discrete local zones rather than across the entire structure width as illustrated in the figure below (Figure 2-16). As the initial contact interface is irregular, the zones have been observed to fail in such a way that contact remains irregular throughout the impact process. It is unlikely that the ice will fail simultaneously across the entire structure width. This contributes to the scale effect discussed previously, which reduces the global pressure applied to the structure as structure width increases.

Ashby et al., (1986) illustrated this phenomenon using a brittle wax sheet interacting with a cylindrical indenter. As illustrated in figure (Figure 2-16) (after Ashby et al., 1986), the load at various time intervals is highly dynamic and is transmitted through several zones of high pressure. A detailed description of the mechanics involved during non-simultaneous failure relating to ice-structure interaction can be found in Jordaan (2001), Ashby et al. (1986) or Blanchet & DeFranco (1996).

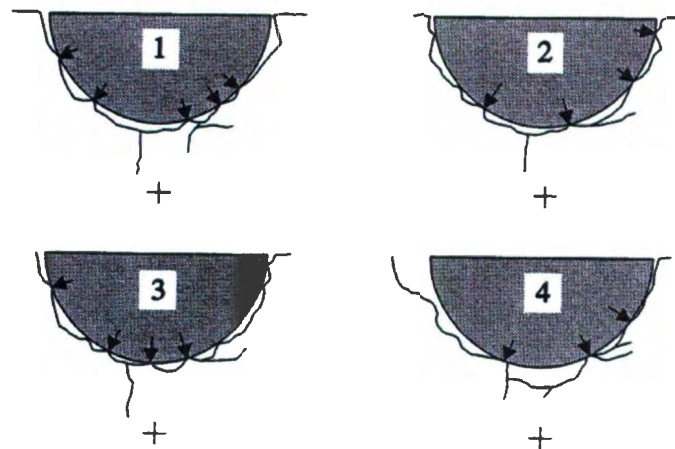


Figure 2-16 Non-simultaneous failure illustration (Ashby et al., 1986).

Blanchet & DeFranco (1996) present a comparison of various models for non-simultaneous failure.

It is noted that whilst it is important to understand the mechanics of ice structure interaction, if an established rubble pile is present, non-simultaneous failure of the approaching ice sheet on a sloping structure will likely be less significant. Non-simultaneous failure will be of greater significance when a structure is free of rubble. Cases like these include narrow structures where the clearing ability of the structure keeps the slope free of rubble or alternatively interaction of very large sloping offshore structures with thick multiyear floes with limited kinetic energy would likely result in limited rubble formation placing a greater significance on non-simultaneous failure.

2.6.2 Scale Effect in Flexural Strength

Lavrov (1971) reported that experiments were done in the USSR by Troshchinskii as early as 1939 at the Luga River which revealed that the flexural strength measured from cantilever beams cut from the ice cover were different than smaller samples taken from the same ice sheet. Since then some debate has taken place over whether a scale effect (also known as a size effect) exists in the flexural strength of ice (Dempsey et al., 1999, and Parsons et al., 1992, Jordaan and Pond, 2001). Iyer (1983) distinguishes between a scale effect and a size effect. According to Iyer (1983) a scale effect is a reduction in pressure with increasing structural width due to a change in failure mechanisms such as non-simultaneous failure. Iyer considers a size effect to be inherent in the material; essentially the presence of flaws causes a reduction in flexural strength due to increased sample size. One could argue that the size effect falls under the umbrella of a scale effect since for practical design of offshore structures, the design beam size increases as the width of the structure increases. With an increase in beam size there is an increased variation in flaw sizes and formations, thus an increased probability of the ice sheet containing a critical flaw path to initiate failure. It is common in industry to consider any pressure reduction with increasing structure width a scale effect.

One of the most comprehensive studies of flexural strength has been carried out by Timco and O'Brien (1994). This study incorporates the data produced by many other researchers combining 1556 tests from freshwater ice and 939 measurements from sea

ice. For this reason it was chosen to be the standard published in CSA-S471 (2004). Brine volume is the critical variable in defining flexural strength in this model. Timco And O'Brien argue that beam size has no significant effect on flexural strength, whilst many other researchers suggest the opposite. This will be discussed in more detail in Chapter 3.

2.7 Probabilistic Design Methodology

2.7.1 Risk and Safety

Andre Gide once said that "*Man cannot discover new oceans unless he has the courage to risk losing sight of the shore*". Risk, is a function of the probability of an unwanted outcome occurring and the consequences of the occurrence of such an outcome. Risk to humans is often defined in terms of annual probabilities of injury or death for an individual. Published levels of risk have been reported by the World Health Organization for various activities and occupations. The United States Environmental Protection Agency reports risks to humans and the environment due to specific environmental pollutants for various levels of exposure.

Safety involves the reduction of risk to a level which is considered to be acceptable to protect human life, property and the environment. Many engineering problems are

concerned with the analysis and mitigation of risk. Risk management in engineering often involves maintaining an acceptable level of risk to the public whilst providing economically viable solutions to problems. A detailed discussion of risk and safety can be found in Jordaan (2005).

2.7.2 Offshore Structure Safety Classes and Reliability

There is a difference between the total risk to humans or the environment and the target levels of safety or reliability used in structural design. In the case of an offshore structure in a harsh environment, total risk includes causes such as ship collisions, wave loads, and ice loads among many others, making the overall safety of the structure quite difficult to estimate. The target levels of annual reliability used in structural design are more manageable. The structure must be designed such that the probability of exceeding the load capacity for the structure is less than the target annual exceedence probabilities discussed below for specific safety classes.

The Canadian Standards Association (CSA) has two safety classes for verifying the overall safety of a structure or any of its structural elements. Safety Class 1 is for loading conditions whereby failure of the structure or individual structural elements would result in a great risk of life and/or a high potential for environmental damage. Safety Class 2 is for structures whereby failure would result in a small risk to life and a low potential for

environmental damage (CSA-S471, 2004). If specific loading hazards can be identified sufficiently ahead of time to carry out a predefined emergency response plan that ensures personnel safety and environmental protection, then, for the particular loading condition, the structure may be designated Safety Class 2. It is also noted that a safety class may be assigned to the structure as a whole, or to individual structural elements. Thus a structure designated a safety class 1 structure as a whole, may have individual structural components designed for safety class 2 (CSA-S471, 2004).

In order to meet the design objectives in each of the safety classes, target reliability levels have been selected. These target reliability levels serve as a basis for limit state design. For a safety class 1 structure, the annual target reliability level is $(1-10^{-5}) = 0.99999$, or an annual exceedence probability of 10^{-5} . For a safety class 2 structure, the annual target reliability level is $(1-10^{-3}) = 0.999$, or an annual exceedence probability of 10^{-3} (CSA-S471, 2004).

2.7.3 Uncertainty

A major consideration in decision making or structural design is the analysis of uncertainties. Uncertainties arise in a number of ways. Uncertainties that arise from natural variation in environmental parameters cannot be reduced by collecting more information. For example, the maximum wave height occurring next year at a given site cannot be predicted with absolute certainty, regardless of the amount of wave height data

available for that site (Nessim et al., 1995). Uncertainty also arises when using quantitative methods to analyze problems where the problem is defined in terms of parameters and models since these are only approximations of reality. When using functional relationships the uncertainty in the output parameter is a function of both the uncertainty in the input parameters as well as the uncertainty in the functional relationships.

Maes (1990) has discussed the importance of the ability to reduce conservatism in structural design codes if a reduction in uncertainty is achieved with the use of more accurate models based on new data. The source of the uncertainty has an important effect on how it should be treated in estimating design loads. Nessim et al. (1995) introduce three classifications of uncertainty with respect to sources. These classifications are *basic* uncertainty, *model* uncertainty, and *distribution* uncertainty. *Basic* uncertainty is defined as uncertainty regarding the physical parameters that affect the load magnitude. These are parameters such as environmental conditions or material properties which are not known with certainty at the time the structure is built. *Model* uncertainty is defined as uncertainty regarding the error in the calculated value of a physical parameter due to the model used in the calculation. These uncertainties can be reduced with new data and the development of better physical models. *Distribution* uncertainty is defined as uncertainty surrounding a probabilistic distribution assigned to represent an uncertain parameter in a model.

The effect of uncertainty in design problems is illustrated in the Figure 2-17 below (after Fuglem, 1997). The solid curve represents an exceedance distribution for ice loads on a structure. This distribution is assigned by the designer given the information available at the time. The second curve represents the exceedance curve after obtaining additional information, thus reducing uncertainty. As the level of uncertainty is reduced, the design load corresponding to a specified acceptable level of risk is reduced.

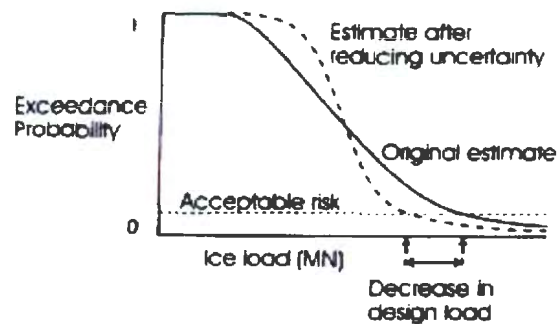


Figure 2-17 The effect of uncertainty in design problems

Even when there is considerable uncertainty it is still often possible to achieve a design that is conservative enough to ensure safety, and still be economical. If the level of uncertainty is very high, it may be cost effective to proceed first with more in depth analysis to reduce uncertainties to a level which brings the design load lower. Some techniques are discussed in the following sections for dealing with uncertain input parameters.

2.7.4 Extreme Value Analysis

For the purpose of design using probabilistic methods, a distinction is made between *frequent* events and *rare* events. Frequent events are environmental processes which are discrete events that occur at multiple discrete points in time over the course of the year. Level first year ice interaction with offshore structures are generally considered to be a frequent event for most ice environments. Rare events are discrete events that occur on average less than once per year (CSA – S471, 2004). For the Grand Banks of Newfoundland, an iceberg impact is considered a rare event. Since we are concerned with level ice interaction with sloping offshore structures, frequent events will be the focus of this discussion.

Frequent ice loading events can be treated using an extreme value approach as developed in Jordaan et al. (1993). Jordaan et al. made the observation that pressure data from ship rams on a specific area, ranked and plotted in the form of an exceedance distribution, were of exponential form in the tail of the distribution (Figure 2-18). The distribution was fit to the tail only since the analysis was mainly concerned with the extreme pressures.

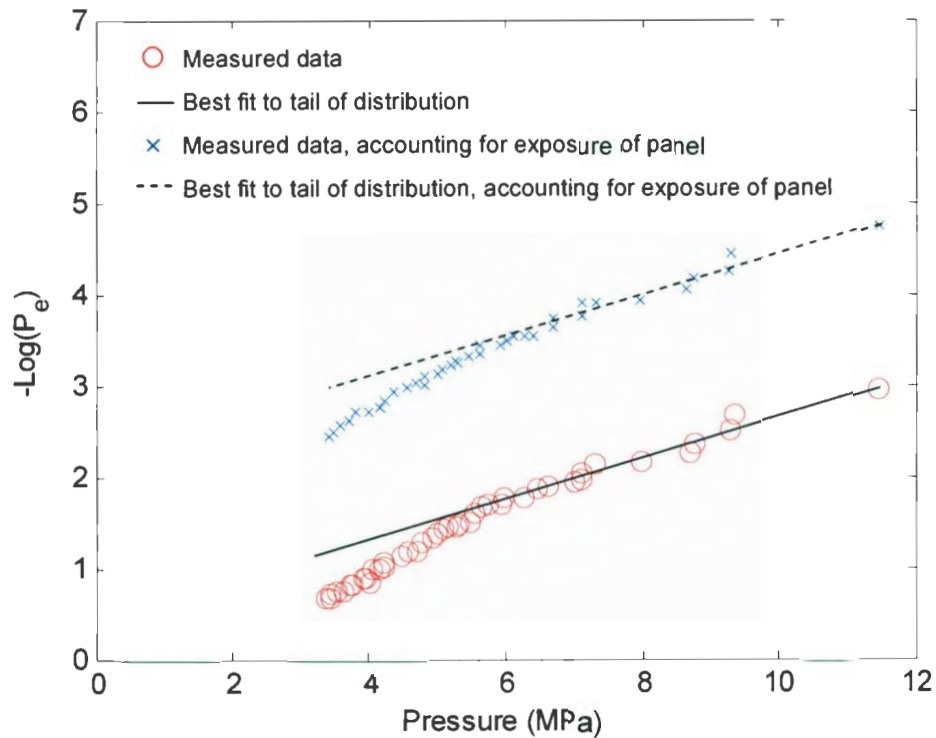


Figure 2-18: Best fit to the tail of local pressure data (Jordaan et al., 1993)

The resulting cumulative distribution function is $F_X(x)$, where X is the force or pressure under consideration. If there are N events in a year, we consider the largest pressure value Z , where:

$$Z = \max(X_1, X_2, \dots, X_i, \dots, X_N) \quad \text{Equation 2-9}$$

Where X_i is a random quantity denoting the maximum load for a given event (ie. one impact). A Poisson arrival process of loading events is often assumed, although it is not necessarily a constant floe arrival rate. The resulting expression for the distribution of the extreme load Z is then:

$$F_Z(z) = \exp\{-v[1 - F_X(z)]\} \quad \text{Equation 2-10}$$

Where ν is the number of arrivals in a year or whichever period is of interest. As mentioned above, the tails of extreme distributions are often exponential. The probability of exceedence is then given by the equation below:

$$p_e = \exp\left[-\frac{(x - x_0)}{\alpha}\right] \quad \text{Equation 2-11}$$

Where p_e is the probability of exceedence, given by $1-F_X(x)$ and x_0 and α are constants. This causes the expression for the distribution of the extreme load Z to take the form of the double exponential or the Gumbel distribution shown below.

$$F_Z(z) = \exp\left\{-\exp\left[-\frac{(z - x_0 - x_1)}{\alpha}\right]\right\} \quad \text{Equation 2-12}$$

Where $x_1 = \ln \nu$

The parameter α represents the decrease of pressure with area. Jordaan et al. (1993) determined the design curve $\alpha = 1.25a^{-0.70}$, with x_0 approximated as zero. Figure 2-19 below, taken from Jordaan et al. (2005), shows the analysis of alpha versus area for two data sets.

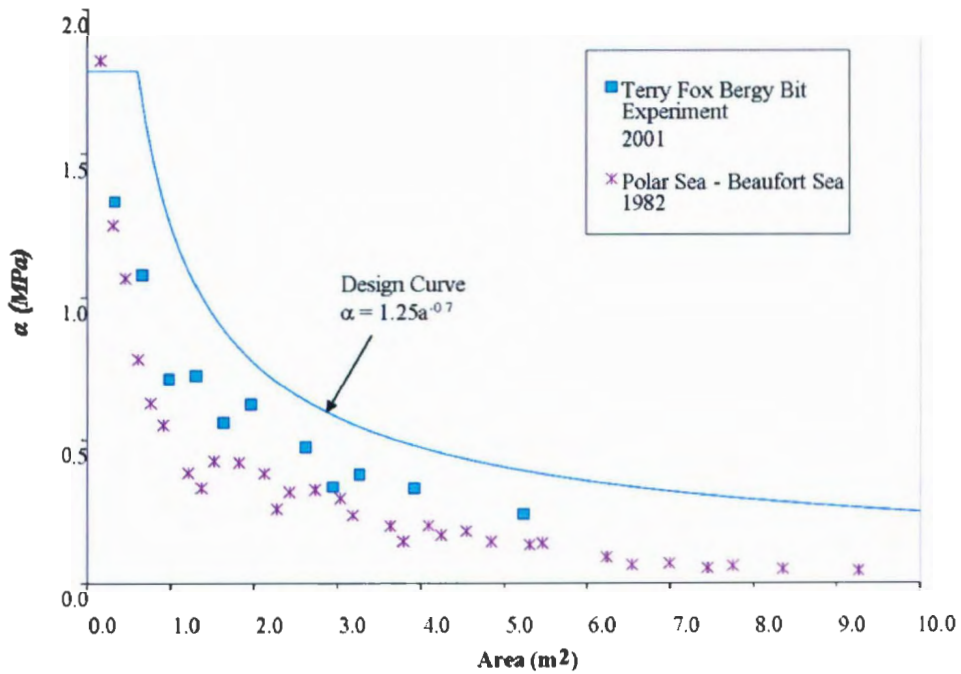


Figure 2-19 The scale effect in alpha vs. area, after Jordaan et al. 2005.

The figure below (Figure 2-20) shows the effect of considering design loads based on the probability of exceedance of 10^{-2} and 10^{-4} . It is noted that increasing the exposure (ie. the number of impacts per year) has a similar effect in that the design curve is shifted as the probability of an extreme load increases with increased exposure.

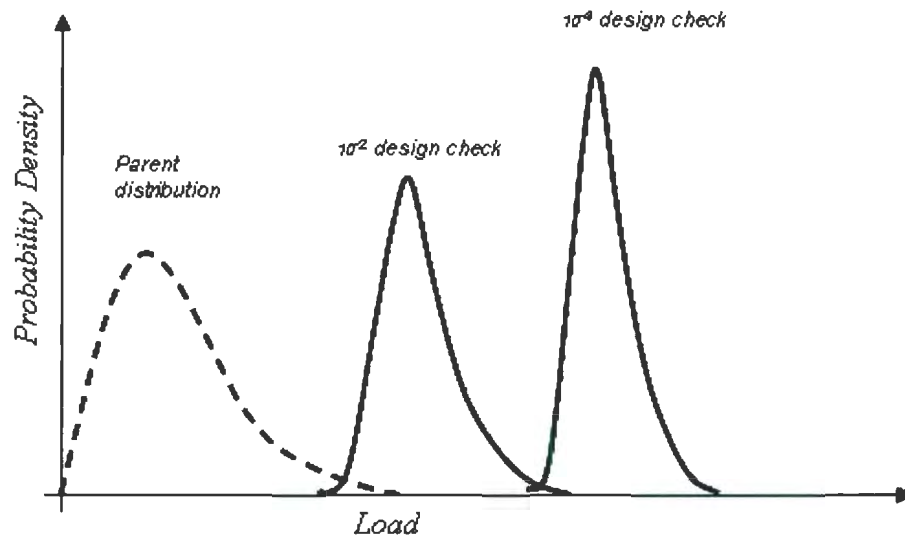


Figure 2-20 Effect of extremal analysis based on the parent distribution for 100 and 10,000 year return periods.

This strategy of determining extreme loads works best for local pressures, however when considering global loads, the peak force is strongly dependent on vessel size. For considering global loads, Monte Carlo simulation is more appropriate. In this case, the Monte Carlo simulation forms the basis for the determination of the parent distribution $F_X(x)$. Monte Carlo simulation is discussed in some detail in the following section.

2.7.5 Monte Carlo Simulation

In analysis of engineering problems more often than not it is difficult to find the required solution in closed form. A powerful way to solve problems of this nature numerically is the Monte Carlo method, which is very flexible and has been widely used in many

industries. Monte Carlo simulation has proven to be particularly useful for the generation of global loads on offshore structures and analyzing reliability as discussed by (Melchers 1987 and Melchers 1989, Jordaan 2005).

In Monte Carlo simulation, a model is run repeatedly, using different values for each of the uncertain input parameters each time. The values of each of the uncertain parameters are generated based on the probability distribution for the parameter. If there are two or more uncertain input parameters, one value from each is sampled in each repetition in the simulation.

With many input variables, one can envision Monte Carlo simulation as providing a random sampling from a space of m dimensions, where m is the number of random variables that are inputs to the model. One could also envision Monte Carlo as providing a simulated set of sample values for the joint distribution of all of the random variable inputs to the model. Over the course of a simulation many iterations can be made, typically in the area of 1000 iterations or more, producing a set of sample values for each of the model output variables (Cullen, 1999). These output values can then be treated statistically as though they were an experimentally observed set of data.

A flowchart such as the one shown below (Figure 2-21) taken from Brown et al. (2001) can be used to illustrate the general process of applying Monte Carlo simulation to a model. For each input to the model which is a random variable, a probability distribution

is specified. Random samples can then be simulated from each of the input distributions. One sample from each input distribution is selected, and the set of samples is entered into the model. The model is then executed as it would be for any deterministic analysis. The simulated model results are stored after every repetition and the process repeats itself for the user specified number of simulated years (or any other specified duration). The results may then be analyzed similar to experimentally collected data as the simulation essentially forms the parent distribution $F_X(x)$.

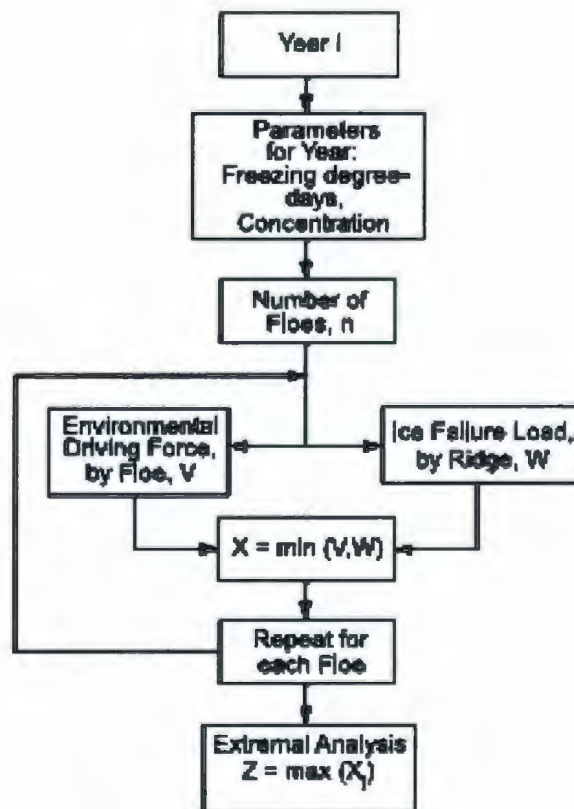


Figure 2-21 Sample flow chart showing Monte Carlo simulation (taken from Brown et al., 2001).

Using Monte Carlo techniques it is possible to represent uncertainty in the output of a model by generating sample values for the model inputs, and running the model repetitively. Instead of obtaining a single number for model outputs as in a deterministic simulation, a set of samples is obtained. These can then be represented as cumulative density functions (*cdf's*) and summarized using typical statistics such as the mean and variance of the dataset.

Although the generation of sample values for model input parameters is probabilistic, the execution of the model for a given set of samples in a repetition is deterministic. The advantage of Monte Carlo methods is that these deterministic simulations are repeated in a manner that yields important insights into the sensitivity of the model to variations in the input parameters, as well as the likelihood of obtaining any particular outcome. Monte Carlo methods also allow the modeler to use any type of probability distribution for which values can be generated on a computer.

3 FRACTURE OF ICE: FLEXURAL FAILURE

3.1 Flexural Strength

For elastic materials, such as steel, the tensile strength can be obtained by performing a tensile test, whereby the specimen is deformed, usually to fracture, with a gradually increasing tensile load that is applied uniaxially along the axis of the specimen. Using the tensile strength approach it can be quite difficult to prepare brittle specimens, such as ice, to the required geometry for testing. Once prepared, the specimen must be gripped for testing in such a way that it ensures that the specimen fails in tension and not locally at the gripping point. The tensile test is further complicated for brittle materials since they tend to fail after a very small amount of tensile strain, which necessitates that a tensile specimen be perfectly aligned to avoid any bending stresses which can develop which are difficult to account for. For these reasons, for brittle specimens such as ice the stress-strain tensile behavior is more often determined using the flexural strength.

The flexural strength is obtained more suitably for brittle materials in a transverse bending test, in which a rod specimen having either a circular or a rectangular cross section is bent until fracture. This bending is achieved using either a three point loading or a four point loading as shown below in Figure 3-1. At the point of loading, the top surface of the beam is placed in a state of compression, whilst the bottom surface is placed in a state of tension. Stress is computed based on the thickness of the specimen, in addition to the bending moment, and the moment of inertia of the cross section. Since the

tensile strength for ice is much lower than its compressive strength, and since fracture occurs on the tensile specimen face, the flexure test is a reasonable substitute for the tensile test. The stress at the fracture using this flexure test is known as the *flexural strength*.

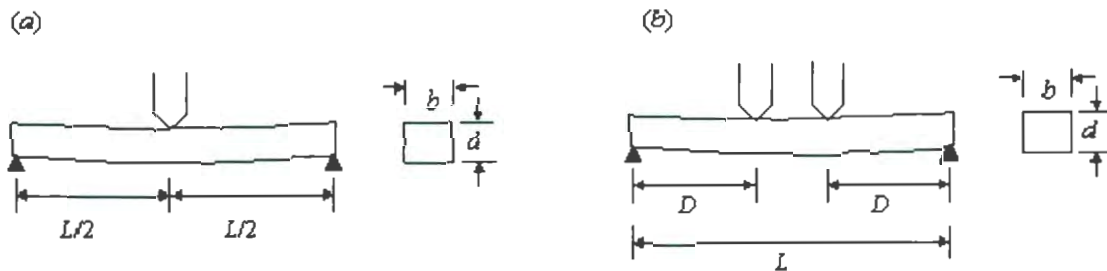


Figure 3-1(a) Three point loading setup. (b) Four point loading setup.

For a three point loading setup, the flexural strength is given by the equation below:

$$\sigma_f = \frac{3F_f L}{2bd^2} \quad \text{Equation 3-1}$$

For a four point loading setup, the flexural strength is given by the equation below:

$$\sigma_f = \frac{3F_f D}{bd^2} \quad \text{Equation 3-2}$$

Where F_f is the peak load occurring at fracture of the specimen. It is noted that the flexural strength of a material is in general greater than the tensile strength. When a specimen is loaded in flexure as shown in Figure 3-1 the top portion of the specimen is in compression, whilst the bottom portion is in tension. This leads to a reduced tensile area,

which leads to a reduced probability of the sample containing a critical flaw pathway to initiate failure.

The cantilever beam test is also a potential method for determining the flexural strength. The cantilever beam test can be performed insitu on the floating beam. A cantilever shape is cut into the ice and loaded at the tip. The loading may be downward (into the water) or upwards (out of the water) as shown in the figure below (Figure 3-2). The flexural strength can then be obtained from the equation below:

$$\sigma_f = \frac{6F_f L}{bd^2} \quad \text{Equation 3-3}$$

Where L is the length of the cantilever beam as shown in Figure 3-2.

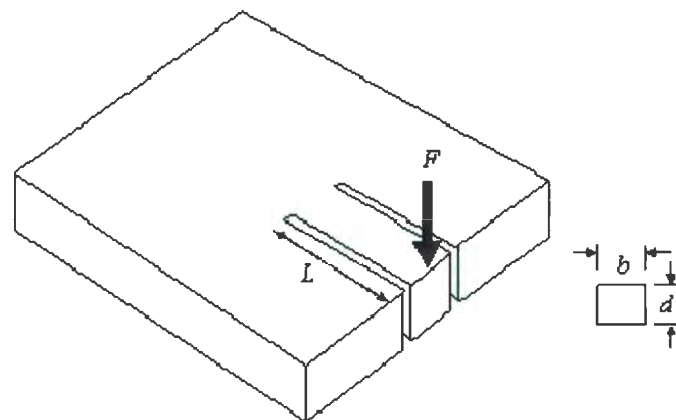


Figure 3-2 Shows arrangement for insitu cantilever beam testing.

3.2 Scale Effect in Flexural Strength – Review of Relevant Literature

Parsons et al. (1992) conducted a study of simply supported beams under three point loading with the intention of studying the size effect in ice during flexural failure. The purpose was to determine if the flexural strength in bending, or the tension in the extreme fiber, decreases as the stressed volume increases. Beams 2m x 0.2m x 0.2m were prepared from the top of the sea ice in Allen Bay, North West Territories. The beams were then tested at a calculated strain rate at the extreme fiber of $\dot{\epsilon} = 10^{-3} s^{-1}$. Beams of 2.0, 1.0, 0.45 and 0.2m spans with thickness equal to the width equal to a tenth of the span were tested at the same strain rate. The original top sheet of the ice was placed in tension in cases. In addition to sea ice, the group also conducted tests on fine grained columnar freshwater ice as well as iceberg ice.

The results of this experimentation showed a decrease in the flexural strength of the sea ice beams with increasing stressed volume. The freshwater ice showed little to no scale effect. The results are shown below in Figure 3-3 reproduced from Parsons et al., (1992).

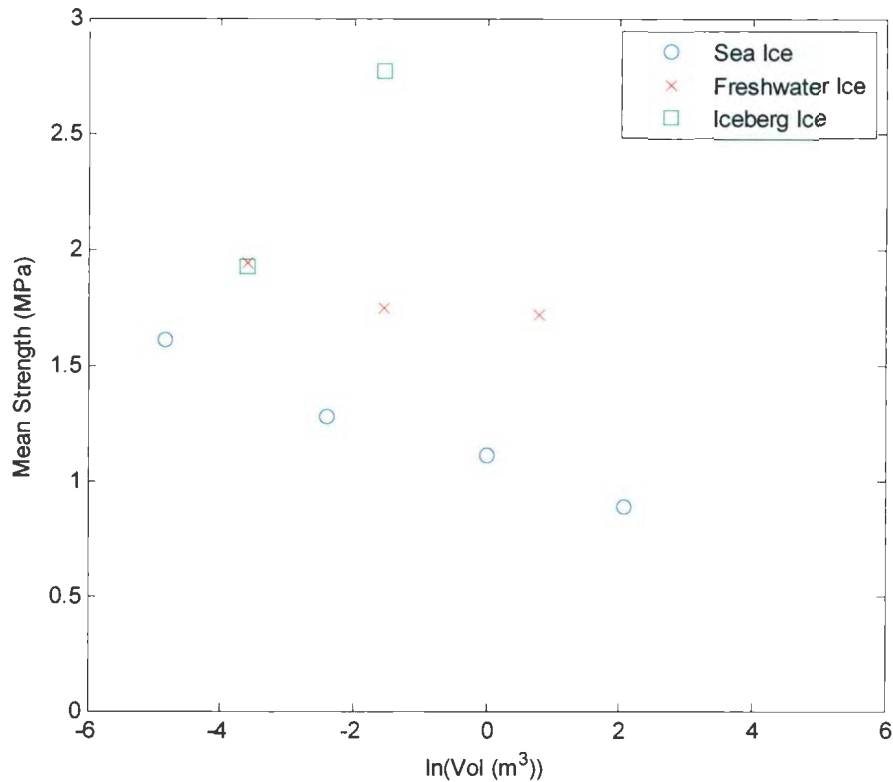


Figure 3-3 Iceberg, sea, and freshwater ice flexural strength vs. volume after Parsons et al., 1992.

A study conducted by Timco and O'Brien (1994) states that the results reported by Parsons et al., (1992) show that there is not a large scale effect for flexural strength of sea ice. Instead, an argument is made that the flexural strength of sea ice is governed by brine volume alone. The study involved the compilation of 14 investigators representing 939 sea ice measurements and 5 investigators representing 1556 freshwater ice measurements.

In this work, the beam size was broken into two sections, large beams and small beams. Where a small beam is considered to be one in which the cross sectional area of the failure plane is less than 100cm^2 , whilst a large beam has a cross sectional area of the failure plane greater than 100cm^2 .

An exponential fit was developed for the flexural strength as a function of the square root of the brine volume. The equation developed is given below:

$$\sigma_f = 1.76e^{-5.88\sqrt{v_b}} \quad \text{Equation 3-4}$$

Where v_b is the brine volume which is obtained from the equation below:

$$v_b = S \left(\frac{49.185}{|T|} + 0.532 \right) \quad \text{Equation 3-5}$$

Where T is the temperature of the ice where $-0.5^{\circ}\text{C} \geq T \geq -22.9^{\circ}\text{C}$ and S is the salinity of the ice. The fits for Equation 3-4 are shown in the figures below (Figure 3-4 and Figure 3-5).

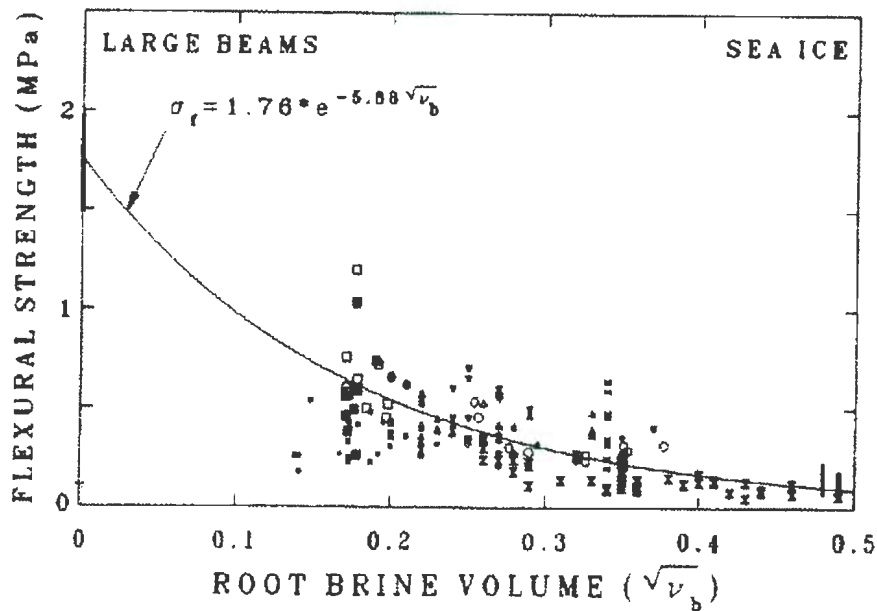


Figure 3-4 Large beam sea ice flexural strength as a function of the square root of brine volume (Timco and O'Brien, 1994).

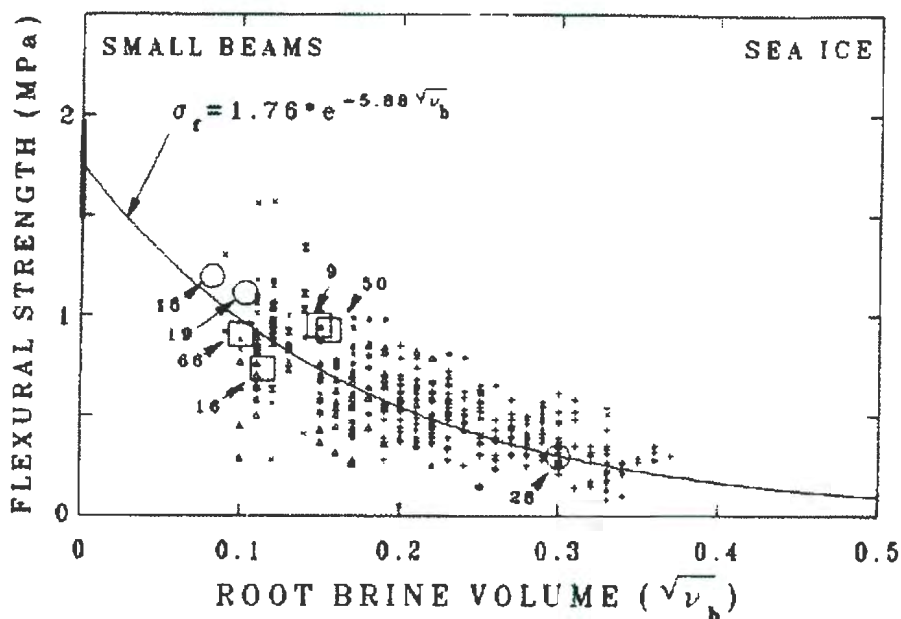


Figure 3-5 Small beam sea ice flexural strength as a function of the square root of brine volume (Timco and O'Brien, 1994).

This method for predicting flexural strength has been accepted by much of the ice community and has made its way into the Canadian Safety Association's (CSA – S471, 2004) recommended practice. The main benefit taken from the paper would be the ability to predict perhaps the mean flexural strength for a given area knowing the salinity and average air temperature. This method does however neglect the size effect found by many researchers. By neglecting the size effect one must assume the same flexural strength for a 100m wide structure as for a 1m wide structure, which could lead to design loads being higher than necessary when used in a probabilistic model. In addition to this, the methodology described above does not account for the large scatter found in the data. For example, for a root brine volume of approximately $0.10 \text{ m}^{3/2}$ the spread in flexural strength ranges from approximately 0.25 MPa to 1.6 MPa. It is the belief of the author that the size effect may account for some of this variation in flexural strength.

A model developed by Williams and Parsons (1994) combines the effects of both the brine volume and the size effect. The study considered the statistical significance of brine volume, sample size, crystal size, ice temperature and strain rate. Brine volume was found to have the most significant effect, with sample size being the next most significant factor effecting the flexural strength of ice.

Williams and Parsons (1994) took a similar approach to that of Timco and O'Brien (1994) in that they combined the datasets of many studies conducted in the past. The database used for their study contained 1771 sea ice and 650 freshwater ice beams. The equation developed which incorporates both brine volume and beam volume is given below:

$$\sigma = \sigma_0 \exp(a\sqrt{v_b}) \left(\frac{V}{V_1}\right)^b \quad \text{Equation 3-6}$$

Where σ_0 , a and b are coefficients to be determined, V_1 is the reference volume of 0.01m^3 obtained from the Institute for Marine Dynamics (IMD) standard test beam size configuration of $1\text{m} \times 0.1\text{m} \times 0.1\text{m}$. It is noted that for freshwater ice $a = 0$. For sea ice, the coefficients σ_0 , a and b are determined from linear regression. Williams and Parsons found the coefficients to be as shown below:

$$\sigma = 1760 \exp(-5.395\sqrt{v_b}) \left(\frac{V}{V_1}\right)^{-0.084} \quad \text{Equation 3-7}$$

With a root mean square residual on the measured strengths of 186kPa.

A three dimensional plot of flexural strength versus brine volume and beam volume is shown below (Figure 3-6), where beam volume is plotted on a log scale (Williams and Parsons, 1994). It is clear from this figure that in addition to brine volume, beam volume plays a significant role in determining flexural strength.

It is the feeling of the author that this approach, using beam volume in addition to brine volume provides a better solution for the determination of flexural strength. It is also necessary to consider the sensitivity of ice loads on offshore structures to flexural strength. In Section 3.3 a closer examination will be conducted on the effect of flexural strength on ice loads.

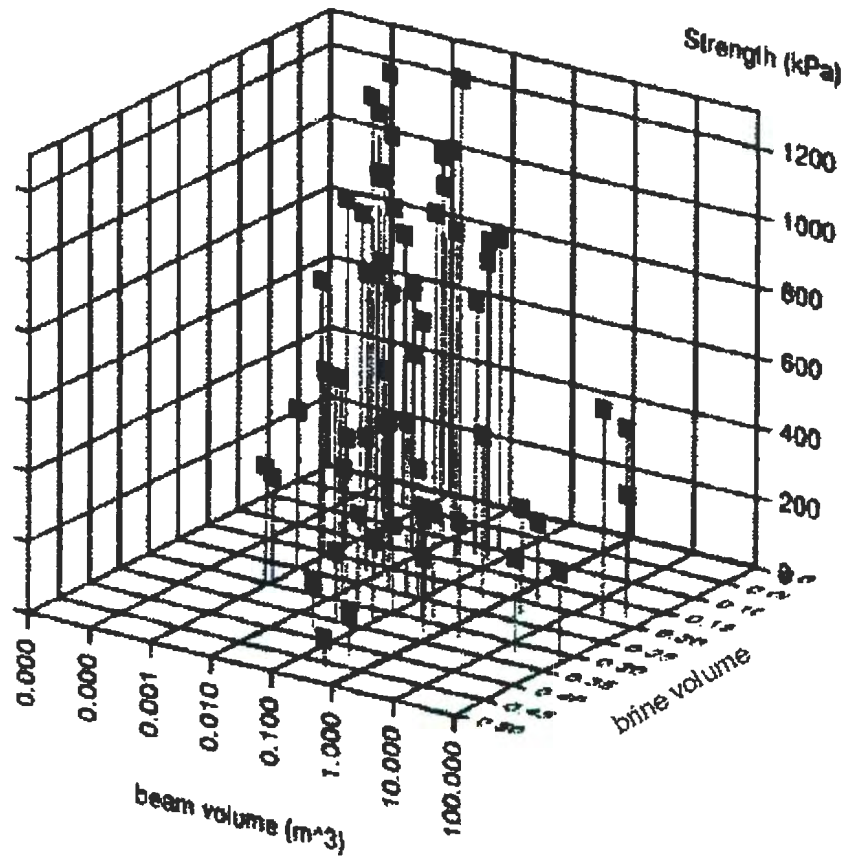


Figure 3-6 A three dimensional plot of flexural strength versus brine volume and beam volume is shown with beam volume plotted on a log scale (Williams and Parsons, 1994).

3.3 Sensitivity of Ice Loads on Sloping Structures to Flexural Strength

When designing a sloping offshore structure, it is important that one considers the sensitivity of the derived ice loads to all input parameters in order to ensure that a safe model or design has been developed. In the later chapters of this work, the Croasdale model has been used in the development of a probabilistic ice load model for a case study involving the Confederation Bridge. For this reason, the sensitivity of the Croasdale model to variations in input values should be studied in detail (See Appendix A for full sensitivity analysis). Here the sensitivity of ice loads predicted by the Croasdale model to flexural strength is discussed in detail.

If one refers back to Section 2.4.1 where the Croasdale model is described in detail, the breaking term (H_B) is the only component which is dependent on the flexural strength.

The breaking term is given by the equation below:

$$H_B = \varepsilon_1 \sigma_f D \left(\frac{\rho_w g h^5}{E} \right)^{0.25} \left[D + \left(\pi^2 / 4 \right) l_c \right] / D \quad \text{Equation 3-8}$$

It is possible to consider the sensitivity of the breaking term to flexural strength by varying the flexural strength whilst keeping all other variables constant. The table below (Table 3-1) lists sample values for the variables which are required for deriving the total horizontal load on a structure by using the Croasdale model.

Flexural Strength	Range 200 - 900 kPa
Ice Thickness	0.7 m
Rubble Height	0.0 m
Rubble Porosity	0.2
Angle of Rubble Pile	35 degrees
Width of Structure	14 m
Structure Slope Angle	52 degrees
Freeboard Height	5.0 m
Ice Internal Friction Angle	40 degrees
Cohesive Strength of Ice	4.0 kPa
Ice-Ice Friction Coefficient	0.1
Ice-Structure Friction Coefficient	0.12
Density of Water	1030 kg/m ³
Density of Ice	900 kg/m ³
Youngs Modulus of Ice	3.0 GPa
Poisson's Ratio	0.3

Table 3-1 The constant values used for considering the sensitivity of flexural strength on ice loads.

The figure below (Figure 3-7) shows the result of varying flexural strength on the breaking term as well as the total vertical and horizontal ice loads determined by the Croasdale model. These values were determined whilst keeping all other variables constant as listed in Table 3-1.

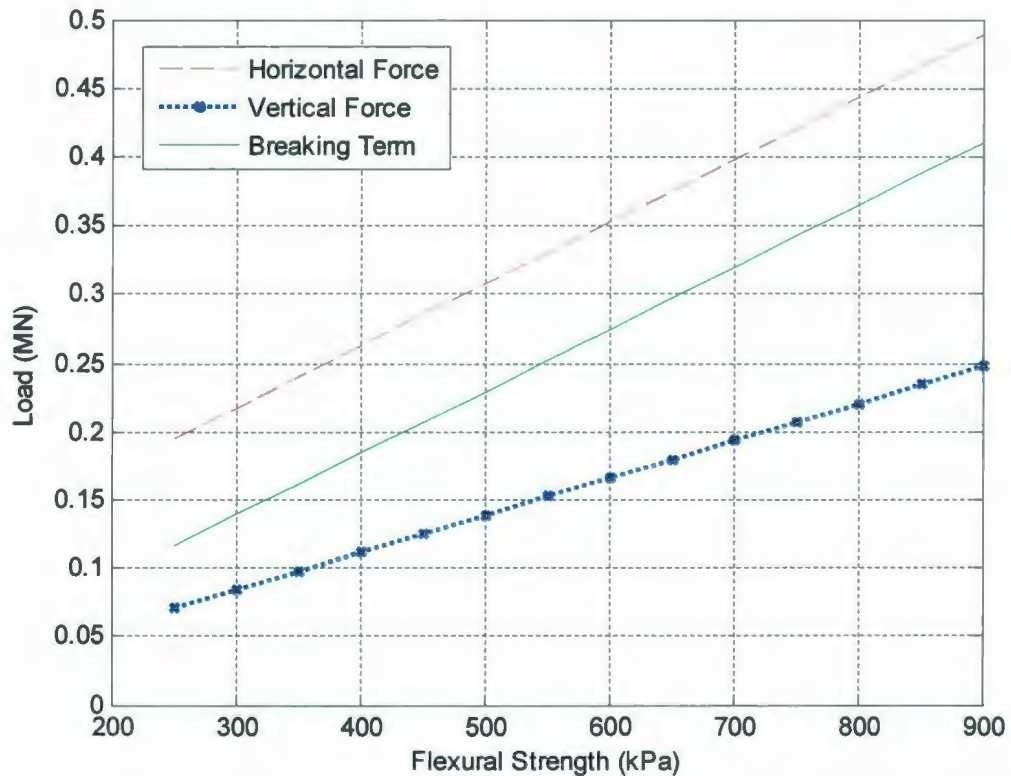


Figure 3-7 Ice load as a function of flexural strength without ice rubble formation.

One can see from Figure 3-7 that for the case outlined above, the flexural strength of the ice is very significant as varying the flexural strength from 250 – 900kPa leads to an increase in the breaking term from 0.11MN to 0.41MN.

There may be cases however where the flexural strength is not as significant as the above results may suggest. As mentioned previously, it is only the breaking term in the Croasdale model which is directly affected by the flexural strength. One particular load case which results in large ice loads on sloping structures is the development of a rubble

pile. One can see from the figure below (Figure 3-8) that by adding rubble to the structure, the flexural strength becomes less significant. An additional figure (Figure 3-9) shows the effect of varying rubble height on vertical and horizontal ice loads compared to the breaking term for a flexural strength constant at 500 kPa.

While the flexural strength of ice may be of less significance in the case where there is a rubble pile present, there are a number of design scenarios where flexural strength is of great significance. For instance, a ship ramming a level ice feature often results in the ice sheet breaking in flexure. The process occurs without any rubble formation, making the flexural strength of the ice feature of great importance for determining design loads on ice breakers. The possibility of building very large conical or sloping structures in the high arctic where multi-year floes will be impacting is also of interest. Here, the multi-year floes will have limited kinetic energy, leading to the likelihood of relatively small amounts of rubble formation, thus making flexural strength modeling a significant aspect for design of such structures. Finally, as discussed previously the flexural strength of ice is not a large contributor to the maximum load on a conical structure when an established rubble pile is present - from the perspective of breaking the ice sheet in flexure against the structure. However, the flexural strength of the ice sheet plays a significant role in determining the maximum rubble height that the ice sheet can physically support. Considerable effort will be placed in the following sections to examine the flexural strength during full scale ship ramming events.

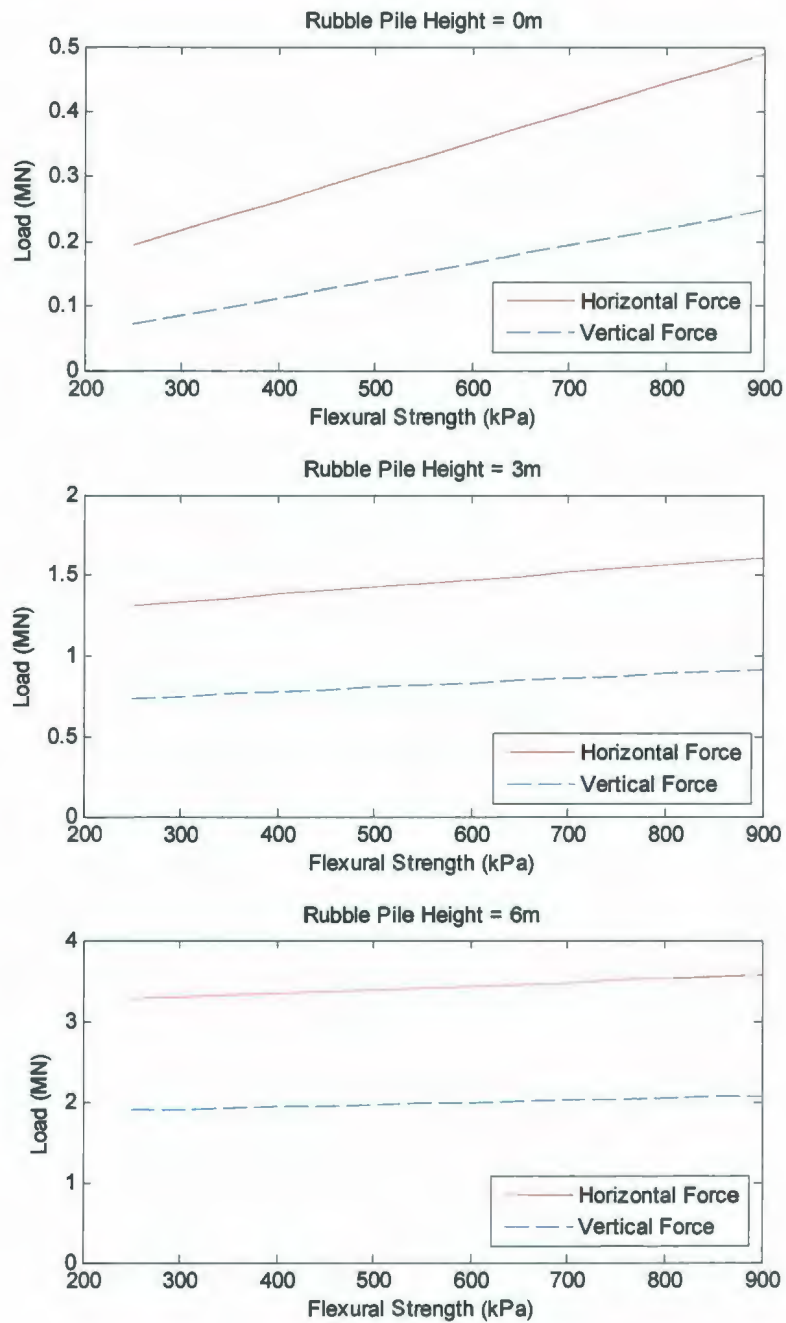


Figure 3-8 Illustrating the decreasing significance that flexural strength holds as a result of introducing a rubble pile. The top, middle and bottom plots have a rubble pile height of 0m, 3m and 6m respectively.

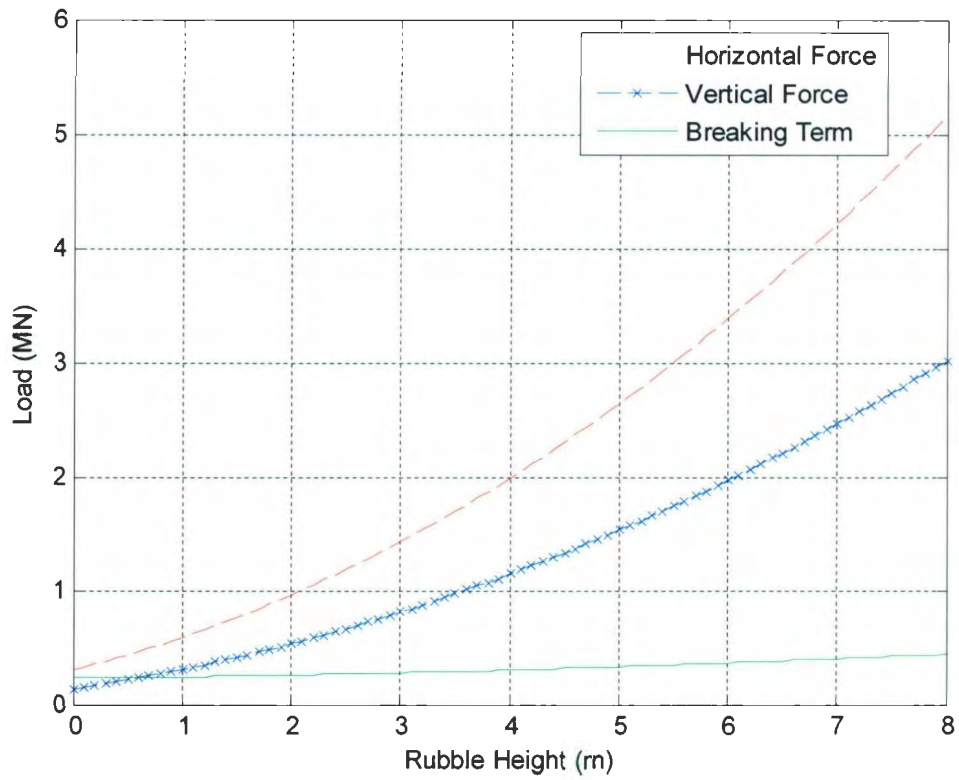


Figure 3-9 The effect of varying rubble pile height whilst keeping the flexural strength constant at 500kPa. The breaking term becomes less significant with increasing rubble formation.

3.4 Full Scale Ice – Ship Interaction

The problem being addressed in this section is that of a vessel ramming into thick first year or multiyear level ice, as illustrated in Figure 3-10. For design purposes, we are interested in determining the maximum ice force being exerted on the bow of the ship. This force, denoted F_{max} , is important for determining both the global and local ice loads used in the design of vessels and offshore structures in ice environments. The ice-ship interactions provide full scale data which can be used to consider the size effect in flexural strength. Ship ram data are ideal for this as the loads causing failure of the ice sheet are not affected by rubble formation like those on sloping offshore structures. The role of flexural failure and ultimately the flexural strength of the ice during ice-ship interaction on the icebreaker Oden will be examined in some detail in this section.



Figure 3-10 The Ice Breaker Oden interacting with thick level ice.

3.4.1 Ship Ramming Process Description

Ships break ice by forcing the ice downwards to break in flexure. In operational conditions the ship has the power to break ice steadily and continuously. As the ice gets thicker the power required increases and the ship tends to slow. At some point the ice force exceeds the available thrust and the ship is brought to a stop. If further progress is needed the ship must back up and begin a process of ramming the ice feature.

During ice-ship interaction there are a number of stages which are present during a typical ship ramming event. Dome Petroleum (1982) described the ice-ship interaction process using five phases. As mentioned previously, this is a description of a typical interaction event and may be slightly different for vessels varying in size and shape. The five phases are listed below and illustrated in Figure 3-11:

1. *Approach Phase:* During the approach phase the vessel accelerates in open water towards the ice feature. The goal is for the vessel to reach a constant speed before interacting with the ice feature. The duration of this phase is dependent on the vessel and the speed desired for the interaction.
2. *Impact Phase:* The impact phase incorporates the first point of contact between the vessel and the ice feature until the vessel begins to ride up the ice feature. This phase is the fastest of the five phases often lasting less than one second. During this phase there is a significant change in the surge velocity of the vessel, as well the vertical velocity of the bow increases from zero to its maximum value. The impact phase is structurally the most critical as the highest stresses of the

interaction are often achieved during this phase. It is distinguishable by the splash of ice and water from the interaction face.

3. *Slide-up Phase:* During the slide-up phase, the ship slides up on its relatively flat bow where the transfer from kinetic energy to potential energy occurs with the ships loss of velocity and gain in height. Some kinetic energy is also dissipated due to the frictional losses during this time. This phase continues until all kinetic energy is converted to potential energy or dissipated. This loss of kinetic energy can also be aided by the impact of the ice knife.
4. *Ice Knife Impact Phase:* If the vessel has sufficient kinetic energy during the slide-up phase, the ice knife will impact the ice feature. The ice knife is intended to stop the vessels forward motion by dissipating kinetic energy in the form of ice crushing. The magnitude of the global ice force will reach a characteristic second peak during this phase which can be of a similar magnitude to that of the initial impact phase. At the end of this phase, the ship is stopped with its bow at the highest vertical position. The stern deck can often be underwater during this phase.
5. *Slide-Down Phase:* During the slide-down phase the ship slides back down the ice feature into the open water. Minor ice crushing can take place during this phase as the vessel returns to the open water.

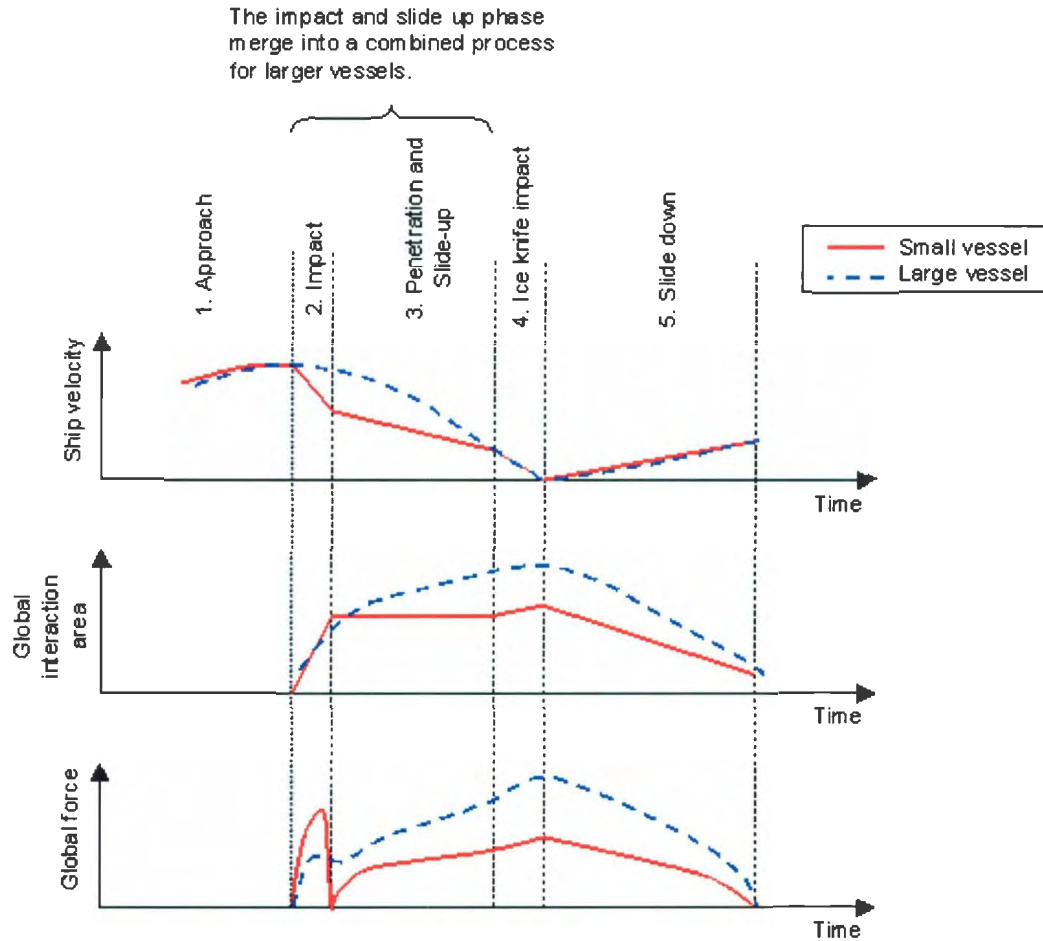


Figure 3-11 Schematic illustration of the phases involved during a ship ramming event (Jordaan et al., 2005).

3.4.2 Case Study: The Icebreaker Oden

The Oden is a Swedish icebreaking vessel which was designed and built in 1988 by Göteverken-Arendal in Gothenburg, Sweden. The Oden was designed to act as a heavy escort icebreaker for the northern Baltic coast of Sweden with the additional purpose of providing icebreaking capability during Arctic expeditions.

The data analyzed in this work was obtained during the International Arctic Ocean Expedition in 1991 where the Oden was part of a three vessel expedition to the central Arctic Basin. The expedition left Tromso, Norway following a course to the west of Spitzbergen, Franz Josef Land, the Lomonosov Ridge, and Makarov Basin, ultimately reaching the North Pole.

The Oden has a rounded landing craft form as shown in Figure 3-12. This design is intended to provide a very clean channel for ships to follow in. The Oden has a length of 107.8m, with a maximum beam of 31.0m and an operational draft of 7.0-8.5m. It has an ice breaking capability of 1.8m ice thickness at 3 knots and was designed with a DnV 1A1 safety classification.

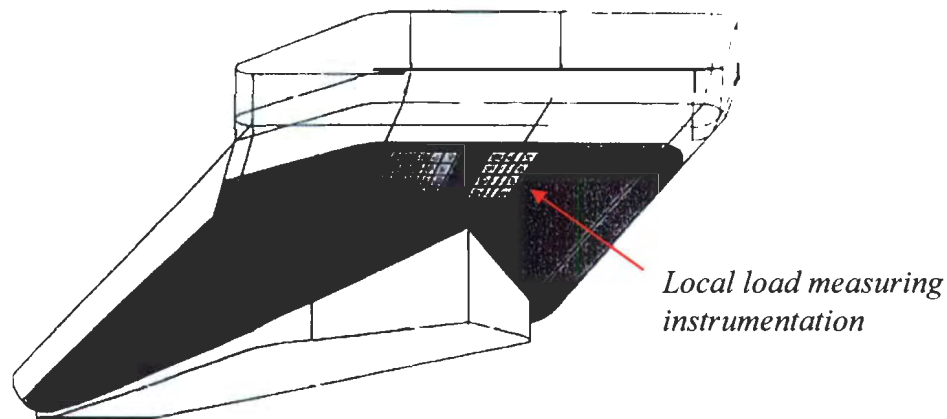


Figure 3-12 The Oden rounded landing craft hull design used for breaking ice in flexure. The local load instrumentation layout is also shown.

During its 1991 voyage with the International Arctic Ocean Expedition, the Oden was subject to 786 recorded ice-ship interaction events. The events were recorded on a 20m² strain-gauged area located on the bow as shown in Figure 3-12 above. The strain gauged area was divided into 32 subpanels, each with an area of 0.65m². This instrumentation was used for measuring local ice pressure.

The global load determination was achieved by using strain gauges on the hull girder, as well as two accelerometers located on the ship. It is the global load that is of interest when considering the flexural strength of the ice sheet.

3.4.3 Simulation of Ice-Ship Interaction – Fmax Program

Jordaan et al. (1996) developed a methodology for the determination of global pressure during ice-structure interaction, using the expression below:

$$P = Ca^D \qquad \text{Equation 3-9}$$

Where P is the global pressure, a is the area which is treated as being normalized (ie. divided by a reference area of, say 1m²) thus making it dimensionless. C therefore has units of pressure (MPa). The parameters C and D can be modeled as lognormal and normal distributions respectively.

Ship ram data from Carter et al. (1996) is used to calibrate the equations for the maximum loads during the interaction. The governing equations of ship motions developed in Carter et al. (1996) are given below:

$$\ddot{x} = \frac{(-k_x x - c_x \dot{x}) - F_h}{M_x} \quad \text{Equation 3-10}$$

$$\ddot{y} = \frac{(-k_y y - c_y \dot{y}) - F_v}{M_y} \quad \text{Equation 3-11}$$

Here F_h and F_v are the horizontal and vertical components of the force due to the ice crushing and the friction occurring at the contact interface. The horizontal and vertical spring constants are given by k_x and k_y respectively. The horizontal and vertical damping coefficients are given by c_x and c_y respectively and M_x and M_y are the equivalent mass at the bow in the x and y directions respectively.

The force components F_h and F_v are determined using the global pressure equation (Equation 3-9) and some geometrical considerations based on the shape of the bow, whilst the area, a is a function of penetration (x, y). The reader is directed to Carter et al. (1996) for an in depth derivation of these parameters. These calculations leave only the penetration values x and y to be determined which are solved numerically using a Runge-Kutta process.

The solution is found by proceeding with a time domain approach using a Runge-Kutta numerical integration algorithm developed by Carter et al. (1996) called F_{max} . At each

time step, the new displacement and thus resulting ice force is determined. From this, the accelerations and displacements of the vessel are determined using the equations above (Equation 3-10 and Equation 3-11). The model is run until the forward motion of the vessel is stopped or the ice fails in flexure. A check is made at each time step to determine whether failure by flexure occurs. The flexural resistance of the ice sheet will increase with thickness and contains a time-dependant decrease in strength due to the viscoelastic nature of ice. If the flexural resistance limit for the ice sheet is reached, the numerical algorithm will stop.

3.4.4 Simulation Results

In this work the intention was to compare the flexural strength observed during a full scale interaction with the flexural strength predicted based on small scale beam test analysis by Timco and O'Brien (1994). As discussed previously in Section 3.2 the work by Timco and O'Brien neglects the size effect which has been determined to be statistically significant by Williams and Parsons (1994).

Here an attempt has been made to determine the flexural strength which provides the best simulation results when compared to the observed maximum force during the icebreaker Oden's 1991 International Arctic Ocean Expedition. This is achieved by performing various simulations with a mean flexural strength ranging from 0.3 to 0.8 MPa with a standard deviation of 0.2 MPa. Values for parameters C and D were assigned based on a

sensitivity analysis conducted by Carter et al (1996). Parameter C is modeled as log normally distributed with a mean of 3.0 MPa and a standard deviation of 1.5 MPa. Parameter D is modeled as normally distributed with a mean of -0.4 and a standard deviation of 0.2.

Recalling from Section 3.2 that Timco and O'Brien (1994) define the flexural strength of ice to be dependent on the brine volume of ice given by Equation 3-4, where brine volume is determined based on the salinity and temperature of the ice by Equation 3-5. As ice develops during the course of the winter, the average salinity of the entire ice thickness decreases as brine is lost from the ice. Brine loss occurs by temperature-dependent brine pocket migration, brine expulsion, and by gravity drainage through cells and channels in the ice. At the end of winter, Arctic first-year ice has an average salinity of 5–10 parts per thousand (ppt), whilst multi-year ice has an average salinity of 0.5-4 ppt (Sanderson, 1980). The areal average air temperature for the Pan-Arctic basin is -23.75°C (Rawlins and Willmott, 2003) leading to approximately -12.8°C average ice temperature, assuming that the ice at the bottom of the sheet (ice-water interface) is -1.8°C .

As there was both first-year and multi-year ice present during the Oden's expedition, the salinity of the ice can be assumed to be approximately 5ppt with an ice temperature of approximately -12.8°C . Utilizing Timco and O'Brien's approach, the predicted flexural strength of the ice is approximately 0.74 MPa.

Adopting the predicted flexural strength developed above for simulations using the F_{\max} program described previously, leads to an overestimation of the simulated loads compared to the recorded field data as can be seen in Figure 3-13. If the simulated loads are systematically higher than the recorded data as they are in Figure 3-13, this implies that the model is failing the ice in a crushing failure when it should often have perhaps failed previously in flexure. A number of simulations were conducted whilst varying the flexural strength of the ice. Some of these results can be seen in Appendix B.

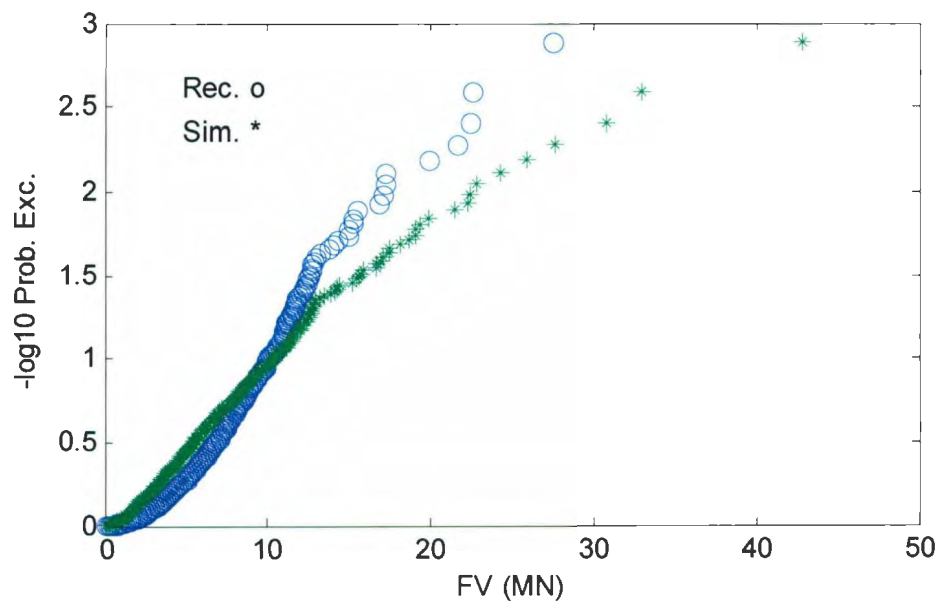
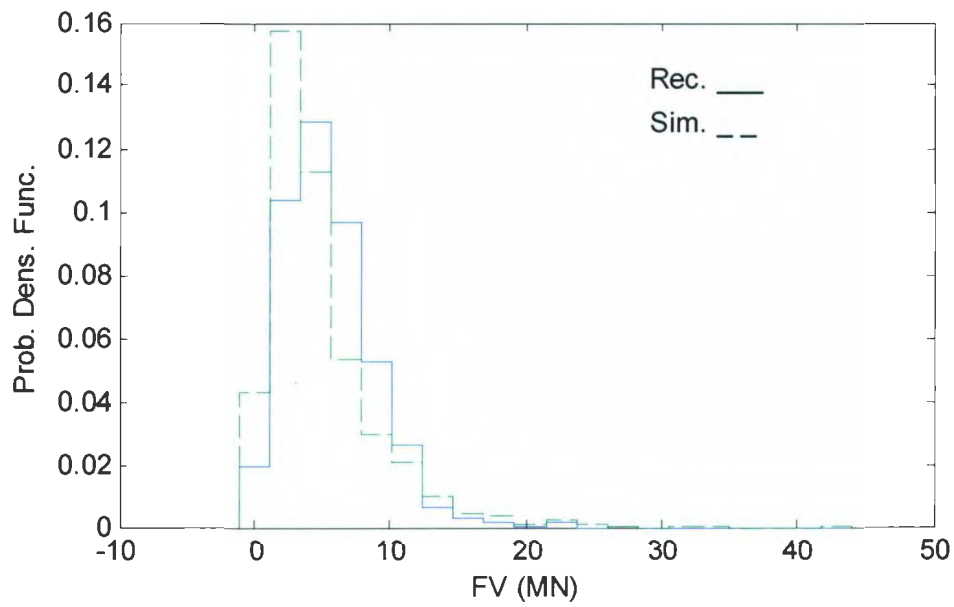


Figure 3-13 Histogram and exceedance probabilities of individual (parent) rams. This simulation utilized a flexural strength of 0.7MPa with a standard deviation of 0.2MPa.

The simulation which produced the best fit to the recorded field data was achieved whilst using a flexural strength of 0.4 MPa with a standard deviation of 0.2 MPa, as can be seen in Figure 3-14. This represents a significant decrease in the predicted flexural strength of the ice due seemingly to an increase in the scale of the interaction. This result confirms the significance of the size effect discussed by Williams and Parsons (1994).

If one considers a sample calculation using the methodology developed by Williams and Parsons (1994), a comparison can be made using Equation 3-7. Considering a sample cantilever interaction with an ice thickness of 3 m, an interaction width of 25 m and a beam of length 26 m. The beam length is determined based on the relationship developed by Croasdale (1994) where the distance to the first crack is given by $\frac{\pi}{4} L_c$, where L_c is the characteristic length given by the equation below:

$$L_c = \left(\frac{Eh^3}{12\rho_w g(1-\nu^2)} \right)^{\frac{1}{4}} \quad \text{Equation 3-12}$$

Where E is Young's Modulus, h is ice thickness, ν is Poisson's ratio, and ρ_w is the density of water. When using the method developed by Williams and Parsons for cantilever beams the volume of ice is multiplied by two to generate a volume as if it were a simple beam test. Thus, the effective ice volume is approximately 3900 m³. This methodology predicts a flexural strength of approximately 0.27 MPa with a residual error of 0.186 MPa, which agrees well with the results simulated in this work.

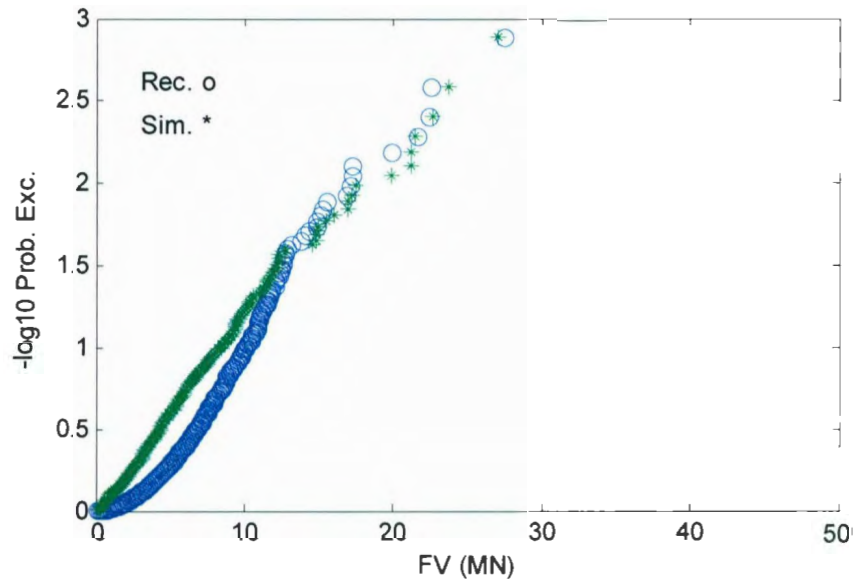
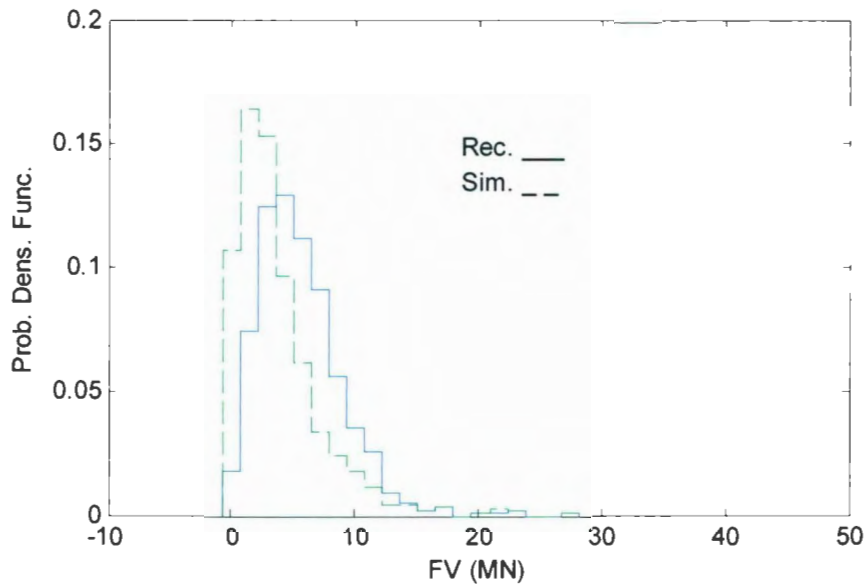


Figure 3-14 Histogram and exceedance probabilities of individual (parent) rams. This simulation utilized a flexural strength of 0.4 MPa with a standard deviation of 0.2 MPa.

3.5 Concluding Remarks

The flexural strength of ice can be a significant factor affecting the ice loads on structures for certain loading scenarios. As was determined in the analysis in Chapter 3, the presence of a rubble pile on a structure decreases the significance of the flexural strength of ice. This is due to the large increase in load associated with the formation of a rubble pile when compared to that of a level ice sheet. The flexural strength of ice remains of great significance however for ship ramming events where flexural failure is a predominant failure model. It is of great importance to model the flexural strength of ice accurately for these cases where the ice load is sensitive to the flexural strength input.

From the results of the simulations described above in Section 3.4.4 it is likely that the flexural strength of ice for a full scale interaction is significantly less than those of small scale beam tests. The methodology developed by Timco and O'Brien (1994) appears to over predict the flexural strength of ice for full scale interactions as it neglects the size effect. For full scale interactions, the methodology developed by Williams and Parsons produces an improved result.

4 PROBABILISTIC MODELING OF ICE LOADS

4.1 Introduction

The objective of this chapter was to develop a probabilistic model to determine design ice loads on a conical structure in a level ice environment. This was achieved by using a Monte Carlo simulation approach. In a probabilistic model such as the one carried out in this study, it is important that input values are not excessively over estimated as this will lead to a compounding effect of safety factors. The accepted practice behind probabilistic modeling is to estimate certain expected values of random quantities, and to develop probability distributions around the values which reflect uncertainties in the random quantities and in the estimation of the parameters (Cammaert et al., 1993). The probability distributions developed in this work are based as much as possible on data available for the specified location.

4.2 Case Study: The Confederation Bridge

The Confederation Bridge (Figure 4-1) is located in the Northumberland Strait, spanning 13km to connect Prince Edward Island to New Brunswick, Canada. The Northumberland Strait is an area which experiences ice formation every winter, with ice as early as mid December and lasting as late as May. Ice forces were therefore a major factor affecting the design of the bridge piers.



Figure 4-1 The ice environment surrounding the Confederation Bridge.

The geometry selected for pier construction (Figure 4-2) consisted of 52° cones with a 14m diameter at the waterline. The 52° cone extends approximately 2.6m above the waterline where there is a 78° cone that rises to 7.0 m above the waterline, from which the pier shaft proper continues. Below the cone, the pier is supported by a 10 m diameter cylindrical shaft, resting on a conical pier base.

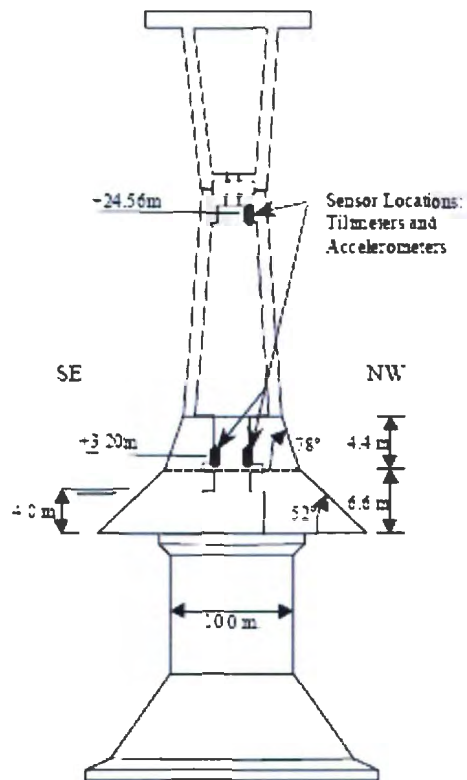


Figure 4-2 Geometry selected for design of the Confederation Bridge piers. Pier dimensions and locations of tiltmeters and accelerometers used for global load measurement are also shown.

A detailed description follows of the probability distributions used to model the ice environment. The probability distributions developed in this work are based as much as possible on data available for the specified location.

4.3 Modeling the Ice Environment

4.3.1 Freezing Degree Days

Freezing degree days are used as an indication of the severity of the ice season. In the present study, freezing degree days (*FDD*) is defined as the *sum of all negative daily average temperatures (°C)* for the period of December 1st through April 30th. A variation of the *FDD* calculation is the accumulated freezing degree day value. Accumulated freezing degree days (*aFDD*) is defined as the *sum of all daily average temperatures (°C)* throughout the period of December 1st through April 30th. The *aFDD* is typically used to indicate where a period of warming has occurred in the air temperature data.

Air temperature data was obtained from Environment Canada for the town of Summerside on Prince Edward Island. This was the closest town to the bridge location with a publicly available temperature data set. The figure below (Figure 4-3) shows the location of Summerside in relation to the Confederation Bridge. Given the close proximity of Summerside to the Confederation Bridge, one can be reasonably confident in the air temperature data accuracy. The data record starts in 1943 and runs until 2007 and contains information regarding the minimum, maximum and average daily air temperatures for this period.

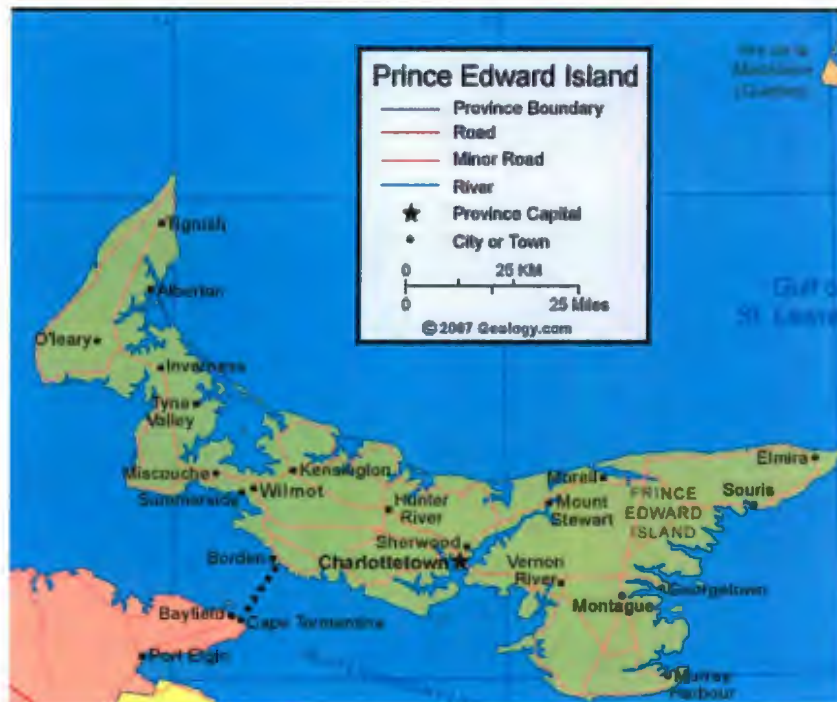


Figure 4-3 Map showing the location of Summerside, Prince Edward Island in relation to the Confederation Bridge. Summerside is located approximately 20km from the North side of the bridge.

Below the extracted *FDD* data are shown for each month (Figure 4-4 to Figure 4-8). A gamma distribution has been fit to each month's *FDD* distribution as it provided the best fit to the data set. The gamma distribution is given by the following:

$$f_x(x) = \frac{x^{\alpha-1} \exp\left(-\frac{x}{\beta}\right)}{\beta^\alpha \Gamma(\alpha)}, \text{ for } x \geq 0, \alpha, \beta > 0. \quad \text{Equation 4-1}$$

Where α and β are coefficients for shape and scale respectively.

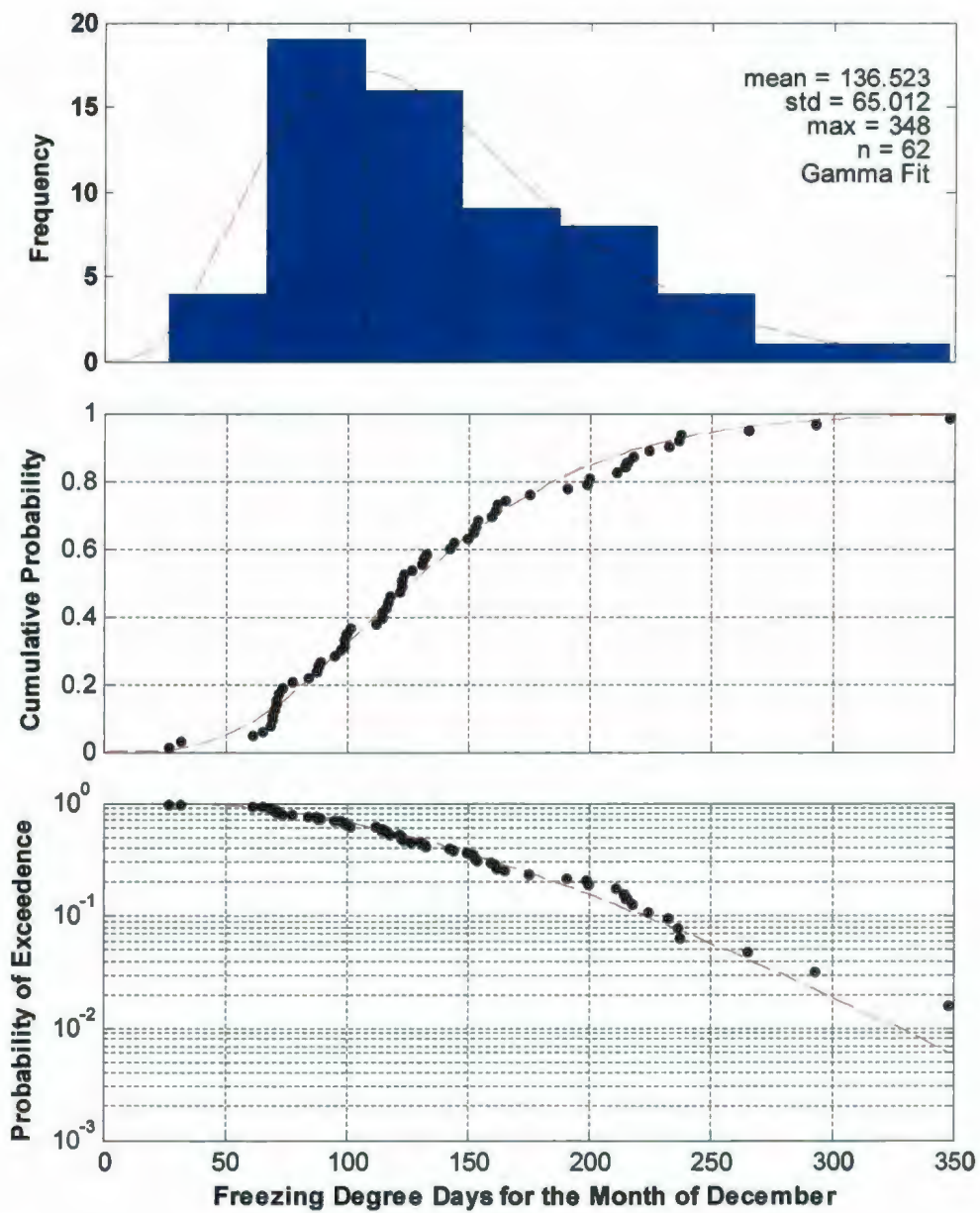


Figure 4-4 Freezing Degree Days for the month of December. Fit with a gamma distribution with $\alpha=3.49$, $\beta=37.3$.

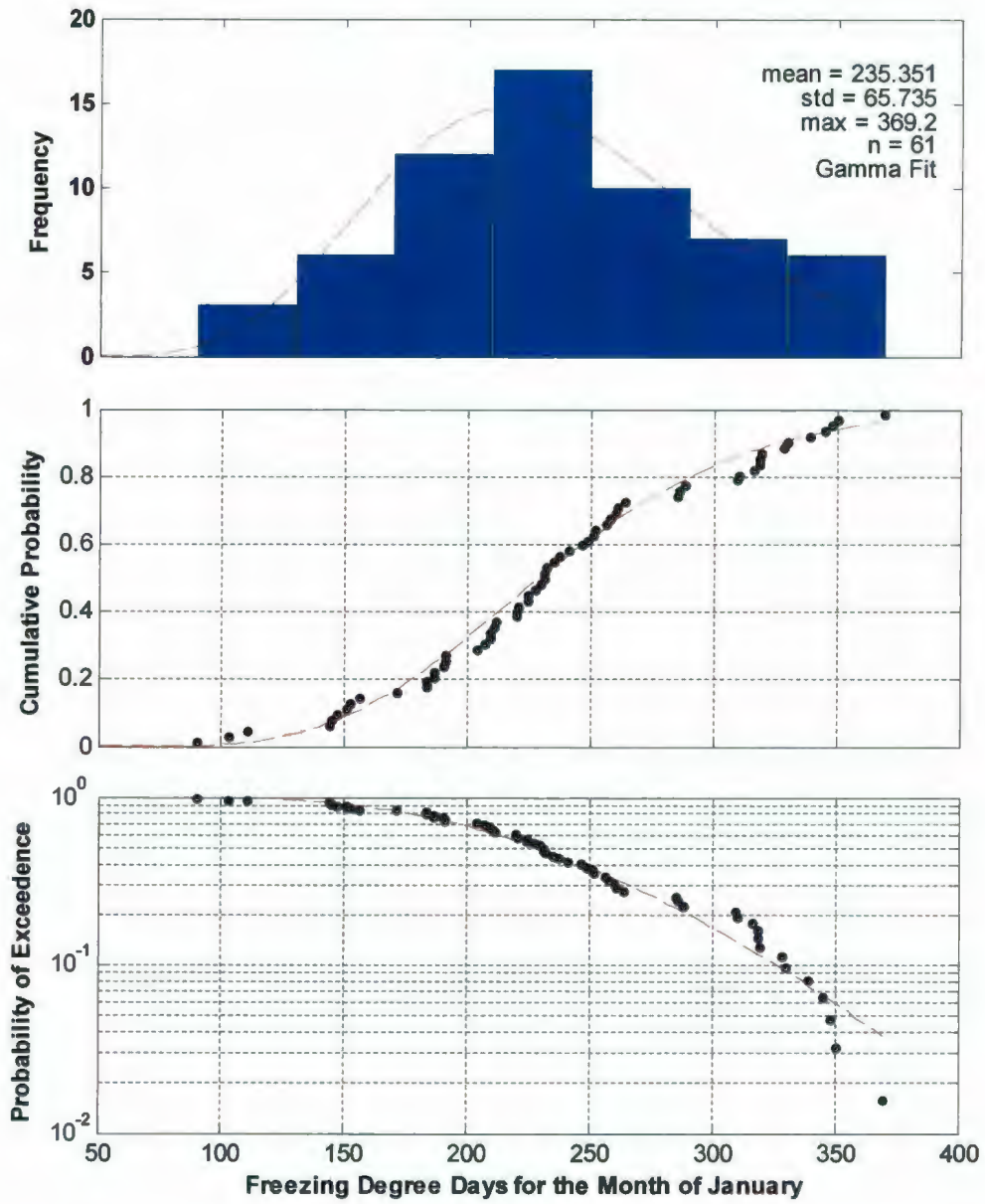


Figure 4-5 Freezing Degree Days for the month of January. Fit with a gamma distribution with $\alpha=220.9$, $\beta=85.4$.

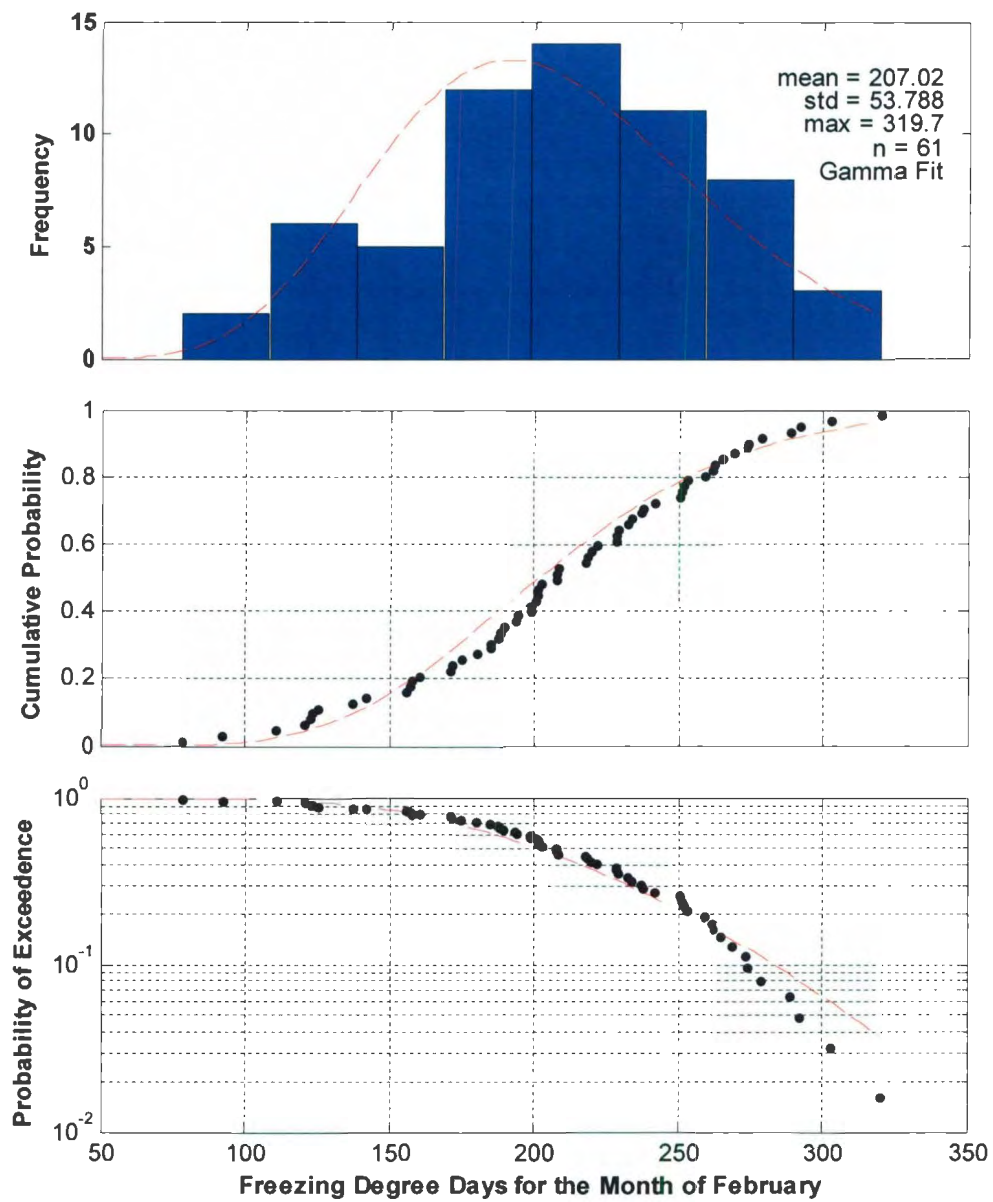


Figure 4-6 Freezing Degree Days for the month of February. Fit with a gamma distribution with $\alpha=194.3$, $\beta=72.3$.

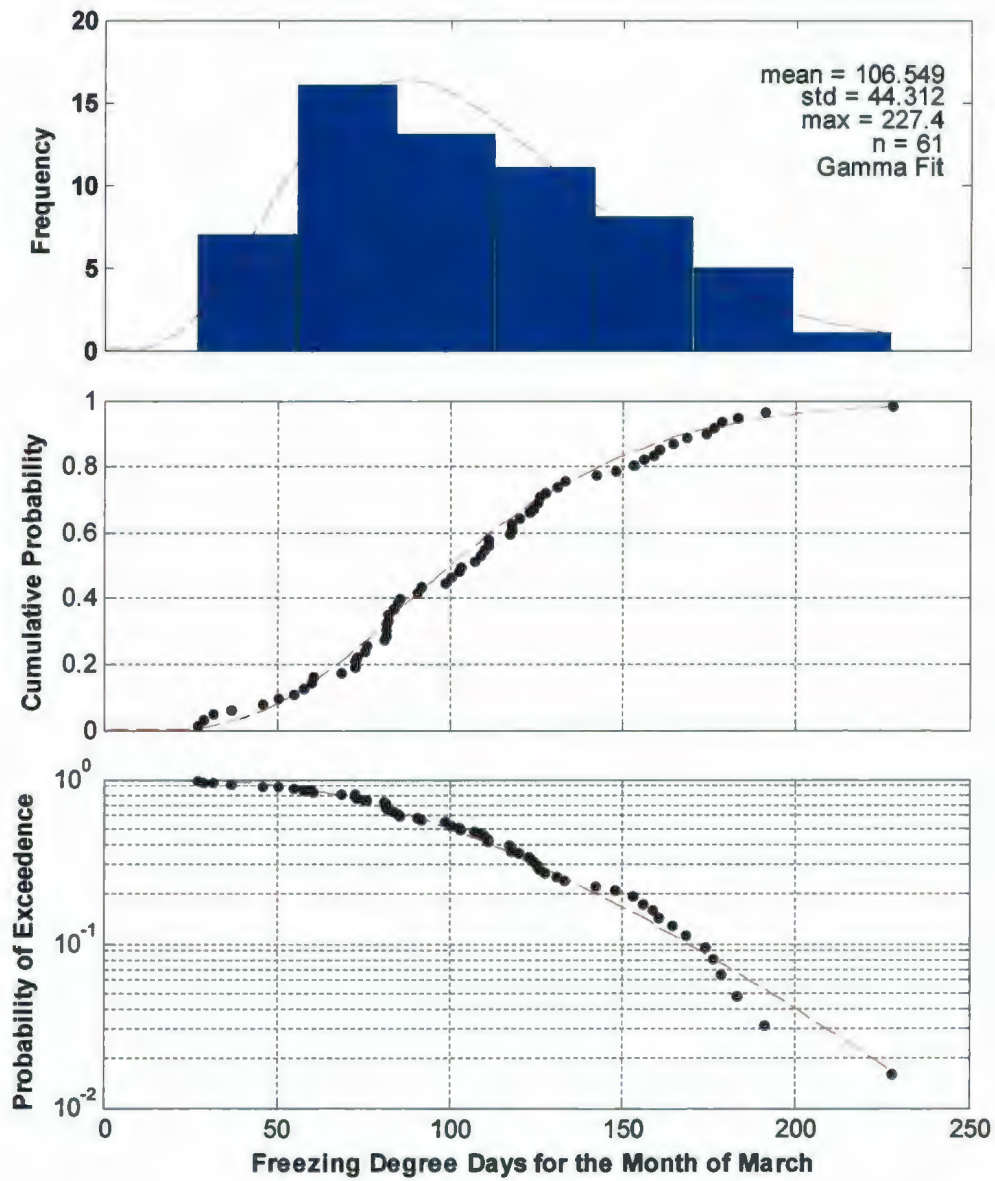


Figure 4-7 Freezing Degree Days for the month of March. Fit with a gamma distribution with $\alpha=100.0$, $\beta=50.1$.

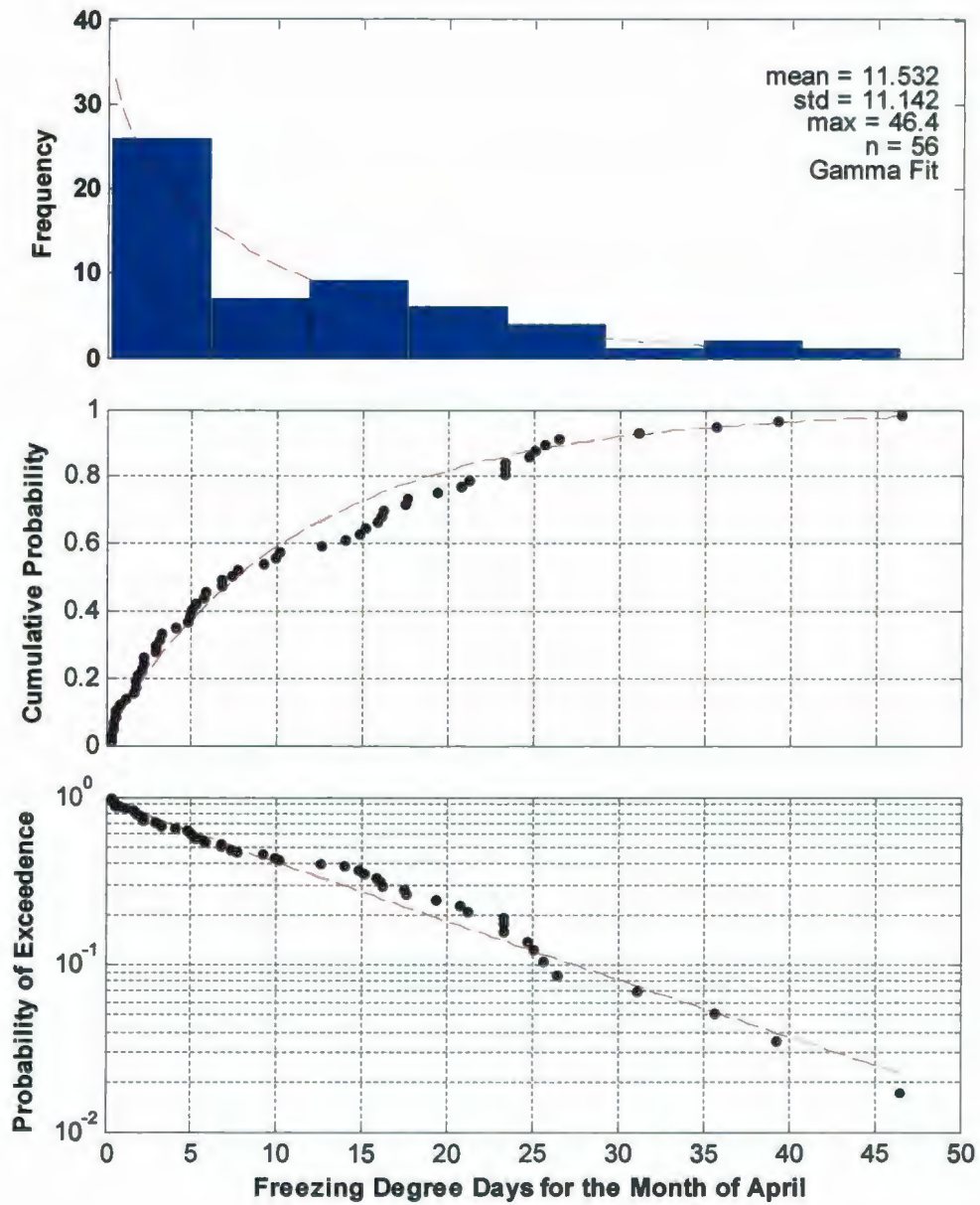


Figure 4-8 Freezing Degree Days for the month of April. Fit with a gamma distribution with $\alpha=0.80$, $\beta=12.3$.

4.3.2 Ice Thickness

The data shown below were obtained from the current archive at the Canadian Ice Service which was collected by the Atmospheric Environment Program of Environment Canada. Measurements were taken at the same approximate location for each year on a weekly basis starting after freeze-up when the ice is safe to walk on, and continuing until break-up or when the ice becomes unsafe to walk on. The location is selected close to shore, but over a depth of water which will exceed the maximum ice thickness. Ice thickness is measured to the nearest centimeter using either a specialized auger kit or a hot wire ice thickness gauge. The depth of snow on the ice at the location of ice thickness measurement is also measured and reported to the nearest centimeter.

The Canadian Ice Service ice thickness data at Summerside, Prince Edward Island is available for the years 1973-1978 as well as 1995 (Figure 4-9). Along with the thickness measurement is an associated date, so its position in the ice season is known. This is important information for modeling ice growth throughout the ice season. There are 82 thickness measurements with a mean of 33.74 cm, standard deviation of 16.6 cm and a maximum thickness measurement of 73.0 cm.

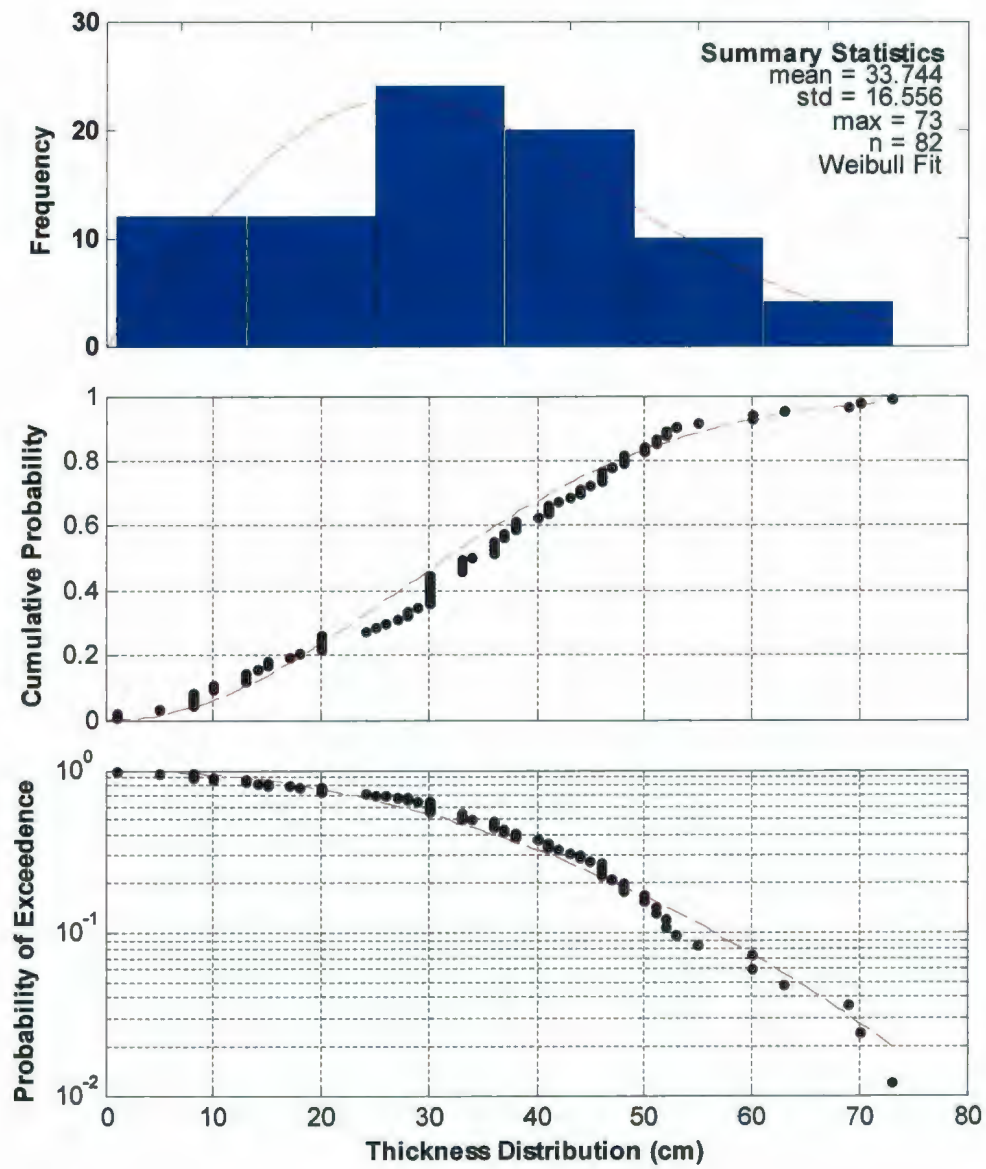


Figure 4-9 thickness distribution for data provided by the Canadian Ice Services.

4.3.3 Ice Thickness Growth

A relationship can be obtained for ice thickness growth in relation to freezing degree days. A number of empirical formulae have been developed by others using this approach. Lebedev (1938) proposed that ice thickness growth (h) can be related to freezing degree days by the following equation:

$$h = 1.33FDD^{0.58} . \quad \text{Equation 4-2}$$

LaBelle et al. (1983) proposed the equation below:

$$h = 0.01\sqrt{8FDD - 501} \quad \text{Equation 4-3}$$

Stefan's Law developed in 1891 and described in detail by Pounder (1965) addresses the ice growth problem using a heat transfer approach. For the ice sheet to freeze the latent heat which must be extracted from the sheet is considered. The rate at which this process occurs for a given time increment is determined to obtain the total amount of heat removed from the sheet of ice. It is noted however that Stefan's equation is considered to be the maximum theoretical insitu ice growth curve, given by:

$$h = 3.4FDD^{0.50} \quad \text{Equation 4-4}$$

Stefan's Law is considered to be a maximum as it assumes that the ice sheets surface temperature is the same as the air temperature, neglecting the insulating effect of snow cover.

Whilst the formulae above were developed for ice in different locations, with differing climates and snow conditions, they still provide useful insight into the ice growth analysis. For the purpose of simulation, Stefan's equation can be used as a maximum bound for simulated values.

If one plots the Canadian Ice Services (CIS) ice thickness data discussed previously with the corresponding freezing degree day value, a relationship can be obtained similar to those by Levedev (1938) and LaBelle (1983). A power curve was fit to the data set resulting in the equation $h = 1.36FDD^{0.52}$ as shown below (Figure 4-10).

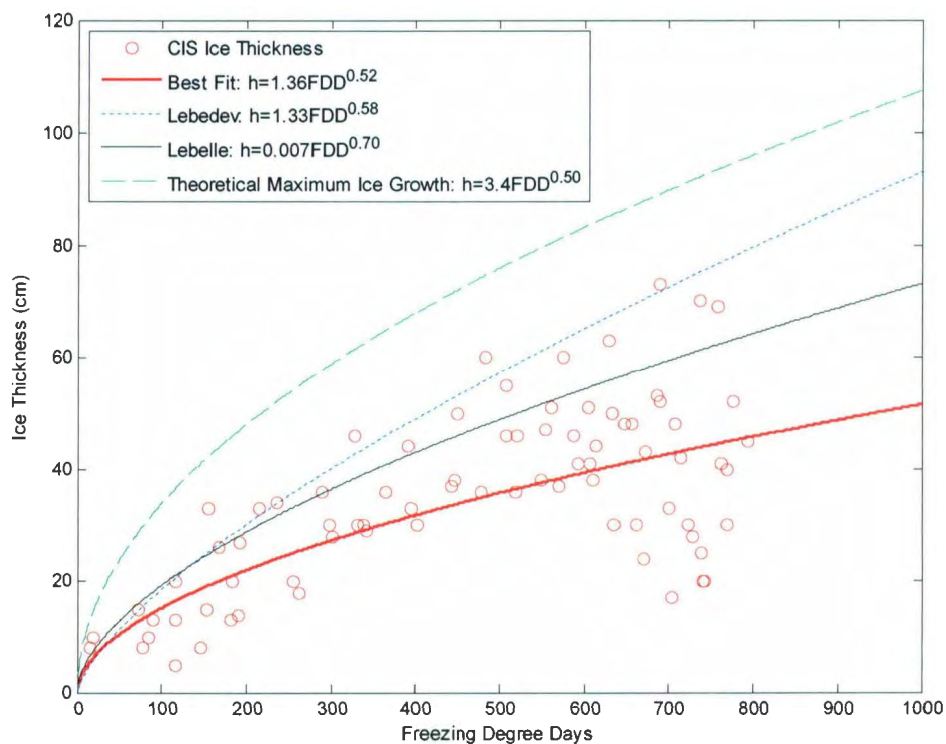


Figure 4-10 Shows the result of a power law best fit through the CIS data set in relation to the models described above.

In order to simulate the ice thickness for an ice floe, the equation $h = 1.36FDD^{0.52}$ may be used along with a random component determined based on the residuals of the best fit curve. The residuals of the data and the best fit curve are obtained and the histogram below shows that they fit a normal distribution (Figure 4-11). Knowing the mean and standard deviation of the residuals which are normally distributed, a random number can be sampled from this distribution. Adding this random normally distributed number to the ice thickness predicted by the best fit curve allows one to simulate a random ice thickness based on the CIS sample data set.

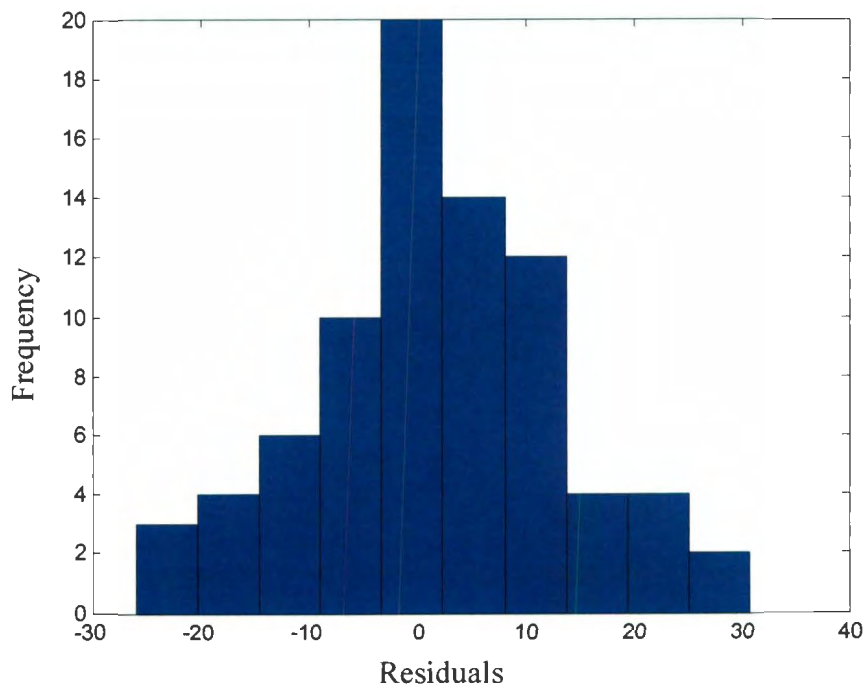


Figure 4-11 Histogram showing the residuals for the ice growth curve shown above is normally distributed.

Figure 4-12 below shows a sample result of 2000 simulated ice thicknesses based on 2000 freezing degree day values sampled randomly from a uniform distribution between 0 and 1000. If the simulation yields values which exceed Stefan's maximum theoretical ice growth curve $h = 3.4FDD^{0.50}$, then they are resampled.

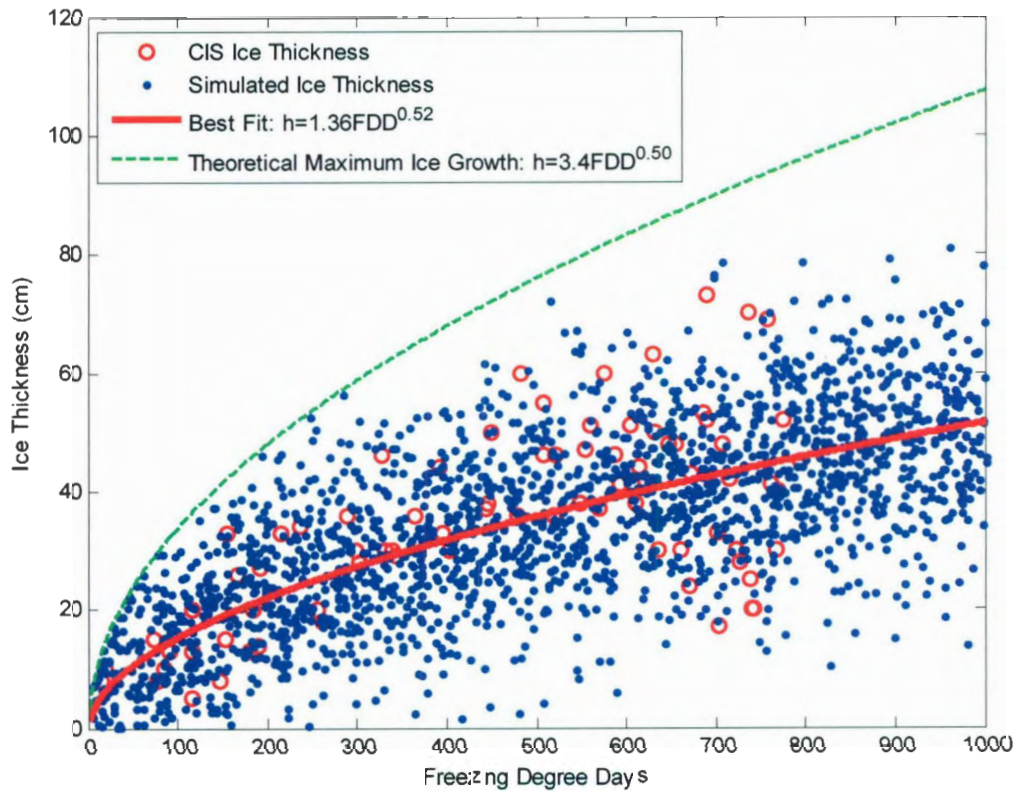


Figure 4-12 The result of 2000 simulated ice thickness values based on a distribution of freezing degree days. The ice thickness values are based on the curve $h = 1.36FDD^{0.52}$.

4.3.4 Season Length

Season length data was obtained from an ice break up model developed by Bercha and Associates (Bercha et al, 1991). The ice break up model was developed as part of the Northumberland Strait Bridge Crossing Project. The season length data was reported with a date of last ice observed for 36 seasons between 1943 and 1990, along with its Julian date (Table 4-1).

Date Last Ice	Julian Date	Date Last Ice	Julian Date
20-Apr-43	110	2-May-73	122
15-Apr-44	106	17-Apr-74	107
8-Apr-45	98	25-Apr-75	115
23-Apr-46	113	9-Apr-76	100
20-Apr-47	110	21-Apr-77	111
17-Apr-49	107	20-Apr-78	110
3-May-50	123	24-Apr-79	114
26-Apr-51	116	20-Apr-80	111
5-May-52	126	24-Mar-81	83
28-Apr-53	118	15-Apr-82	105
5-Apr-54	95	3-May-83	123
10-Apr-55	100	27-May-84	148
20-Apr-56	111	17-Apr-85	107
25-Apr-57	115	23-Apr-86	113
21-Apr-69	111	13-May-87	133
13-Apr-70	103	24-Apr-88	115
11-Apr-71	101	24-Apr-89	114
24-May-72	145	15-Apr-90	105

Table 4-1 Table displaying the date of when the last ice was observed in the Northumberland Strait along with its Julian date.

The report defines the date of last ice based on when less than 1/10 ice concentration is observed throughout the strait. For the purpose of this study, the Julian Date associated with the date of last ice is taken to be the ice season length.

It is noted that these last ice dates will likely be conservative since the bridge is located approximately midway in the Strait whilst the current moves the ice predominantly in a south-east direction, clearing finally on the east side. Thus the bridge location will likely be free of ice earlier than the strait as a whole. Nevertheless the values displayed above provide a good estimate of the season length in the Northumberland Strait.

Matching the last ice date with its associated freezing degree day value from historical Environment Canada data, one can plot the freezing degree day value with its associated Julian date or season length, obtaining the figure below (Figure 4-13). Although the data are somewhat limited, a power law can be used to represent the season length as a function of freezing degree days. The season length expression developed is given by the equation below:

$$\text{Season Length} = 4.5 FDD^{0.50} \qquad \text{Equation 4-5}$$

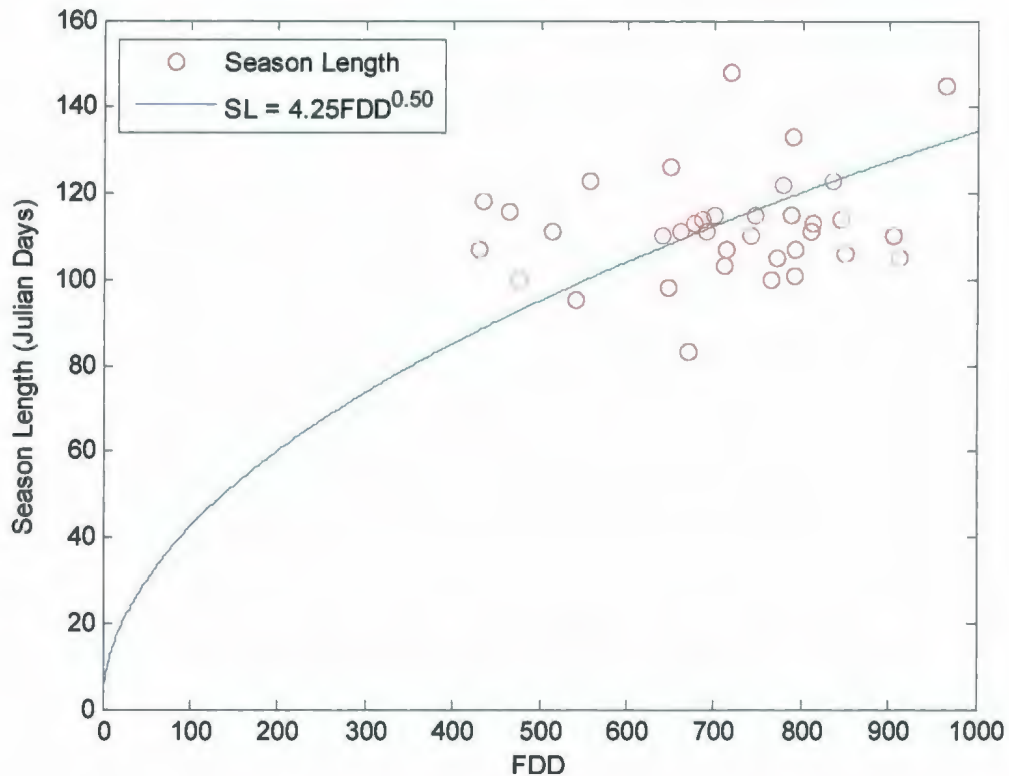


Figure 4-13 Season Length vs. FDD from ice clearing data obtained from the Northumberland Strait Bridge Crossing Project. A power law has been used to represent the data given by the equation: $Season\ Length = 4.25\ FDD^{0.50}$.

4.3.5 Ice Floe Size

Two different data sets were used and combined in order to obtain the floe size distribution for the Northumberland Strait. One set of data was obtained from a series of oblique aerial photographs taken in March and April of 1964 and 1965. The second data set was obtained from aerial sampling of digital X-band synthetic aperture radar (SAR) imagery on February 19th and 20th, 1988. Both of these data sets were developed by

Bercha and Associates (Bercha et al., 1988a and 1988b). The distributions for both sets of data are shown below (Figure 4-14 to Figure 4-16).

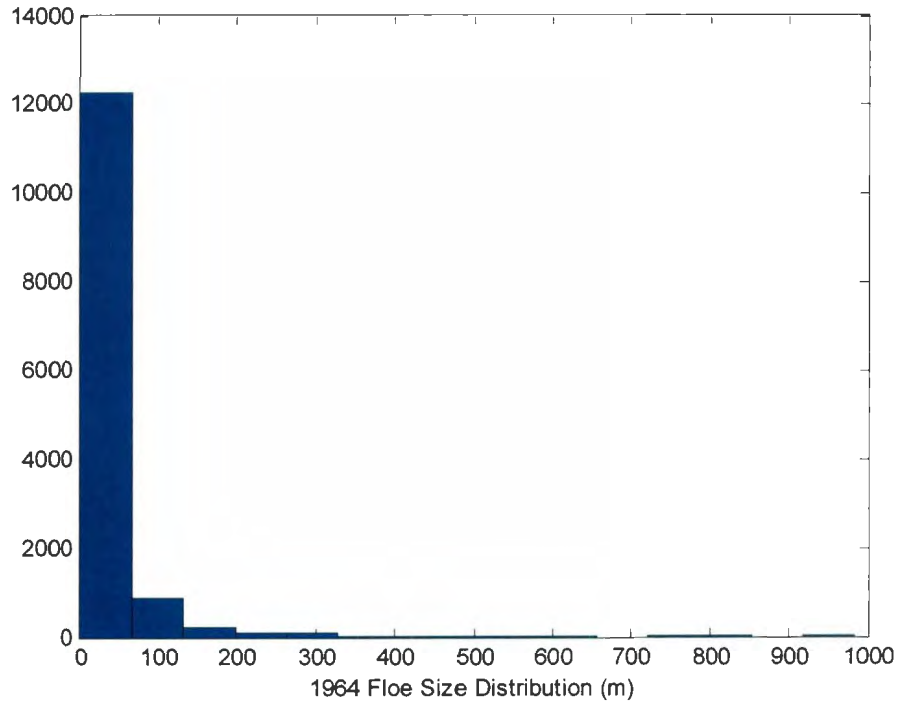


Figure 4-14 Floe size distribution for the 1963-64 ice season – obtained from aerial photographs.

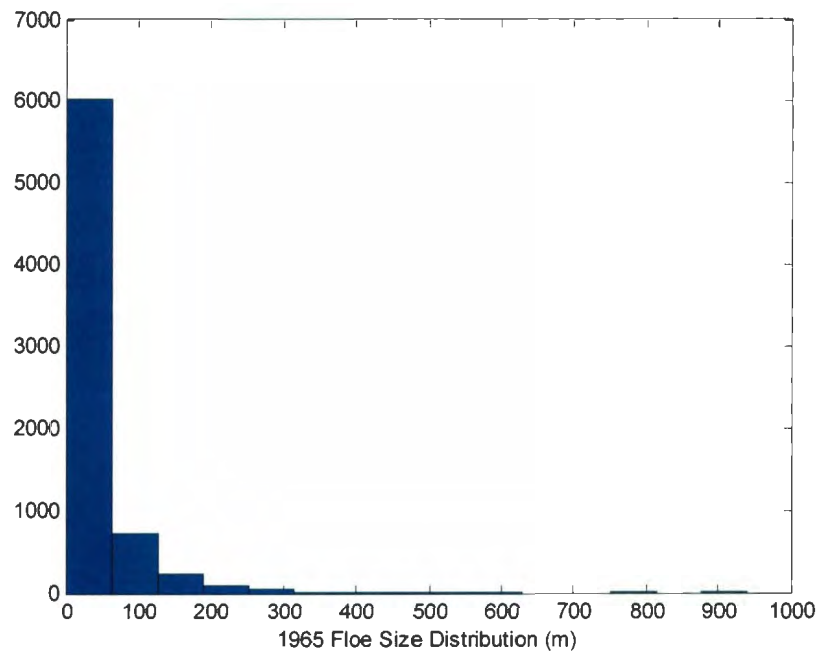


Figure 4-15 Floe size distribution for the 1964-65 ice season – obtained from aerial photographs.

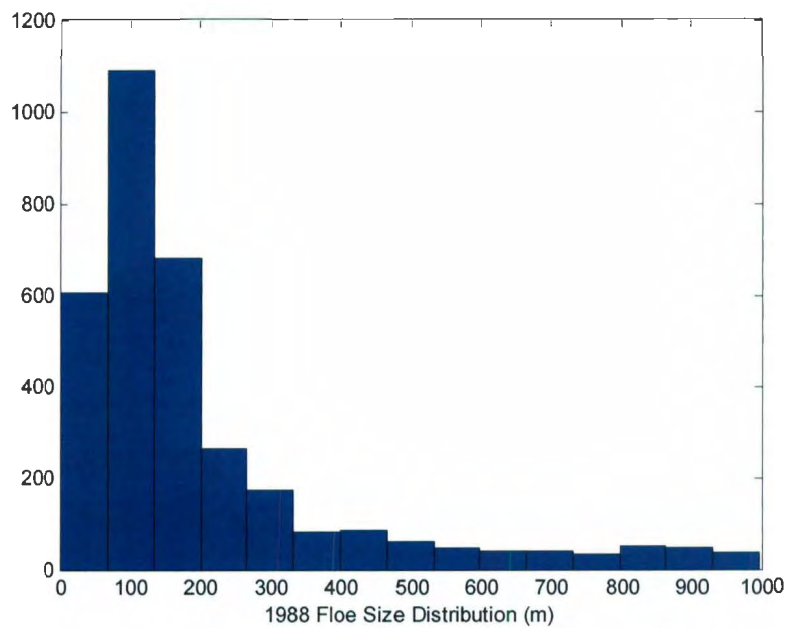


Figure 4-16 Floe size distribution from the 1987-88 ice season – obtained from aerial sampling of digital X-band SAR imagery.

The data sets from the 1964-65 and 1965-66 ice seasons show a large quantity of floes in the 0-50m diameter range, whilst the data set from the 1987-88 ice season shows a larger quantity of floes greater than 100m in diameter. This could be the result of limited resolution of the SAR imagery (Bercha et al, 1988b). It is noted however that other reports of floe properties (Williams et al, 1993) have reported a large concentration of floes with diameters greater than 100m. By combining all three years of data, a reasonable distribution of floes sizes is thought to have been obtained as shown in the figure below (Figure 4-17).

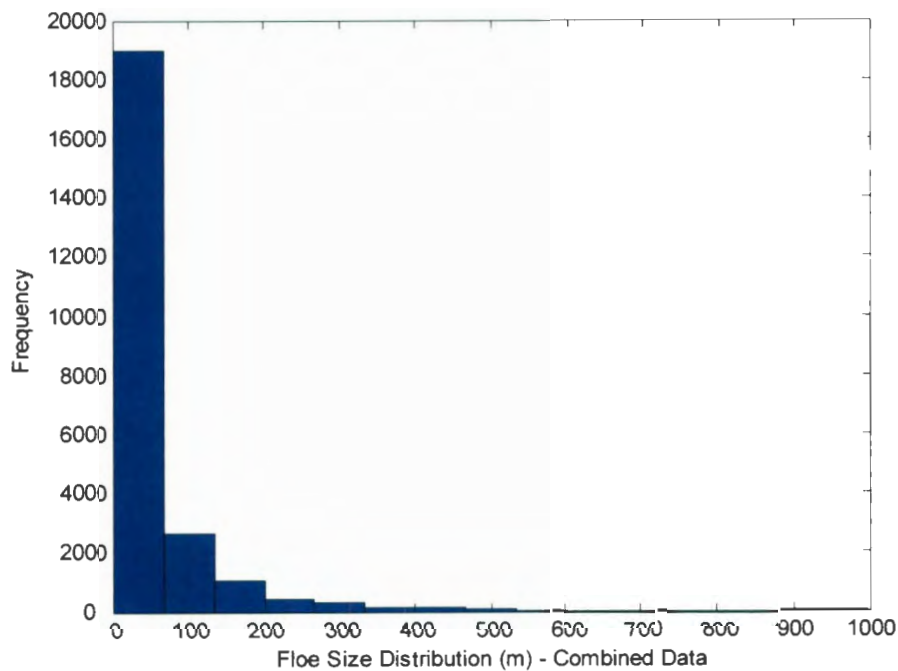


Figure 4-17 Floe size: distribution obtained by combining all floe size data.

4.3.6 Number of Ice Floes per Year

If one takes the average total annual amount of ice seen by the bridge as 3000km (Kubat and Frederking, 2001), then the floe size distribution data from 1964, 1965 and 1988 can be used to simulate the number of ice floes per year. For each year simulated the number of floes per year required to meet the 3000km average ice seen by the structure is determined, where the floe size for each floe is sampled from the floe size distribution discussed in Section 4.3.5. This process is repeated for a set number of years. Here, 2000 simulated ice seasons were considered to be adequate to determine the mean of 54000 floes per year with a standard deviation of 4600 floes per year. The number of floes per year was found to be normally distributed (Figure 4-18).

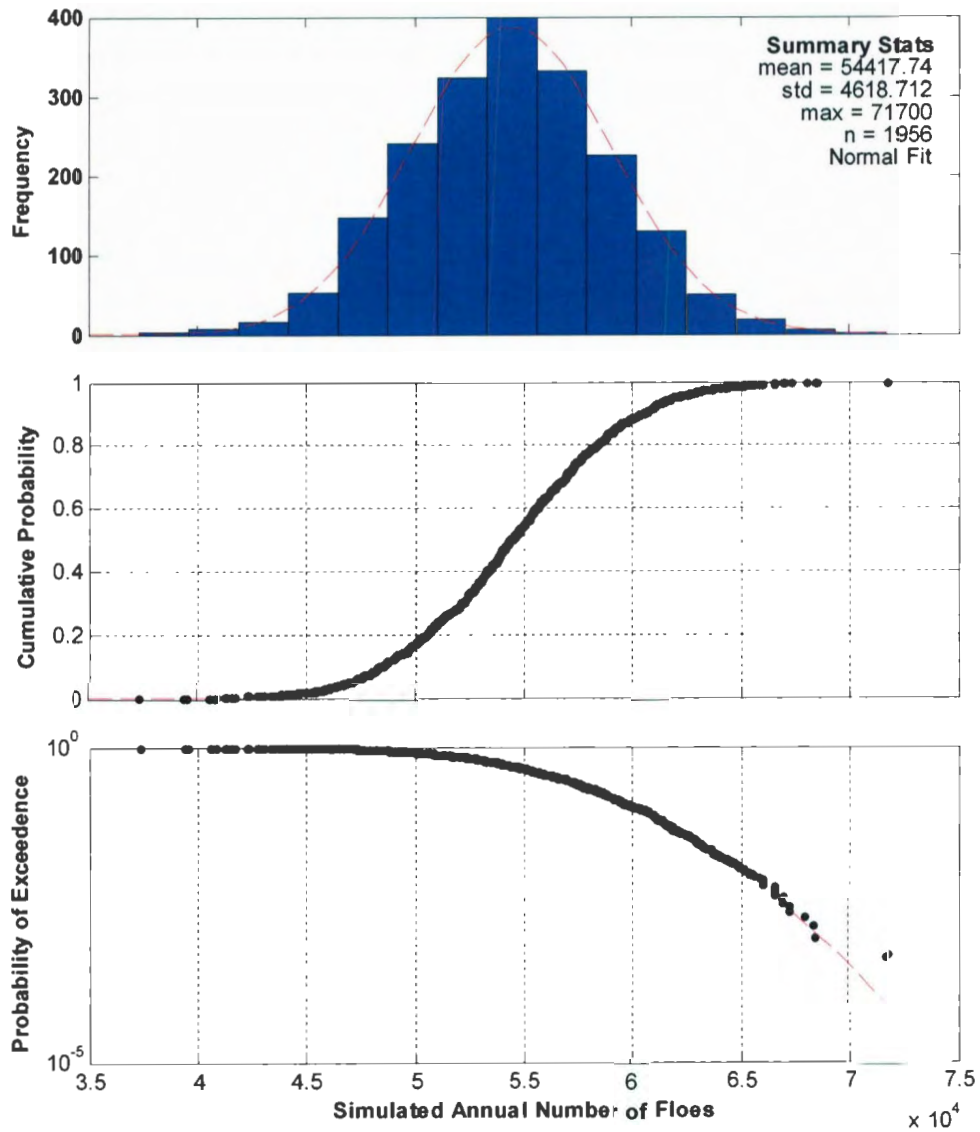


Figure 4-18 Simulated annual number of floes interacting with a bridge pier in the Northumberland Strait, fit with a normal distribution.

If a critical floe size is defined such that one is concerned only with floes that have a diameter greater than or equal to the diameter of a Confederation Bridge Pier (14m at waterline), then the number of critical floes per year is substantially less than the number of floes per year. If one considers the cumulative distribution function for the combined flow size data set (Figure 4-19), one can see that approximately 51% of the floes are less than the critical floe size.

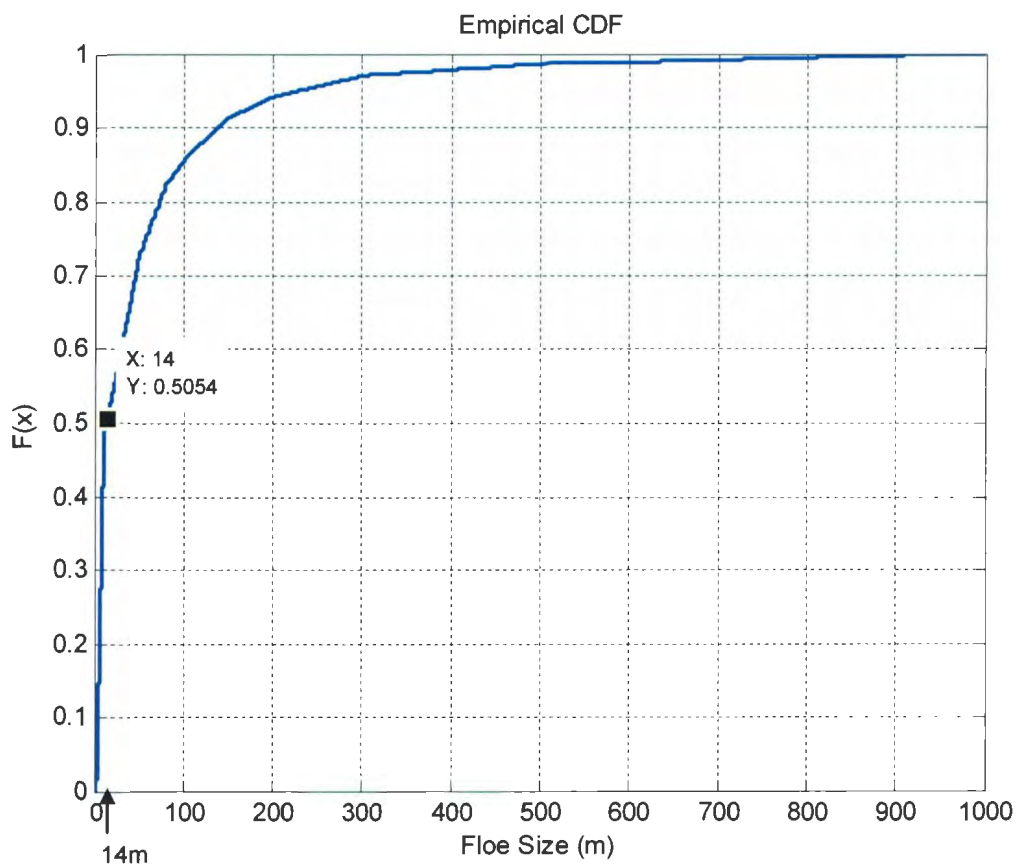


Figure 4-19 Cumulative distribution function showing the proportion of floes with a floe size less than the critical floe size (14m).

Imposing this reduction in the number of floes per year discussed above, the mean number of critical floes per year is reduced to 26600 floes per year, with a standard deviation of 2200 floes per year. A sample of this new distribution of critical floes per year is shown below (Figure 4-20).

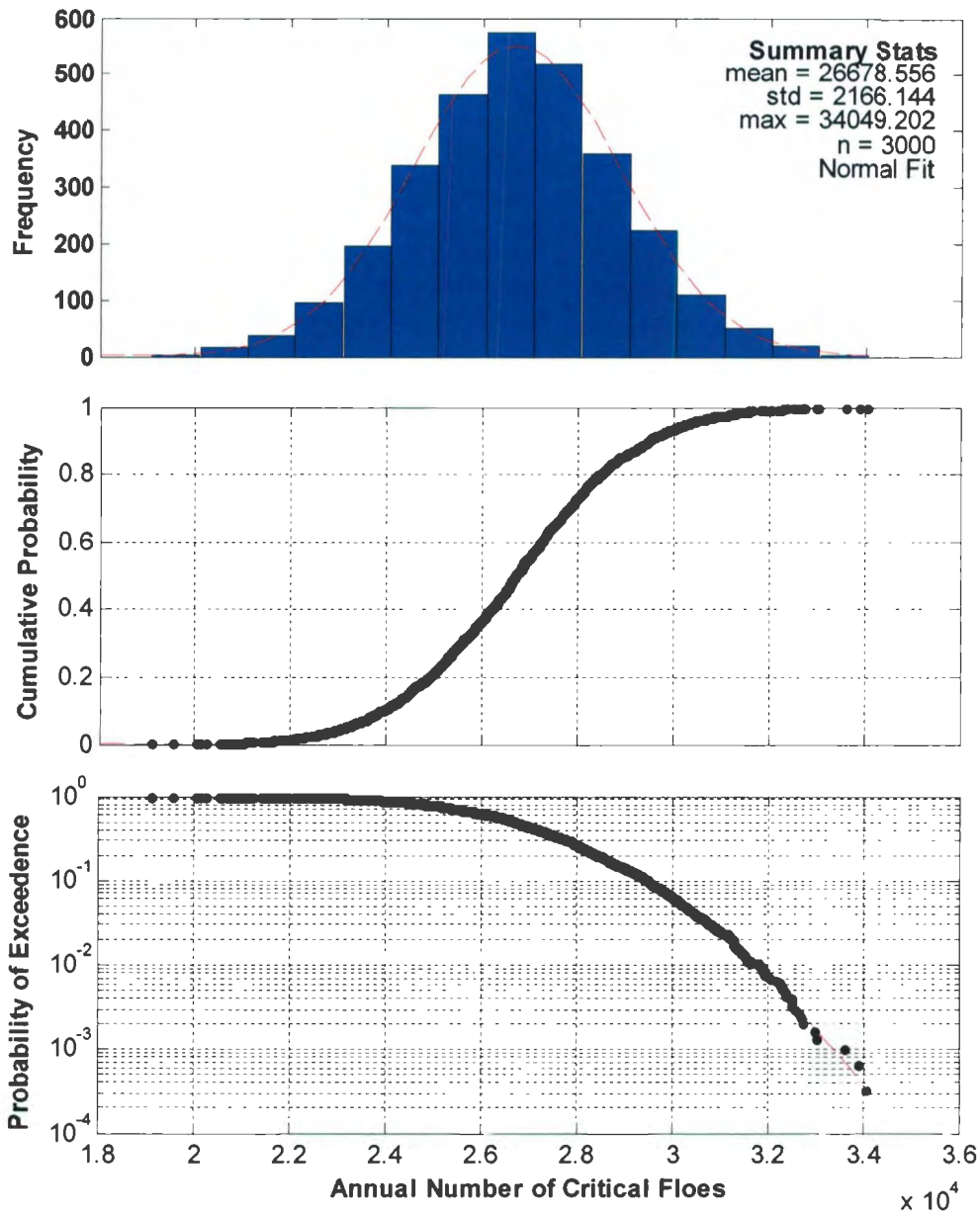


Figure 4-20 The annual number of critical floes per year resulting from considering only floes greater than or equal to the diameter of the confederation bridge piers (14m).

4.3.7 Ice Velocity

Jordaan (1983) determined that the resulting distribution of the size and velocity of impacting ice floes on structures was different than the input distributions describing all ice features in a given area. This result is due to the fact that floes with zero velocity cannot impact the structure and further to this fewer ice structure collisions occur when ice is moving slowly, compared to faster moving ice. This results in a skewing of the colliding ice feature velocities towards the faster moving ice. This result can be accounted for in the model by using Bayesian inference and is generally referred to as Bayesian Updating since the general ice velocity population is updated to include this effect.

It should be noted that Bayesian Updating was not incorporated in this work. This is due to the fact that the Croasdale model which is being used to determine the ice forces acting on the structure does not consider the velocity of the floe. Further to this, Brown and Mayne (2000) have shown that the velocity of the floe has little effect on the formation of rubble on the structure and thus the peak loads acting on the structure. It is briefly described below however for the interest of the reader after Jordaan (1983).

Bayes' Theorem can be written as:

$$P(A_i|B) = \frac{P(B|A_i)P(A_i)}{\sum_{j=1}^n P(B|A_j)P(A_j)}$$

Equation 4-6

where $P(A_i|B)$ denotes the probability of event A_i conditional on the event B . The collision velocity is updated from the input velocity distribution using Bayes' Theorem. If "c" is the event of a collision, then the probability density of velocity f_v should be amended to $f_{v|c}$ using the following expression.

$$f_{v|c}(v) = \frac{vf_v(v)}{\int_{all\ v} uf_v(u) du}, \quad \text{Equation 4-7}$$

in which the term $f_{c|v}$ in the numerator has been written as "v". This simply states that the probability of collision given velocity "v" is proportional to "v".

4.3.8 Rubble Height

Mayne and Brown (2000) reported rubble height data obtained for level ice interaction with the Confederation Bridge from the first two years of the Confederation Bridge Monitoring Project. The figure below (Figure 4-21) shows the observed rubble heights for the reported level ice thickness during the event.

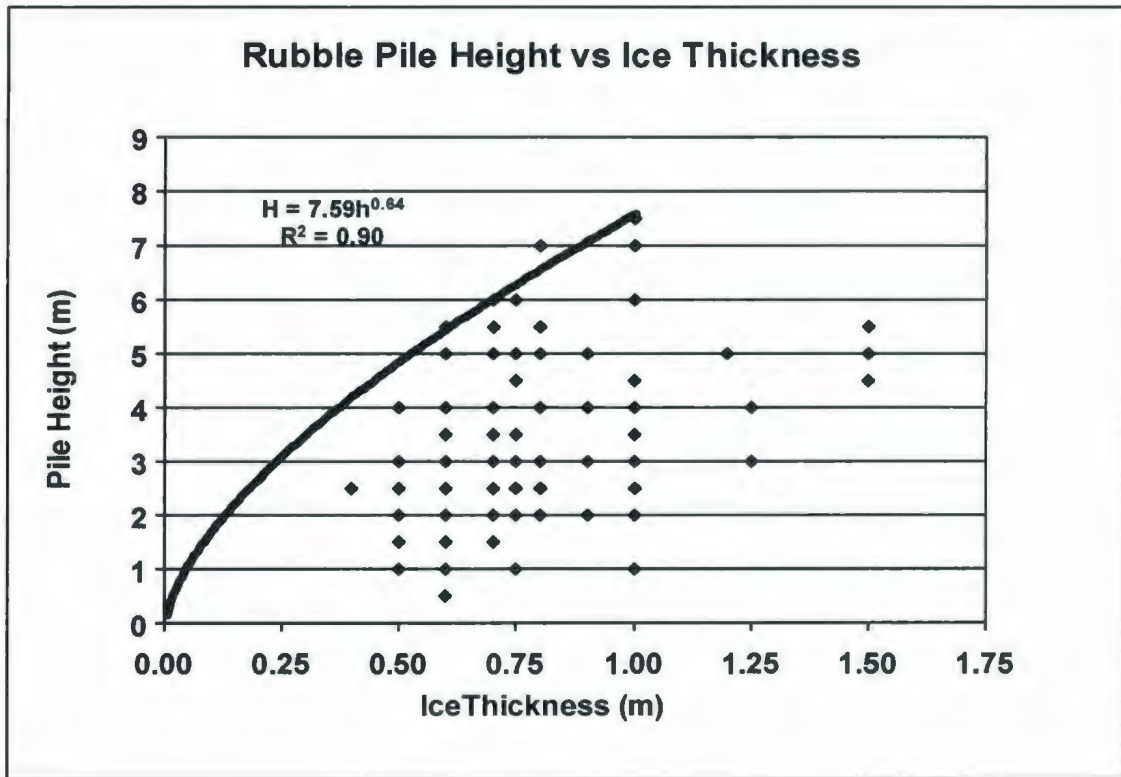


Figure 4-21 Level ice thickness effect on the rubble pile height (Mayne and Brown, 2000)

Mayne and Brown (2000) developed an upper bound equation for the observed rubble height as a function of level ice thickness. This equation was achieved by applying a regression analysis to the peak rubble heights only. The equation obtained is given below:

$$h_R = 7.59h^{0.64} \qquad \text{Equation 4-8}$$

This equation represents an upper bound for the data set obtained.

Using the data set above, one can develop a rubble model to be used for probabilistic analysis. The equation $h_R = 7.59h^{0.64}$ is used to obtain the ratio between the observed rubble height and the upper limit rubble height predicted by Equation 4-6 above for a given ice thickness. Figure 4-22 shows that this ratio fits a Weibull distribution well.

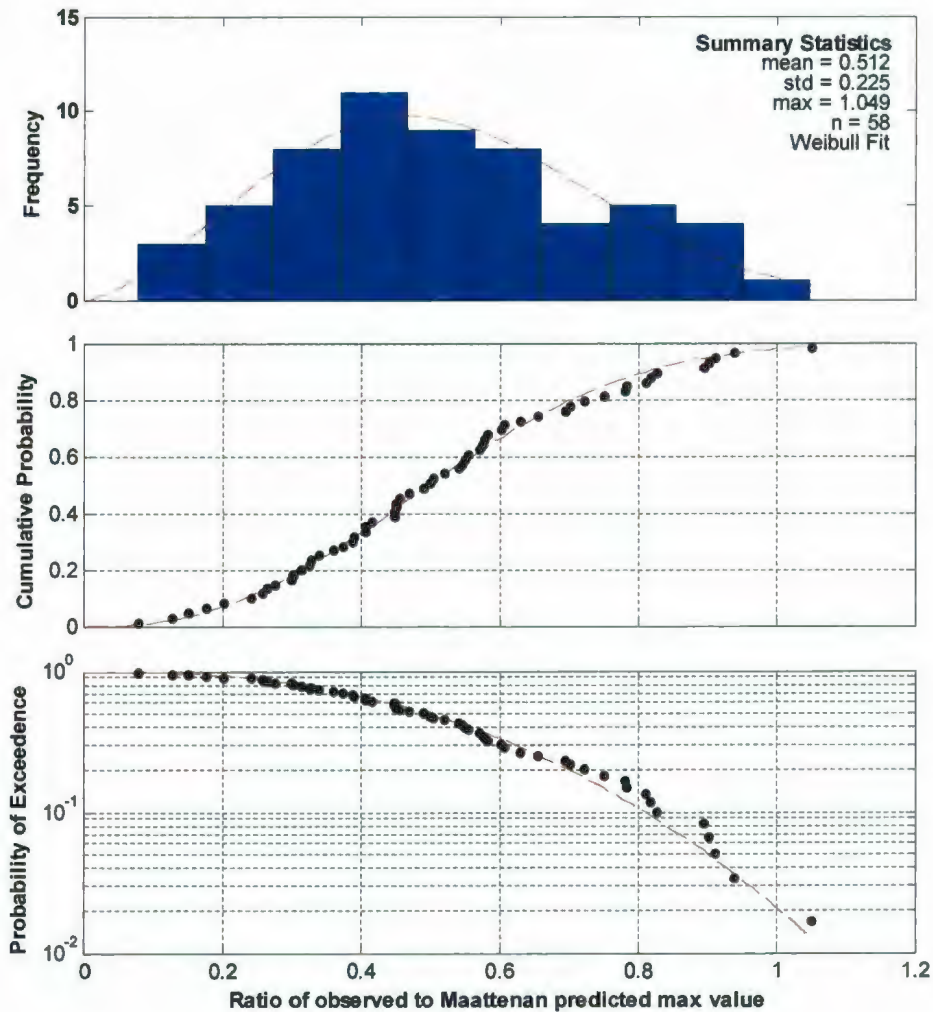


Figure 4-22 A Weibull distribution is fit to the ratio of the observed rubble height to the upper limit rubble height predicted by the curve $h_R = 7.59h^{0.64}$ for a given ice thickness.

In order to generate a rubble height for each sample in a given floe, a random sample from this Weibull distribution is taken and multiplied by the upper bound equation, allowing one to simulate the rubble height.

Figure 4-23 below shows a sample result of 1000 simulated rubble heights based on 1000 ice thickness values sampled randomly from a uniform distribution between 0 and 1.5m. This method will predict several rubble height values in excess of the upper bound curve. This is acceptable as the upper bound curve is intended to be the expected maximum curve not the absolute maximum curve.

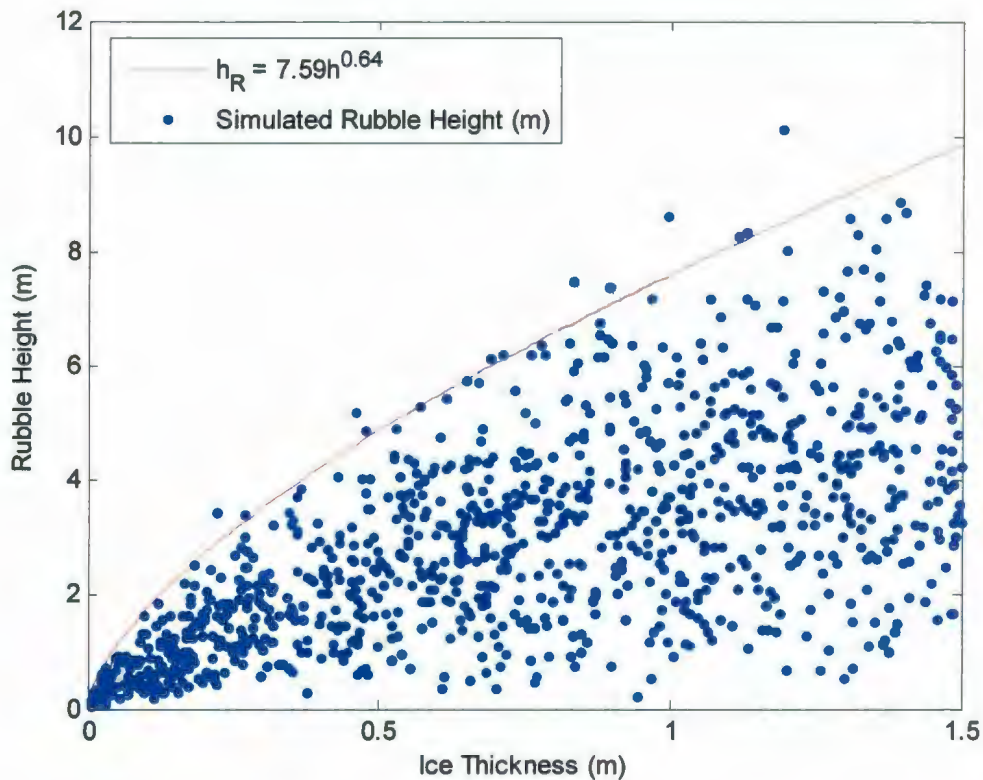


Figure 4-23 Sample results from the rubble model discussed above. Results are obtained by using 1000 randomly sampled ice thickness values from a uniform distribution between 0 and 1.5m.

4.3.9 Rubble Pile Angle

During ice-structure interaction with sloping or conical structures, the angle of the rubble pile resting on the slope of the structure has a significant effect on the horizontal and vertical components of the load seen by the structure. By decreasing the angle of the rubble pile whilst maintaining the same rubble height, the increase in load occurs from

the increased volume of ice over the structure. The figure below (Figure 4-24) shows the effect of the rubble angle in the deterministic solution for ice loads using the Croasdale model, whilst keeping all other variables constant.

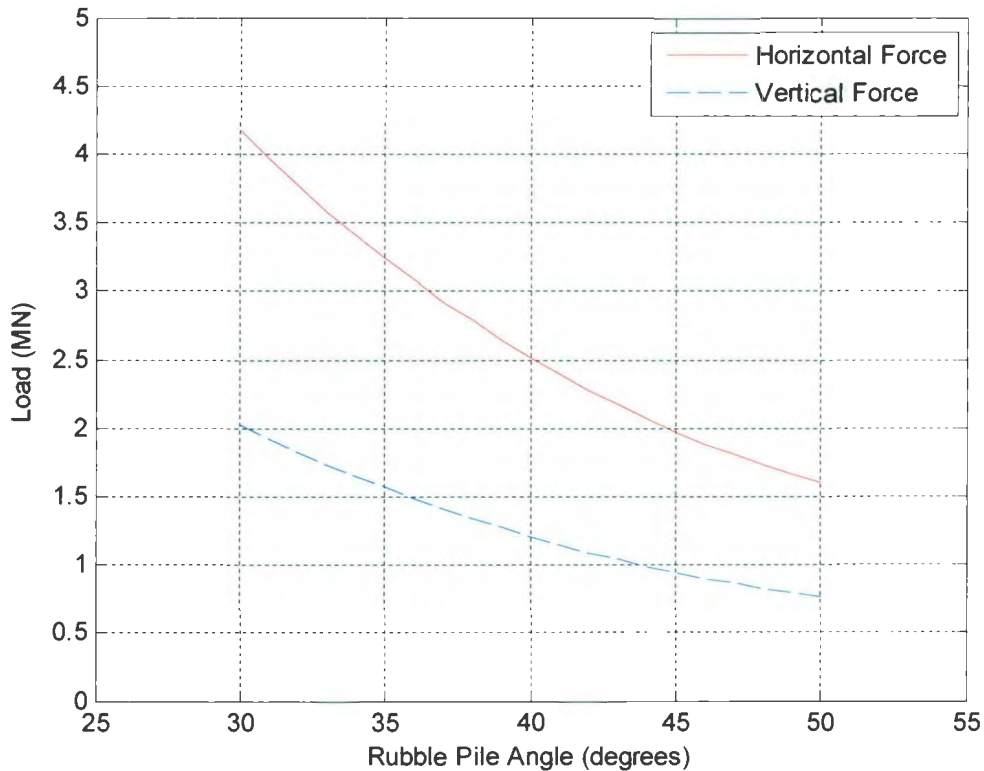


Figure 4-24 The effect of varying the ice rubble pile angle acting on a conical structure as predicted by the Croasdale model.

Cammaert et al. (1993) reported that observations on the 56° Kemi-I structure by Määttänen showed that the slope of the rubble pile varied from 30° to 50° with the majority of rubble pile angles observed between 40° and 45°. As the slope of the Confederation Bridge is 52° one would expect this range to be slightly lower, perhaps 37-42°. This information lends itself to being modeled as a normal distribution with a mean

of 40.0° and a standard deviation of 4° . It should be noted that the Croasdale model requires that the angle of the rubble pile be less than the slope of the conical structure (52° for the case of the Confederation Bridge). The result is the sample distribution shown below (Figure 4-25).

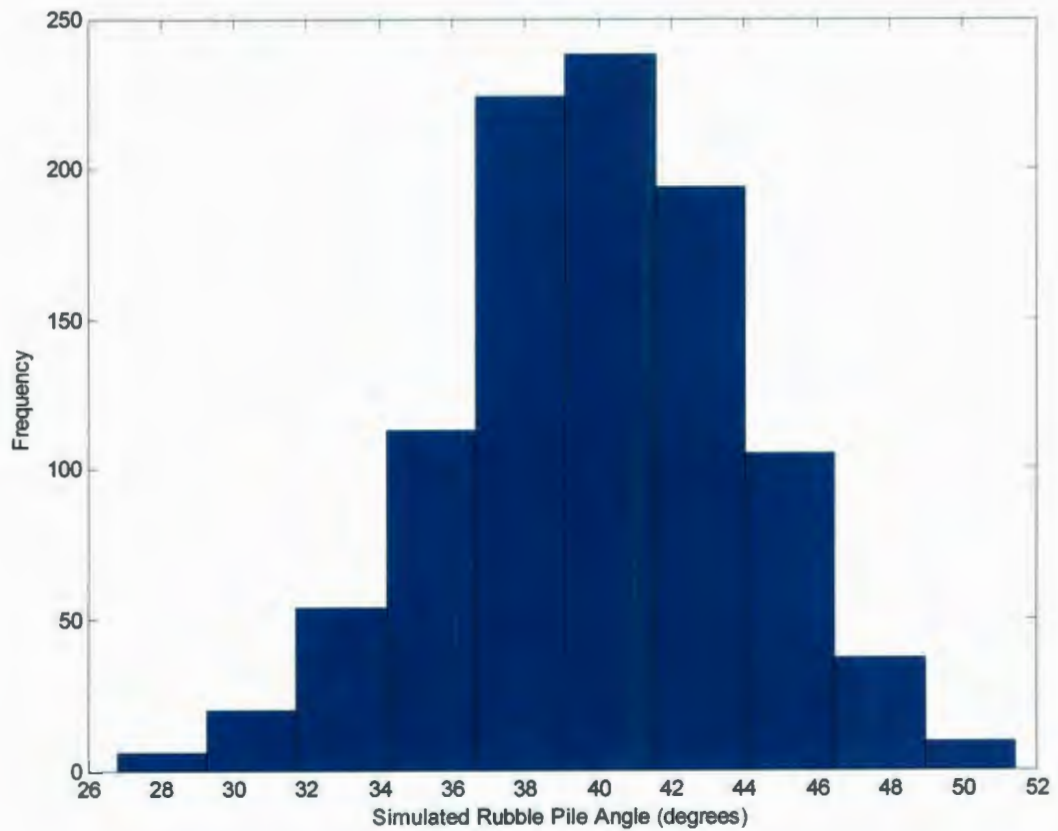


Figure 4-25 Simulated rubble pile angle using a mean of 40° and a standard deviation of 4° . The simulated rubble angles are limited such that they do not exceed 52° .

4.3.10 Friction

During ice-structure interaction with sloping or conical structures, the ice-structure dynamic friction coefficient of the slope has a significant effect on the horizontal component of the load seen by the structure. The figure below (Figure 4-26) shows the effect of increasing the friction coefficient in the deterministic solution for horizontal load using the Croasdale model, whilst keeping all other variables constant.

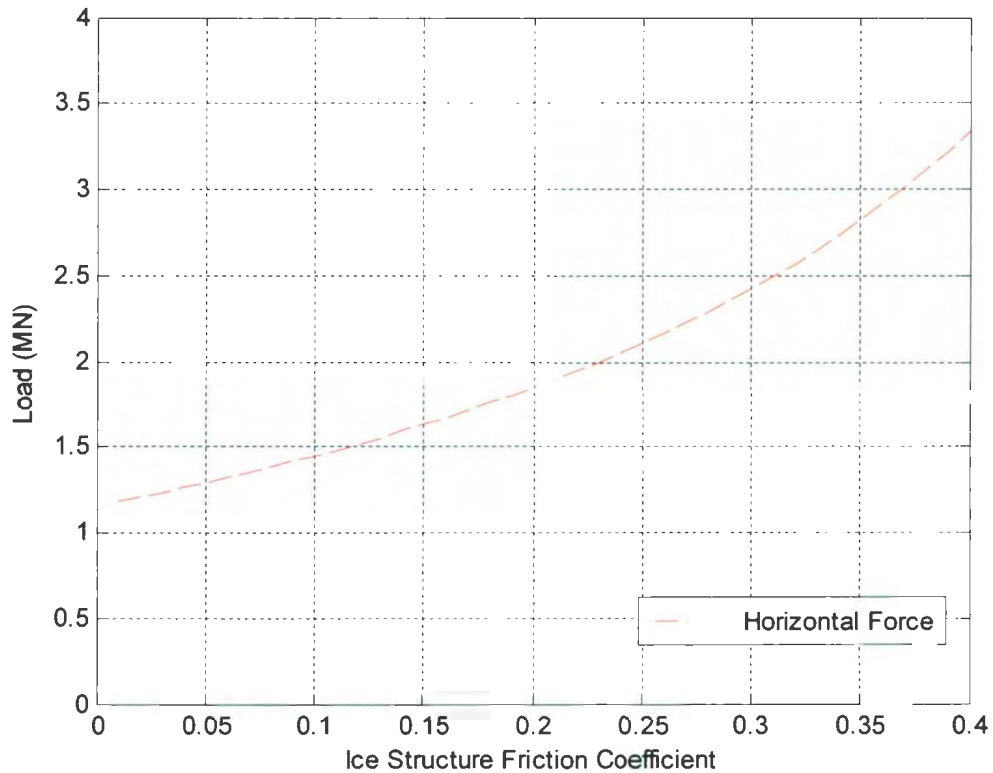


Figure 4-26 The effect of varying the dynamic friction coefficient, between sea ice and a conical structure, on the horizontal load predicted by the Croasdale model.

Studies by Forland and Tatinclaux (1985), and Terashima and Takashi (1997) report surface roughness as the most critical factor affecting the dynamic friction coefficient. Both report dynamic friction coefficients in the range of 0.01 to 0.25 for relatively smooth concrete. It is noted by Forland and Tatinclaux (1985) that abrasion of the concrete surface over time due to ice structure interaction will lead to an increased surface roughness, increasing the coefficient of friction.

To model the dynamic friction coefficient probabilistically, for the purpose of this study, a normal distribution is suggested with a mean of 0.15 and a standard deviation of 0.10, limited such that values outside the range 0.01 – 0.30 are resampled. A sample distribution to this effect is shown below (Figure 4-27).

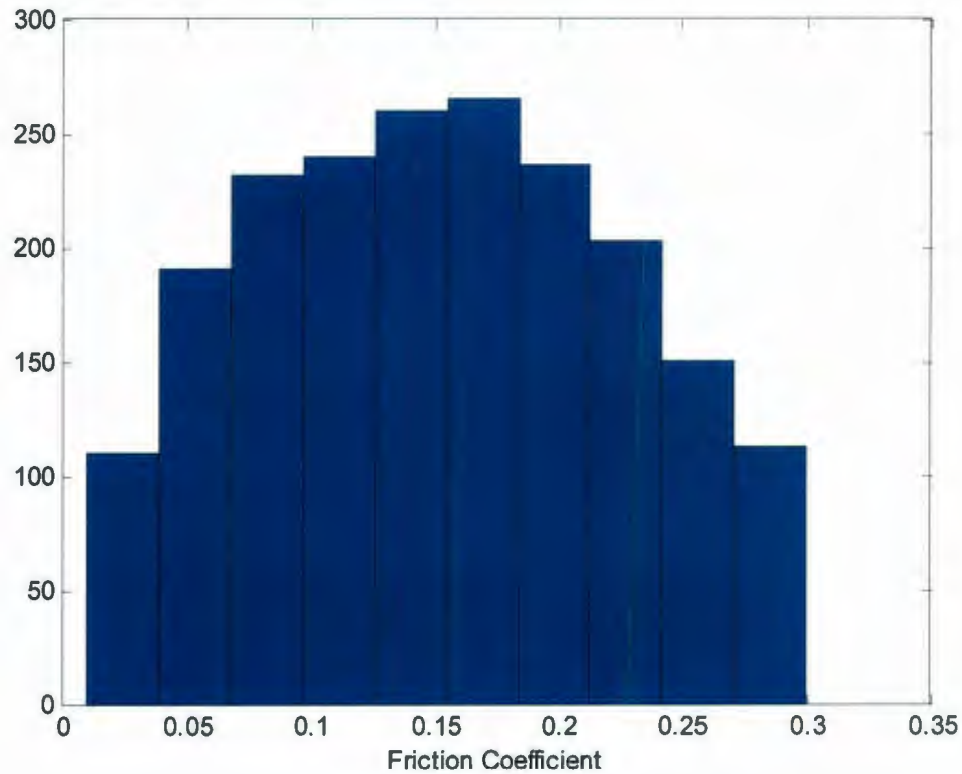


Figure 4-27 Simulated dynamic ice-structure friction coefficient between sea ice and concrete.

4.3.11 Flexural Strength

As was discussed in detail in Chapter 3, the flexural strength of ice is largely dependent on the brine volume as well as the scale of the interaction. It was determined that the expression developed by Williams and Parsons (1994) for flexural strength as a function of brine volume and ice volume is likely to be the most accurate for full scale interactions.

Taking the salinity of ice in the Northumberland Strait to be approximately 2ppt with a mean ice temperature of -2.5°C the flexural strength can be determined. In this work a normal distribution for flexural strength is used with a mean flexural strength of 0.250MPa with a standard deviation of 0.18MPa.

4.4 Simulation Process

In this section, a description of the simulation process is provided in point form. The program begins by having the user specify the total number of years to be simulated. The total number of years to be simulated (n) is typically over 3000 to provide more confidence in extrapolating the fits to higher order exceedance probabilities. The process below is conducted for each year.

1. For the period of December through April, the total freezing degree days for each month is simulated based on the gamma probability distribution described in Section 4.3.1.
2. The length of the ice season is determined based on the relationship derived in Section 4.3.4 whereby, $SeasonLength = 4.25 FDD^{0.5}$.
3. The number of floes per year is simulated based on the normal distribution fit to the data set discussed in Section 4.3.6.

4. The size of each floe is determined by first sorting and ranking the critical floe size data which was described in Section 4.3.5. Next a random number is sampled from a uniform distribution between 0 and 1 which will act as the simulated rank. Based on the random number generated, linear interpolation is used to get the floe size associated with the simulated rank.
5. For each floe, a random uniform discrete number is sampled between 1 and the simulated season length. This assigns each floe randomly to a day within the ice season. Linear interpolation is used to assign a corresponding freezing degree day value to each floe based on its position in the season.
6. The ice thickness of each floe is determined based on the freezing degree day value assigned to each floe. Thickness (h) of each floe is derived based on the equation developed in Section 4.3.3 whereby, $h = 1.36FDD^{0.52}$. The residual was found to be normally distributed with a mean of 0 and a standard deviation of 11.5. In order to simulate the variation about the curve, a random number is sampled from a normal distribution with a mean of 0 and a standard deviation of 1 which is then multiplied by the standard deviation of the residual and added to the thickness value determined by the thickness equation above.

7. A sampling interval is determined based on the radial distance from the structure to the first circumferential crack. Croasdale (1994) derives this equation as
$$First\ Crack = \frac{\pi}{4} Characteristic\ Length .$$
 For each interval of each floe, a number of parameters are sampled. Rubble height is sampled based on the model described in Section 4.3.7. The angle of the rubble pile angle is sampled from a normal distribution with a mean of 40° and a standard deviation of 4° . The flexural strength of the ice is sampled from a normal distribution with a mean of 0.25 MPa with a standard deviation of 0.18 MPa. The ice-structure friction coefficient is sampled from a normal distribution with a mean of 0.15 and a standard deviation of 0.10, limited to the range of 0.01-0.30.
8. For each interval of each floe, the horizontal load and vertical load is calculated using the Croasdale model. The maximum horizontal load for each floe is stored.
9. The annual maximum horizontal load is determined for each year. In addition to this load, the contributing ice thickness, freezing degree day, rubble height, season length and vertical force is stored.
10. An exceedance probability plot is used to show the maximum annual horizontal loads for n years of simulations. From this the 100 year and 10,000 year design loads are typically obtained.

Using the pier geometry described in Section 4.2 and the simulation methodology described in Section 4.4, the results of the probabilistic model are developed. As mentioned previously, the primary objective is to determine the 100 year and 10,000 year design loads. In addition to this objective, it is important to consider the factors that contributed to the maximum annual ice loads. These factors are those such as the rubble height, rubble pile angle, ice thickness, ice structure friction coefficient, and freezing degree day value. These factors serve as a reality check to ensure that the extreme values are realistic, meaning that there are no records of values in excess of these extreme values, or that there are no physical limits which would cause an extreme value to be impossibly high. These factors are also important for design as they may indicate potential areas that can be improved upon to reduce loads. For example, during the design phase of the Confederation Bridge, some consideration was given to cladding the concrete piers with stainless steel or high density plastics to reduce the friction coefficient, thus reducing the extreme ice loads. It is noted however that the construction of the concrete piers was later determined to be of superior quality and the steel cladding was not required.

An exceedance probability plot is shown below (Figure 4-28) for the maximum annual horizontal ice loads for the Confederation Bridge simulation. From Figure 4-28 it can be seen that the 100 year design load is approximately 10.7 MN whilst the 10,000 year design load is approximately 16.0 MN. A double exponential (Gumbel) probability distribution is fit to the annual maximum ice loads. When fitting a probability

distribution to extreme data it is of greatest importance to fit the '*tail*' of the probability of exceedence curve. The double exponential probability distribution provides a good fit to the data shown in Figure 4-28 below.

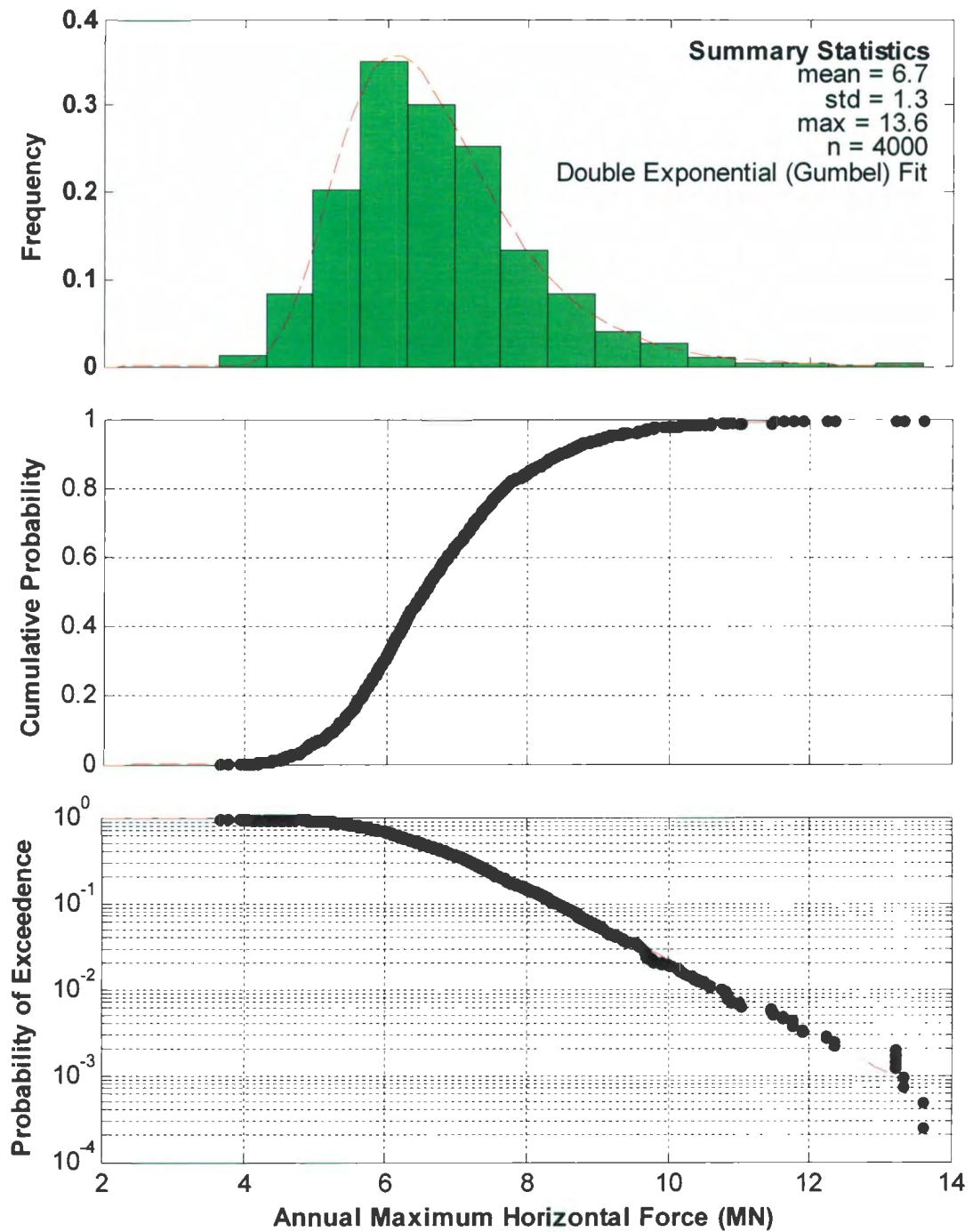


Figure 4-28 Annual maximum horizontal ice forces for level ice interaction with the Confederation Bridge.

Plots showing the contributing input variables which give rise to the maximum annual horizontal ice loads for inputs such as rubble height, rubble pile angle, ice-structure friction coefficient, and ice thickness can be seen below (Figure 4-29).

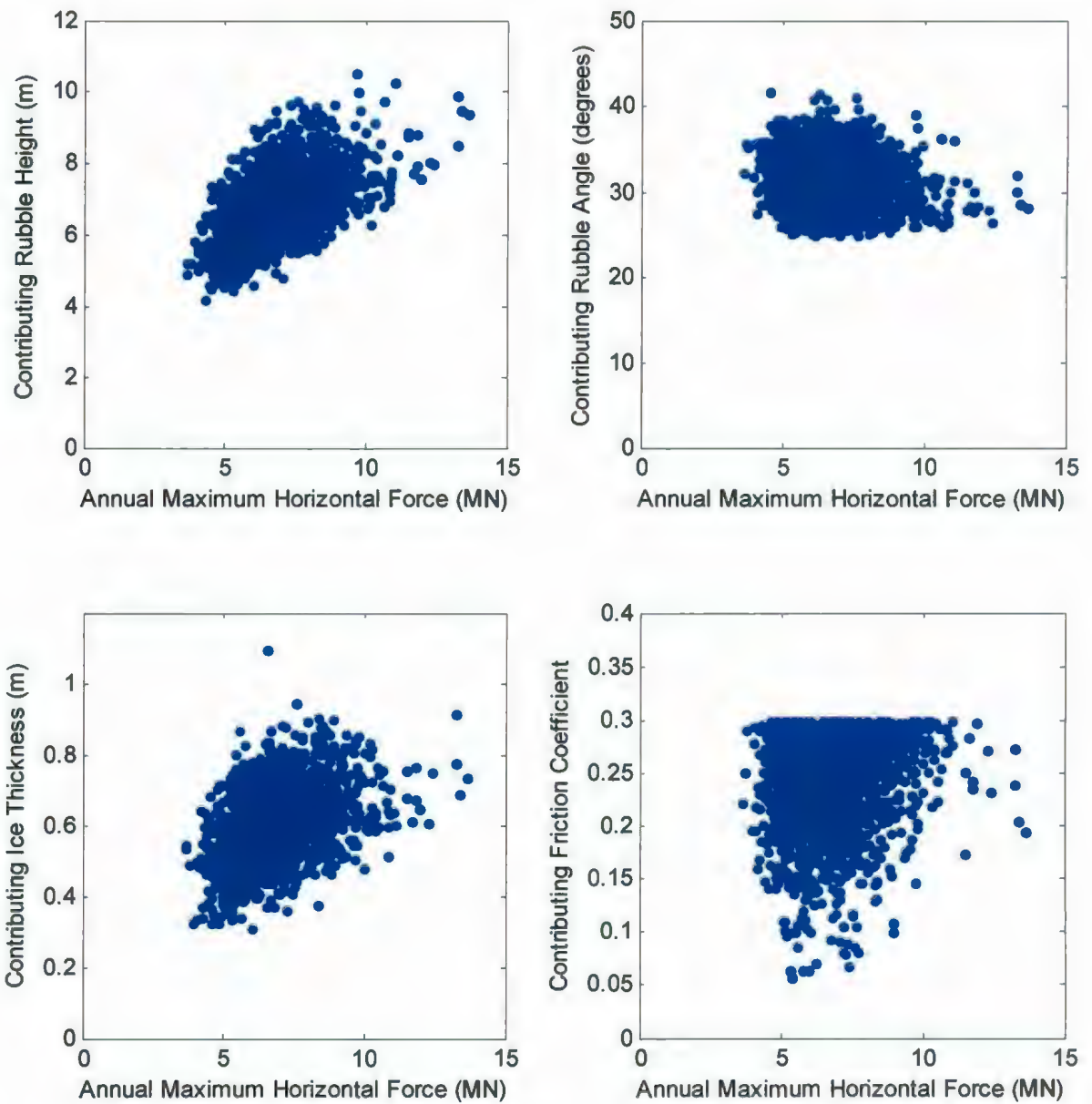


Figure 4-29 The contributing input variables which give rise to the maximum annual horizontal ice loads. (a) rubble height, (b) rubble pile angle, (c) ice thickness, and (d) ice – structure friction coefficient.

4.5 Concluding Remarks

The probabilistic model developed in Chapter 4 predicts a 100 year ice load (10^{-2} exceedance probability) of 10.7 MN and a 10,000 year (10^{-4} exceedance probability) ice load of 16.0 MN for level ice interacting with the 14 m waterline diameter conical bridge piers of the Confederation Bridge. The double exponential (Gumbel) probability distribution was fit to the simulated annual maximum horizontal ice loads and used to predict the 10,000 year ice load.

Uncertainties arise when using quantitative methods to analyze these types of problems where the input parameters and models are approximations of reality. The uncertainty in the results obtained is thus a function of the uncertainty in the input parameters as well as the functional relationship used to obtain ice loads. Model uncertainties can be improved upon by obtaining new data and developing better physical models. While it would be favorable to reduce the uncertainty in any design, it is often not financially viable to conduct field programs to gather full scale data. In addition to this, improved physical models often require a significant increase in computational effort. Accordingly, the sensitivities of any model must be studied in detail along with application of sound engineering judgment to determine a safe final design load.

5 VALIDATION OF THE PROBABILISTIC MODEL

5.1 Introduction

In Chapter 4, a probabilistic model was developed to simulate the loads produced by level ice acting on a Confederation Bridge pier in the Northumberland Strait. This was achieved by using a Monte Carlo methodology to simulate both the ice environment in the Northumberland Strait and the ice interaction with the structure. Once this had been accomplished the annual maximum ice loads could then be derived. As was discussed in Chapter 4, the uncertainty in the results obtained is a function of both the uncertainty in the input parameters as well as the functional relationship used to obtain ice loads.

When developing a probabilistic model to simulate reality, it is imperative that the input variables are represented as accurately as possible. By placing factors of safety on various input parameters, their effect is to overstate the calculated values of the 100 year or 10,000 year simulations. Any factors for safety should be applied to the calculated 100 or 10,000 year ice loads after the simulation is complete. In practice the calculated 100 year ice load for example, is typically multiplied by a factor of safety of 1.35 to account for uncertainty.

The construction of the Confederation Bridge was completed in 1997, at which time the Confederation Bridge Ice Monitoring Program began gathering full scale ice-structure interaction data. There is 10 years worth of data which exists for ice interactions with the

Confederation Bridge. It is the intention of this Chapter to compare the ice loads predicted by the probabilistic model developed in Chapter 4, with published data observed by ice load monitoring programs such as the Confederation Bridge Ice Monitoring Program.

5.2 Monitoring Ice Loads Acting on the Confederation Bridge

The Confederation Bridge Ice Monitoring Program began gathering ice load data in 1997 upon the completion of the construction of the bridge. The Confederation Bridge Ice Monitoring Program has instrumented two main bridge piers (piers P31 and P32) which are used to provide an estimate of ice loads acting on the structures. The ice force monitoring program has the capability to measure global ice forces and to observe the mechanics of ice structure interaction as well as record the prevailing ice conditions at the bridge. Initially, the ice monitoring program had the capability to measure local ice pressures however the panels have since been removed due to excessive damage caused by ice-structure interaction.

The global ice force on a bridge pier is measured by using biaxial tiltmeters which are placed at three locations in each of the instrumented bridge piers. The tiltmeters have the ability to measure tilts as low as 0.1 micro radians (μ rad), which corresponds to an ice load of approximately 3 kN (Brown, 2006). The dynamic response of the system is obtained by using accelerometers to measure the lateral acceleration. The global load

measuring capability of pier 31 of the Confederation Bridge was calibrated by applying a static loading during a full scale pull test using the CCGS Terry Fox (Figure 5-1). The data acquisition system obtains data at 0.034 second intervals but stores only the average load over 500 intervals (or 17 seconds). The exception is if a preset trigger load is exceeded, in this case all data are stored for a 170 second duration.



Figure 5-1: CCGS Terry Fox performing full scale pull test (Mayne, 2007)

The Confederation Bridge Monitoring Program is also capable of observing the ice structure interactions using four time-lapse video cameras and two sonars. Three of the cameras observe the ice failure mechanics, whilst the fourth observes the prevailing ice conditions in the Strait.

In 1999 the National Research Council – Canadian Hydraulics Centre (NRC-CHC) collaborated with the Department of Fisheries and Oceans through the Bedford Institute of Oceanography and the Public Works and Government Services of Canada to initiate an additional research program to study ice loads acting on the Confederation Bridge. This program instrumented two bridge piers (piers P23 and P24). Calibration of the tiltmeters for this project was done using wind loading during a heavy wind event during a period with no ice in the strait. Direct calibration of the tiltmeters using a method such as that used by the Confederation Bridge Monitoring Project (Figure 5-1) was not possible. For this reason the global loads calculated by the Confederation Bridge Monitoring Program might be considered more reliable; nevertheless these ice loads will also be compared with those predicted by the probabilistic model developed in Chapter 4.

5.3 Ice Observations at the Confederation Bridge

To date the Confederation Bridge Ice Monitoring Program and the National Research Council have accumulated a wealth of ice-structure interaction data. The Confederation Bridge Engineering Summit held in 2007 marked the 10 year operating anniversary of the bridge. Brown (2007) and Frederking et al. (2007) have composed reviews of the ice conditions and ice loads acting on the bridge over the last 10 years, resulting from their associated research programs. The annual maximum ice loads reported by the two research programs vary significantly. Brown (2007) reports a maximum recorded ice load throughout the 10 year measuring period of 8.6 MN whilst Frederking et al. (2007)

reports a maximum recorded ice load of 2.4 MN. A more detailed discussion of the ice loads and ice conditions observed at the Confederation Bridge follows.

Brown (2007) has analyzed the 17 second average tiltmeter data in some detail for the 10 years of operation of the Confederation Bridge Monitoring Program. The results of the annual statistics are combined such that exceedance probabilities can be determined. Figure 5-2 below shows the exceedance probabilities for annual maximum horizontal ice loads acting on pier 31 for eight years of data as measured by the tiltmeter 17 second average files. It should be noted that the actual peak load over the 17 second duration is higher than the loads reported below, however given that the annual peak loads are generally resulting from a semi stable rubble pile or ridge ride up the 17 second average load is expected to provide a reasonable estimate of the peak annual load.

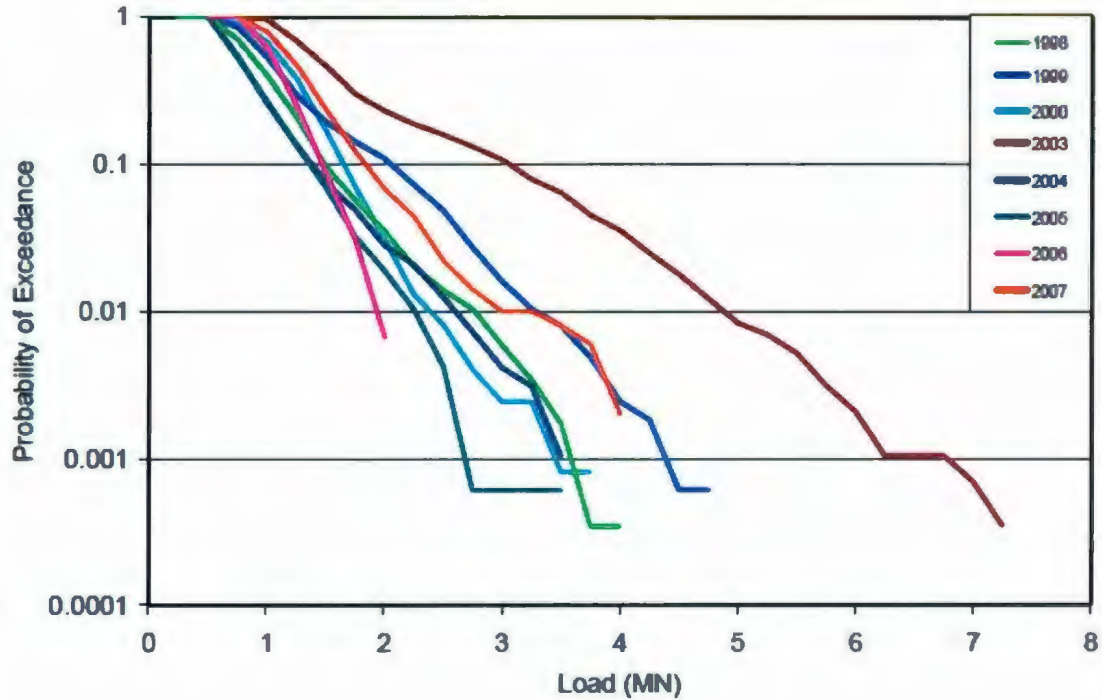


Figure 5-2: Annual maximum horizontal ice load measured by tiltmeters located on pier 31 of the Confederation Bridge using the 17 second average tilt data (Brown 2007).

Brown (2007) has analyzed the event occurring in 2003 which resulted in the largest measured load in Figure 5-2. Part of the analysis conducted by Brown involved analyzing the trigger data which contains the actual peak ice load during the 17 second duration for which the average load was obtained and plotted in Figure 5-2. The analysis of the tiltmeter trigger data requires consideration of the structural response as these devices do not measure the ice load directly. A tiltmeter measures both the static and dynamic load effects which occur during the ice interaction (and the companion wind loading), in addition to the structural response to these load effects (Brown 2006). Analysis of the trigger data for the event occurring in 2003, which resulted in the largest

measured load to date, revealed that the peak load was actually 8.6 MN rather than the 7.25 MN reported in Figure 5-2. Details of the peak loads occurring in years other than 2003 have yet to be published.

The peak load of 8.6 MN is the result of what has been defined as an extreme ice loading event (Brown, 2007) which took place on April 4, 2003. During this event a single floe which was approximately 13 km by 8 km broke free from the land fast ice of Egmont Bay on the south side of Prince Edward Island to the west of the Confederation Bridge. The floe consisted of level ice with an average thickness of 1 m with imbedded ridges with keel depths averaging 4 m (Frederking et al., 2006). Impact with the bridge occurred at 7:00 am and continuous ice failure occurred for the next 4 hours until the driving force of the tide was reduced to the point that the floe stopped. During this 4 hour duration, rubble was always present and a maximum ridge ride up of approximately 9m took place (Brown, 2007). The floe began to move again later that day when the tides changed causing the floe to continue its eastern progression until the floe had passed the bridge axis.

It should be noted that the probabilistic model in Chapter 4 was developed using 62 years of temperature data ranging from 1942 - 2007 at Summerside, Prince Edward Island. This work analyzed the freezing degree day values for these 62 ice seasons resulting in a mean freezing degree day value of 687. Brown (2007) has reported that during the first 10 years of operation of the bridge the mean freezing degree day value was exceeded

only once, occurring in 2003. Table 5-1 below lists the freezing degree day values for the first 10 years of operation of the bridge and a mean freezing degree day value of 526.9 for this period. While this value is lower, it is not expected to have a significant effect.

Ice Season	FDD
1997-1998	411
1998-1999	436
1999-2000	490
2000-2001	560
2001-2002	415
2002-2003	730
2003-2004	650
2004-2005	600
2005-2006	369
2006-2007	608
10 Year Mean:	526.9
62 Year Mean:	687.0

Table 5-1: Freezing degree day values for the first 10 years of operation of the Confederation Bridge.

The annual maximum loads reported by Frederking et al. (2007) from the National Research Council – Canadian Hydraulics Centre in collaboration with the Department of Fisheries and Oceans through the Bedford Institute of Oceanography and the Public Works and Government Services of Canada program vary considerably. Frederking et al. (2007) reports a maximum ice load acting on the Confederation Bridge of 2.4 MN. This 10 year peak load also occurred during the extreme event occurring on April 4, 2003. There is a considerable discrepancy between the maximum 10 year load reported by the two research programs. Given that the Confederation Bridge Monitoring Program calibrated the tiltmeters directly using the CCGS Terry Fox more weight is being placed on the loads derived by this program. Further to this there is little description of the

conditions observed during the maximum load as reported by the NRC-CHC research program.

Figure 5-3 below shows the 10 year annual maximum horizontal ice load of 8.4 MN estimated using the probabilistic model developed in Chapter 4. This compares very well with what was measured by the Confederation Bridge Ice Monitoring Program.

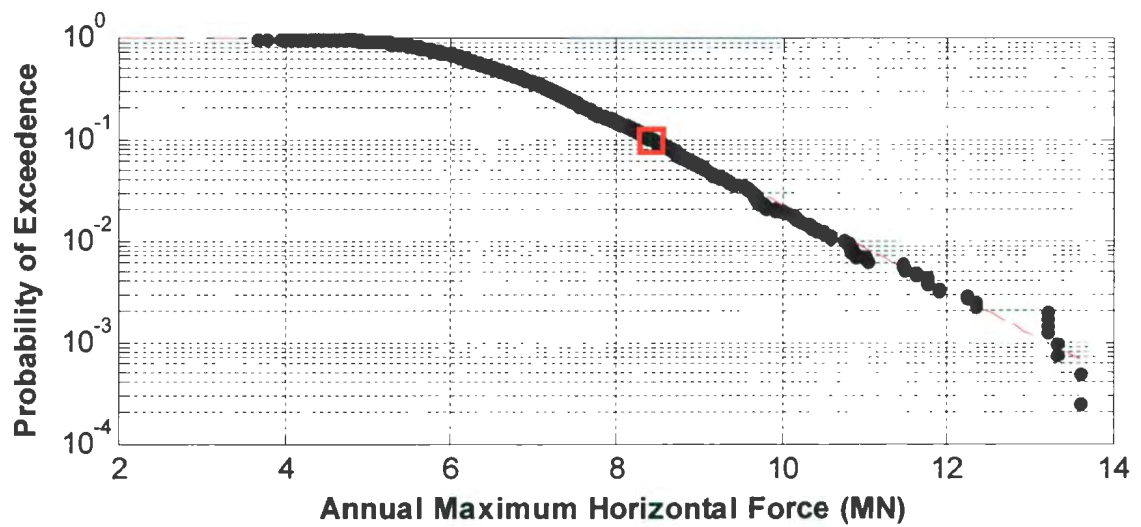


Figure 5-3: Simulated 10 year (10^{-1}) annual maximum horizontal force acting on a bridge pier using the probabilistic model developed in Chapter 4.

5.4 Recommendations for Future Work

One potential area which could benefit from future work would involve modifying the Croasdale model such that it is more suited for a probabilistic model. The Croasdale model was originally intended to be used as a deterministic calculation of the ice load acting on a structure. For this reason the model considers the worst case scenario, which assumes that all components of the load peak at the same instant. When developing a probabilistic model one should incorporate instances when the individual components of the total load peak together and also instances when they do not. The author suggests that some variation in this respect could be implemented in further probabilistic models to improve the accuracy of the results.

Future work on this model could also include more variation in the way the ice interacts with the structure. The Croasdale model assumes that each component of the total load calculation occurs during every interaction with the structure. In other words, the model assumes that the ice pushes through an existing rubble pile to fail in flexure upon making contact with the slope. At this time the ice continues to ride up the slope beneath the rubble pile. One potential variation is for the ice to fail in flexure or crushing on the outside of the rubble pile. This mode of failure could also be caused by the ice sheet pushing partially into the rubble pile and plugging. Croasdale has since described this type of interaction as a 'rubbling' failure. During a rubbling failure the critical factors to be considered are the magnitude of the crushing load which acts on the outside of the

rubble pile, and the amount of protection that the existing rubble pile provides the structure with (Croasdale, personal communication). Another potential variation in the ice interaction with the structure is for the ice floe to split. This form of ice structure interaction results in a significant reduction in the load applied to the structure. These variations could be implemented in the model in order to improve the accuracy of the results.

The effect of ice ridge interaction with the structure could also be studied in more detail. Lemee (2002) has studied ridge loads acting on the Confederation Bridge and has found that the size of the ridge keel has little to no bearing on the total load acting on the structure, as shown in Figure 5-4. It was suggested that this is a result of the efficiency of the cone in breaking up the structure of the keel before it is able to make contact with the pier shaft. Detailed review of the video recording conducted by the Confederation Bridge Ice Monitoring Program and the associated tiltmeter response is recommended. This could be used to distinguish between loads caused by level ice and ice ridges.

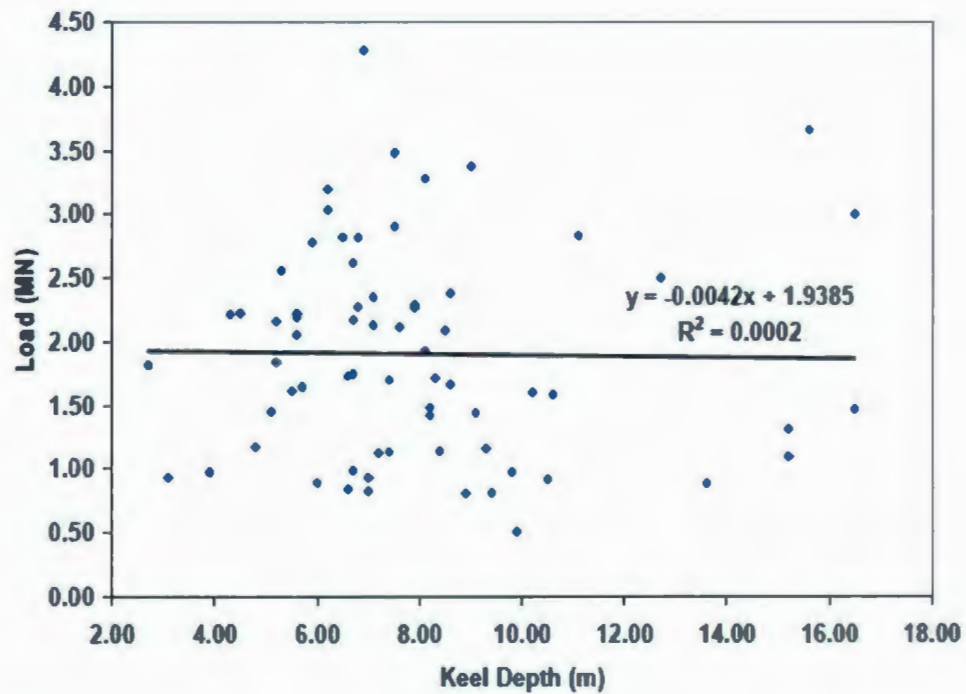


Figure 5-4: Ridge keel depth vs. ice loads acting on the Confederation Bridge (Lemee, 2002). This result shows little correlation between ice load and keel depth.

Event details for all key ice loading events measured by the Confederation Bridge Ice Monitoring Program should be reviewed in detail. Continued work on the detailed structural analysis of the tiltmeter data is recommended to determine the actual peak load for each ice season rather than the peak average load over a 17 second duration which was presented in Figure 5-2. Brown (2007) suggests that this work is ongoing.

5.5 Concluding Remarks

The 10 year (10^{-1}) ice load of 8.4 MN estimated using the probabilistic model developed in Chapter 4 compares very well with the maximum 10 year load reported by Brown (2007) of 8.6 MN. This result suggests that the 100 year (10^{-2}) and 10,000 year (10^{-4}) design ice loads used for the construction of the Confederation Bridge are likely conservative. This result could lead to potential reductions in design loads for the design and development of similar structures in the future.

6 CONCLUSIONS AND RECOMMENDATIONS

In Chapter 3 a sensitivity analysis was carried out to determine which input parameters affected the ice loads as predicted by the Croasdale model. From this analysis it was determined that if a rubble pile was present on the structure, the flexural strength of ice was not found to be a significant factor affecting the ice load. There were however a number of scenarios which were outlined for which the flexural strength of ice was of significance. A ship ramming event is one such scenario for which the flexural strength of ice plays a significant role in limiting the maximum ice load. During a ship ramming event, an ice breaker impacts an extreme ice feature. The maximum ice load occurs as a crushing failure on the bow of the ship, which is limited by flexural failure due to the weight of the vessel on the ice feature. Another scenario for which the flexural strength of the ice may dominate involves the use of conical structures in the Arctic. Here, designers are concerned with thick multiyear floes interacting with large conical structures. In this scenario, ride up is likely to occur with limited rubble formation due to dissipation of kinetic energy, thus making the flexural strength of the ice a critical component affecting the design load. The scale of the interaction has been found in this work to be a critical component affecting the flexural strength of ice due to the presence of a size effect.

The size effect in ice is characterized by a decrease in flexural strength with an increase in beam size. By increasing the beam size there is an increased variation in flaw sizes

and formations, which leads to an increased probability of the ice sheet containing a critical flaw path to initiate failure. The increased probability of containing a critical flaw leads to the size effect observed by a number of researchers.

Research has shown that the most statistically significant parameter effecting flexural strength is the brine volume of the sample. Some argue that the flexural strength of ice is governed solely by the brine volume alone, whilst others have found the beam size to be statistically significant in addition to the brine volume of the sample. It is the belief of the author that the flexural strength of ice is governed by a combined effect of the brine volume and the beam size.

The results presented in Chapter 3 show that the methodology used to predict the flexural strength of ice based solely on brine volume leads to an over estimation of the flexural strength of ice for full scale interactions. This is achieved by using full scale data from the icebreaker Oden during the International Arctic Ocean Expedition in 1991 where the icebreaker Oden was part of a three vessel expedition to the central Arctic Basin. The results of the work show a significant reduction in flexural strength when compared to the methodology which considers brine volume only. The author recommends the use of the methodology presented by Williams and Parsons (1994) when calculating the flexural strength of ice for full scale ice structure interactions.

In Chapter 4 a probabilistic model was developed to determine extreme ice loads acting on the Confederation Bridge in the Northumberland Strait for level ice interaction with the conical bridge piers. A Monte Carlo technique was utilized to simulate the ice environment to derive the annual maximum ice loads on the structure. In order to achieve this, full scale data was obtained from public sources and fitted with probability distributions to model the input parameters.

The model developed in this work simulates the total number of ice floes interacting with a bridge pier in the Northumberland Strait for a given season, as well as individual parameters for each ice floe. Each ice floe is assigned a diameter, an ice thickness, and an ice-structure friction coefficient. For each meter of each floe, a new flexural strength is sampled along with a new rubble height, generated based on the thickness of the ice, as well as the angle that the rubble pile makes with the horizontal axis. The Croasdale model is utilized to calculate the horizontal and vertical ice forces acting on the bridge pier for every meter in each floe. The maximum force acting on the bridge pier for each floe is stored and the annual maximum ice force is obtained from these.

The probabilistic model developed in this work for level ice interactions with the Confederation Bridge piers estimates a 100 year ice load of 10.7 MN and a 10,000 year ice load of 16.0 MN acting on a 52° conical, 14m diameter pier.

In Chapter 5 the author has used published data obtained by both the Confederation Bridge Ice Monitoring Program and the National Research Council to validate the probabilistic model developed in Chapter 4. The model developed is believed to provide a good representation of the level ice loads acting on the Confederation Bridge piers. This result suggests that the 100 year (10^{-2}) and 10,000 year (10^{-4}) design ice loads used for the construction of the Confederation Bridge are likely conservative. This result could lead to potential reductions in design loads for the design and development of similar structures in the future.

The author has also made some recommendations for future work to strengthen the results obtained in this work. The modification of the Crosdale model to account for circumstances where all loads do not peak at the same instant is recommended. This will help to provide a better representation of reality. Further to this, the model developed in this work should be expanded to consider the effects of floe splitting, ice ridges, rafted ice and ice rubbing on the global load. The author recommends a detailed review of the video recordings in the possession of the Confederation Bridge Ice Monitoring Program to identify the tilt response of the structure associated with various modes of failure. This will help to improve the understanding of the loading conditions which govern the design loads acting on the structure.

From this work and the suggestions for future work, a further understanding can be gained regarding the magnitude of the ice loads produced by various ice formations

interacting with conical and sloping offshore structures. Ultimately, the final design load for any structure must consider all of the potential hazards which can be imposed upon the structure, with the appropriate level of reliability in order to ensure a safe structural design in accordance with CSA and ISO standards. Continuing to instrument and monitor offshore structures which have been designed and built for ice environments is key in furthering our understanding of the ice loads acting on offshore structures.

7 REFERENCES

Ashby, M.F., Palmer, A.C., Thouless, M., Goodman, D.J., Howard, M., Hallam, S.D., Murrell, S.A.F., Jones, N., Sanderson, T.J.O., Ponter, A.R.S., 1986. *Nonsimultaneous Failure and Ice Loads on Arctic Structures*. Offshore Technology Conference. pp 399-404.

Bercha, F.G and Associates Limited, 1988a. *Analysis of Photographic Data from 1964-1965*. Report for Public Works Canada.

Bercha, F.G and Associates Limited, 1988b. *High Resolution SAR Data Acquisition and Interpretation for Northumberland Strait*. Report for Public Works Canada.

Bercha, F.G. and Associates Limited, 1991. *The New Ice Break-Up Model*. Northumberland Strait Crossing Project. Appendix D.

Blanchet, D., DeFranco, S.J., 1996. *Global First-year Ice Loads: Scale Effect and Non-simultaneous Failure*. IAHR Ice Symposium 1996, Beijing. pp. 203-213.

Brown, T.G and Mayne, D.C., 2000. *Rubble Pile Observations*, Proc. 10th Intl. Offshore and Polar Engineering Conf., Seattle, USA, p596-599.

Brown, T.G., Jordaan, I.J., Croasdale, K.R., 2001. *A Probabilistic Approach to Analysis of Ice Loads for the Confederation Bridge*. Canadian Journal of Civil Engineering 28. pp. 562-573.

Brown, T.G., 2006. *Analysis of Ice Event Loads Derived From Structural Response*. Cold Regions Science and Technology. Vol. 47. pp. 224-232.

Brown, T.G., 2007. *Ice Force Monitoring*. Confederation Bridge Engineering Summit. Charlottetown, PEI. August 19-22, 2007.

Cammaert, A.B., Jordaan, I.J., Bruneau, S.E., Crocker, G.B., McKenna, R.F., and Williams, S.A., 1993. *Analysis of Ice Loads on Main Span Piers for the Northumberland Strait Crossing*. Contract Report for J. Muller International. Stanley Joint Venture Inc.

Carter, J., Daley, C., Fuglem, M., Jordaan, I.J., Keinonen, A., Revill, C., Butler, T., Muggeridge, K., and Zou, B., 1996. *Maximum Bow Force For Arctic Shipping Pollution Prevention Regulations Phase II*. Industry report prepared for Transport Canada, Ship Safety – Northern Region.

CSA-S471, 2004. *General Requirements, Design Criteria, the Environment, and Loads*. CAN/CSA-S471-04, Part of Code for the Design, Construction and Installation of Fixed Offshore Structures, Canadian Standards Association, 2004.

Croasdale, K.R., 1980. *Ice Forces on Fixed, Rigid Structures, A State-of-the-Art Report by IAHR Working Group on Ice Forces on Structures*, Edited by T. Carsten, CRREL Special Report 80-26, U.S. Army CRREL, Hanover, N.H., pp. 34-106.

Croasdale, K.R., Cammaert, A.B., Metge, M., 1994, *A method for the calculation of sheet ice loads on sloping structures*, IAHR Ice Symposium '94, p874-885.

Cullen, A. C., Frey, H. C., (1999), *Probabilistic Techniques in Exposure Assessment, Handbook for Dealing with Variability and Uncertainty in Models and Inputs*. Plenum Press, New York and London.

Dempsey, J.P., DeFranco, S.J., Adamson, R.M., Mulmule, S.V., 1999. *Scale Effects on the In-situ Tensile Strength and Fracture of Ice. Part 1: Large Grained Freshwater Ice at Spray Lakes Reservoir, Alberta*. International Journal of Fracture. pp. 325-345.

Dome Petroleum, 1982. *Full Scale Measurements of the Ice Impact Loads and Response of the Kigoriak*. Technical report. Report prepared by Dome Petroleum Limited.

Frederking, R., Kubat, I., Prinsenber, S., 2007. *Ice Interaction with Confederation Bridge – Review of NRC Program*. Confederation Bridge Engineering Summit. Charlottetown, PEI. August 19-22, 2007.

Forland, K.A., and Tatinclaux, J.P., 1985. *Kinetic Friction Coefficient of Ice*. US Army, Cold Regions Research and Engineering Laboratory, Report 85-6.

Fuglem, M., 1997. *Decision Making For Offshore Resource Development*. PhD Thesis. Memorial University of Newfoundland. St. John's, Newfoundland.

Hétenyi, M., 1946. *Beam on Elastic Foundation*. University of Michigan Studies, Scientific Series, Vol XVI, The University of Michigan Press.

Hewitt, K.J., 1994. *Molikpaq Ice Interactions Predicted and Actual Performance*. IAHR Ice Symposium, Trondheim Norway.

Hewitt, K.J., Kennedy, K.P., Fitzpatrick, P.J., 1994. *Global Ice Loads on Arctic Structures Interpreted From Foundation Displacements*. 7th International Cold Regions Engineering Specialty Conference.

Hoikkanen, J., 1985. *Measurements and Analysis of Ice Force Against a Conical Structure*, Proc. 8th Intl. Conf. on Port and Ocean Engineering under Arctic Conditions, Vol. 3, Narssarssuaq, Greenland, pp. 1203-1220.

Iyer, S.H., 1983. Size effects in ice and their influence on the design of offshore structures. Proceedings of the 7th International Conference on Port and Ocean Engineering Under Arctic Conditions, Vol. 3. Espoo, Finland.

Jefferies, M.G., Wright, W.H., 1988. *Dynamic response of Molikpaq to ice – structure interaction*. Proceedings OMAE'88, Vol. IV, pp. 201–220. Houston, USA.

Jordaan, I.J. 1983. *Risk Analysis with Application to Fixed Structures in Ice*. Workshop on Sea Ice Management, Memorial University of Newfoundland, St. John's, November.

Jordaan, I.J., Maes, M.A., Brown, P.W., Hermans, I.P., 1993. *Probabilistic Analysis of Local Ice Pressures*. Journal of Offshore Mechanics and Arctic Engineering. 115:83-89

Jordaan, I.J., 2001. *Mechanics of Ice-Structure Interaction*. Engineering Fracture Mechanics 68, pp. 1923-1960.

Jordaan, I.J., Pond, J., 2001. *Scale Effects and Randomness in the Estimation of Compressive Ice Loads*. IUTAM Symposium on Scaling Laws in Ice Mechanics and Ice Dynamics. pp 43-54.

Jordaan, I.J., 2005, *Decisions Under Uncertainty. Probabilistic Analysis for Engineering Decisions*. Cambridge University Press.

Jordaan, I.J., Li, C., Sudom, D., Stuckey, P., Ralph, F., 2005. *Principles for local and global ice design using pressure-area relationships*. 18th International Conference on Port and Ocean Engineering Under Arctic Conditions (POAC).

Jordaan, I.J., Li, C., Mackey, T., Stuckey, P., Sudom, D., and Taylor, R. 2005. *Ice Data Analysis and Mechanics for Design Load Estimation, Final Report*. Prepared for NSERC, C-CORE, Chevron Canada Resources, National Research Council of Canada, Petro-Canada, Husky Energy.

Kim, J.K., and Kotras, T.V., 1973. *Mathematical model to describe the behaviour of a moving ice field encountering a conical structure*, Vol 1 Revised Report, Dec. 28, Arctec Canada Ltd., APOA No. 57.

Kubat, I. and Frederking, R., 2001. *Response of Confederation Bridge to Ice Forces: 2000 Winter Season*. Proceedings of the 16th International Conference on Port and Ocean Engineering under Arctic Conditions. Ottawa, Ontario, Canada.

Lau, M., Molgaard, J., Williams, F.M., and A.S.J. Swamidas, 1999. *Development and Verification of a 3-D Model for Ice Forces on Conical Structures*, Proc. 18th Intl. Conf. on Offshore Mechanics and Arctic Engineering, OMAE Paper No. 1150, St. John's Newfoundland.

Lavrov, V., 1971. *Studies in Ice Physics and Ice Engineering*. Edited by G.N. Yakovlev pp. 26-32.

LaBelle, J.C., Wise, J.L., Voelker, R.P., Schulze, R.H., and Wohl, G.M., 1983. *Alaska Marine Atlas*. Arctic Environmental Information and Data Centre. University of Alaska.

Lebedev, V.V., 1938. *Rost L'Da V Arkticheskikh Rehakh I Moriakh V Zavisimosti Ot Otritsatel'nykh Temperatur Vozdukha (Growth of Ice in Arctic Rivers and Seas in Relation to Negative Air Temperatures)*. Problemy Arkitiki, 5-6, 9-25.

Lemee, E.M., 2002. *Pressure Ridge Interaction with Confederation Bridge*. Masters Thesis. University of Calgary, Calgary, AB.

Määttänen, M., 1975. *Ice Forces and Vibrational Behaviour of Bottom-Founded Steel Lighthouses*. Proc. 3rd International Symposium on Ice Problems, Hanover, New Hampshire, pp 345-355.

Määttänen, M., 1983. *Dynamic Ice-Structure Interaction During Continuous Crushing*. CRREL Report No. 83-5.

Määttänen, M., 1986, *Ice Sheet Failure Against an Inclined Wall*, Proc. 8th Intl. Symposium on Ice (IAHR) 1986, Iowa City, USA, Vol 1, p149-158.

Määttänen, M. and Hoikkanen, J., 1990, *The Effects of Ice Pile Up on the Ice Force of a Conical Structure*, Proc. 10th Intl. Symposium on Ice (IAHR) 1990, Espoo Finland, p1010-1021.

Määttänen, M. and Mustamäki, E.O., 1985. *Ice Forces Exerted on a Conical Structure on the Gulf of Bothnia*, Proc. 17th Offshore Technology Conference, Vol. 4, Paper No. 5054, Houston, pp. 313-320.

Maes, M.A., 1990. *Uncertainties. Why, How and To What Extent Should They Be Considered in Structural Design codes?* Engineering in Our Environment: Proc. Annual Conference and 1st Biennial Environmental Specialty Conference. Hamilton, Ontario.

Mayne, D.C and Brown, T.G., 2000, *Rubble Pile Observations*. Proc. 10th International Offshore and Polar Engineering Conference, Seattle, USA, p 596-599.

Mayne, D.C., 2007. *Level Ice and Rubble Actions on Offshore Conical and Sloping Structures*. PhD Thesis. University of Calgary, Calgary, AB.

Melchers, R.E., 1987. *Monte Carlo Methods for Structural Reliability Analysis*. Transactions of the Institution of Engineers, Australia. Vol. 29, no. 4. pp. 219-222.

Melchers, R.E., 1989. *Structural Reliability Assessment for Major Structures*. Proc of the Institution of Civil Engineers. Design and Construction. Part 1. Vol 87, pp. 343-356.

Morgenstern, N.R. and Price, V.E., *The Analysis of the Stability of General Slip Surfaces*. Geotechnique, Vol. 15, No. 1, 1965, pp. 79-93.

Nessim, M.A., Hong, H.P., Jorcaan, I.J., 1995. *Environmental Load Uncertainties for Offshore Structures*. Journal of Offshore Mechanics and Arctic Engineering, November 1995, Vol. 117.

Nevel, D.E., 1980. Bending and Buckling of a Wedge on an Elastic Foundation, Proc. IUTAM Symp. On Physics and Mechanics of Ice, Copenhagen, Edited by P.Tryde, Springer-Verlag, Berlin, pp. 278-288.

Nevel, D.E., 1992, *Ice forces on Cones from Floes*, Proc. 11th IAHR Ice Symposium , Banff, Canada, Vol 3, p 1391-1404.

Palmer, A.C., Goodman, D.J., Ashby, M.F., Evans, A.G., Hutchinson, J.W., Ponter, A.R.S., 1982. *Fracture and Ice Forces on Offshore Structures*. Symposium on Applied Glaciology, Hanover, NH.

Parsons, B.L., Lal, M., Williams, F.M., Dempsey, J.P., Snellen, J.B., Everard, J., Slade, T., Willams, J., 1992. *The Influence of Beam Size on the Flexural Strength of Sea Ice, Freshwater Ice and Iceberg Ice*. Philosophical Magazine Vol. 66, No. 6, pp. 1017-1036.

Pounder, E.R., 1965. *The Physics of Ice*. Pergamon, London.

Rawlins, M.A., and Willmott, C.J., 2003. *Winter Air Temperature Change Over the Terrestrial Arctic, 1961-1990*. Arctic, Antarctic and Alpine Research, Vol. 35, No. 4, p. 530-537.

Spencer, D., McKenna, R., and Lau, M., (1993). *Ice Model Test of a 60^o Upward Breaking Bridge Pier for the Northumberland Strait Crossing*. Institute for Marine Dynamics, Report No. TR-1993-05.

Terashima, T., and Nakazawa, N., 1997. *Factors Influencing the Coefficient of Friction Between Sea Ice and Various Materials*. 3rd International Conference on Contact Mechanics. Madrid, Spain.

Timco, G.W. and O'Brien, S., 1994. *Flexural Strength Equation for Sea Ice*. Cold Regions Science and Technology 22. pp. 285-298.

Timco, G.W., and Johnston, M.E., 2003. *Ice loads on the Molikpaq in the Canadian Beaufort Sea*. Cold Regions Science and Technology Vol 37 pp 51– 68.

Williams, F.M., Crocker, C.G., and Butt, S., 1993. *Northumberland Strait Ice Properties Measurements*, National Research Council of Canada, Institute for Marine Dynamics, Report TR-1993-06.

Williams, F.M. and Parsons, B.L., 1994. *Size Effect in the Flexural Strength of Ice*. Offshore Mechanics and Arctic Engineering, Vol 4.

8 APPENDIX A

Sensitivity Analysis: Croasdale Model

Here the sensitivity of the Croasdale model to individual parameters is studied. This process aids in the modeling of input parameters as it allows one to determine which input variables have the greatest effect on the load determined. The input parameters which are most significant will then receive the most effort to obtain full scale data to model these inputs as accurately as possible.

To conduct the sensitivity analysis, each input value is first given a constant value as shown in the table below (Table A1). Next, a single input variable will be assigned a range of values, whilst keeping all other inputs constant. A plot of each variable with its effect on the ice loads is then generated and analyzed.

Ice Variables	
Ice thickness	0.7 m
Rubble pile height	5 m
Rubble pile angle	45 degrees
Porosity of ice	0.2
Flexural strength of ice	250 kPa
Ice-structure friction coefficient	0.2
Ice-ice friction coefficient	0.1
Cohesive strength	5 kPa
Structural Constants	
Cone angle	52 degrees
Cone freeboard	5 m
Width of structure	14 m

Table A1: Showing constants used for sensitivity analysis.

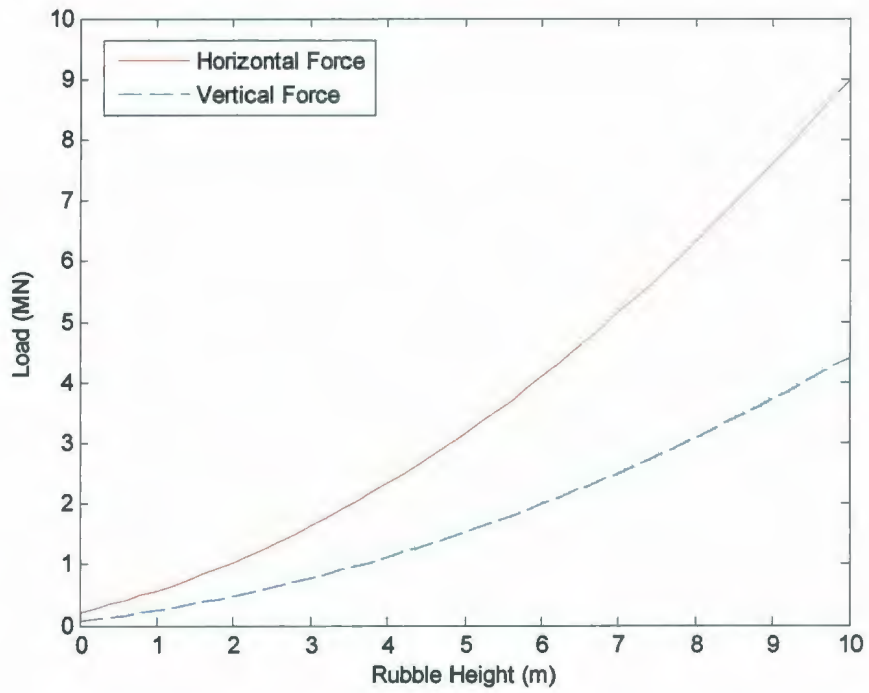


Figure A1: Sensitivity of horizontal and vertical ice loads to rubble height.

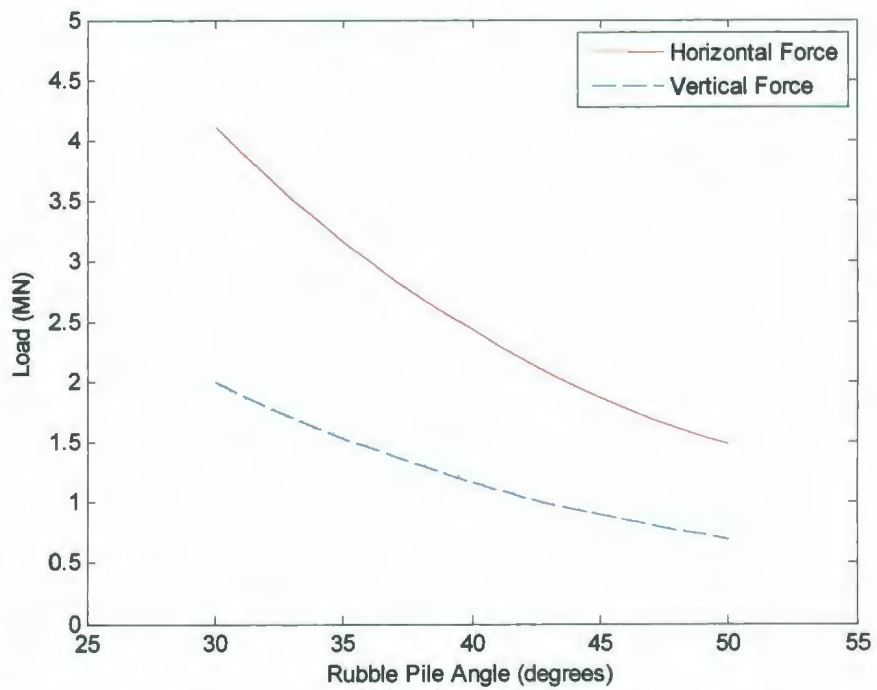


Figure A2: Sensitivity of horizontal and vertical ice loads to rubble pile angle.

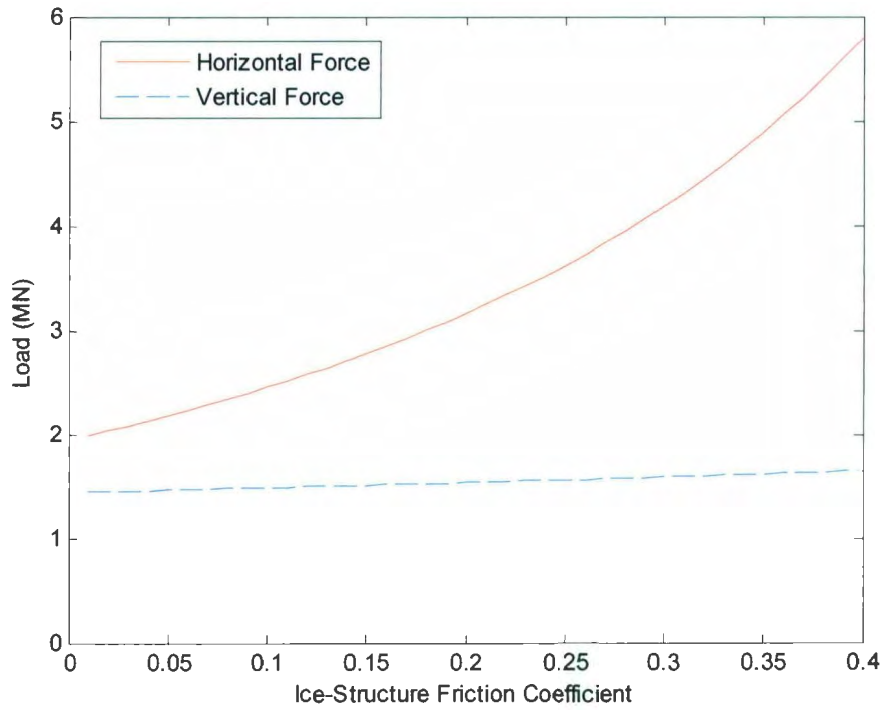


Figure A3: Sensitivity of ice loads to the ice-structure friction coefficient.

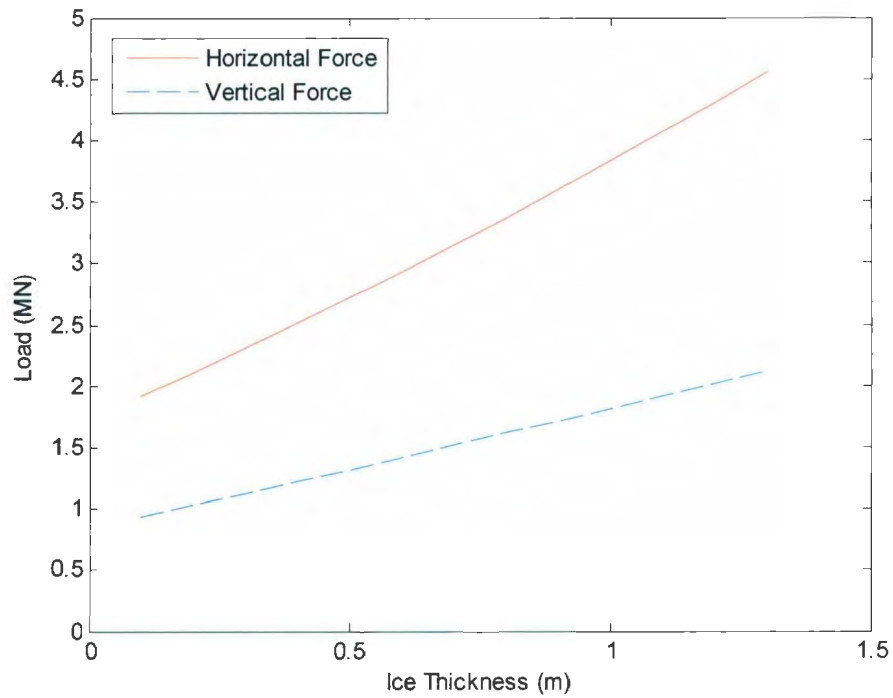


Figure A4: Sensitivity of horizontal and vertical ice loads to ice thickness.

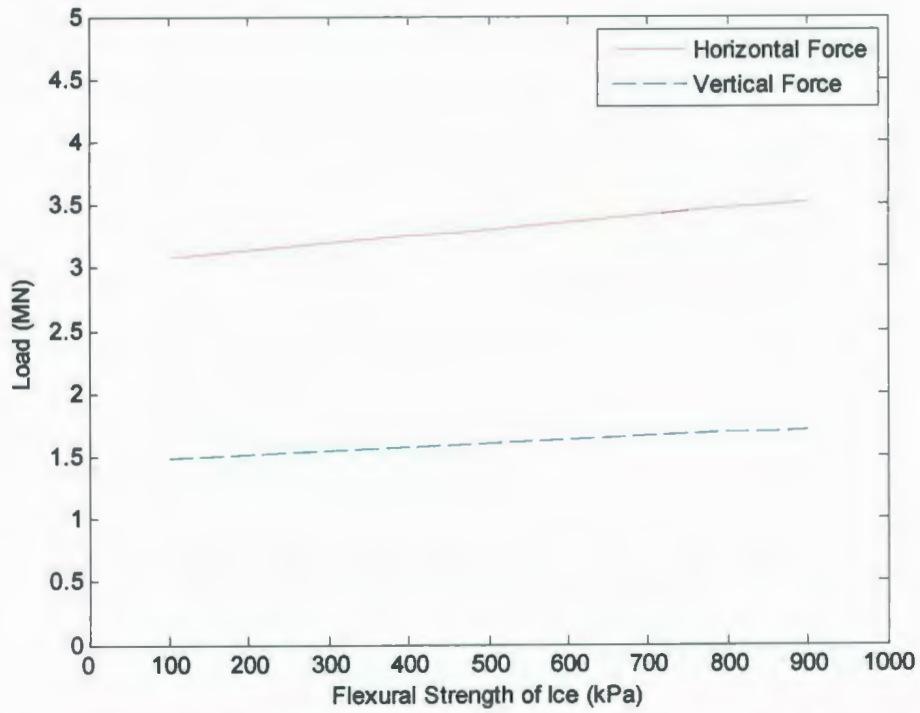


Figure A5: Sensitivity of horizontal and vertical ice loads to the flexural strength of ice.

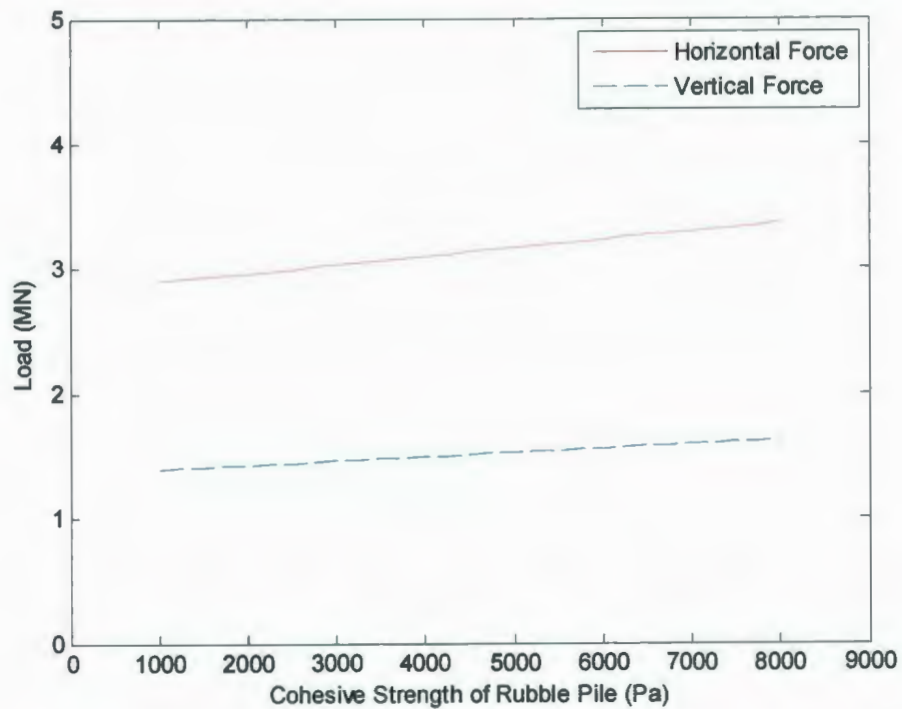


Figure A6: Sensitivity of ice loads to the cohesive strength of the rubble pile.

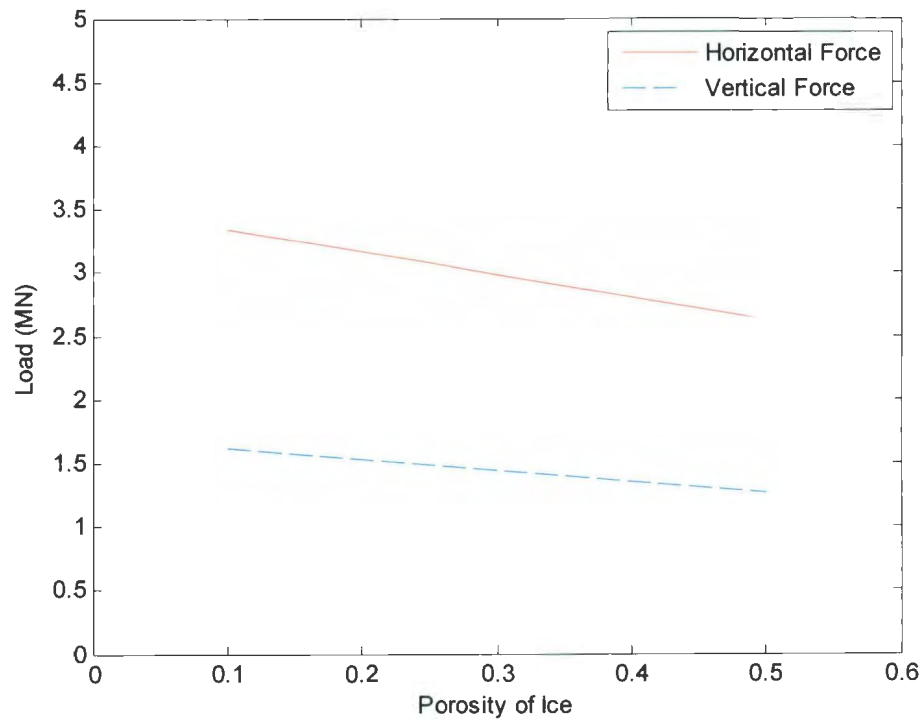


Figure A7: Sensitivity of horizontal and vertical ice loads to the porosity of ice.

9 APPENDIX B

Ship Ram

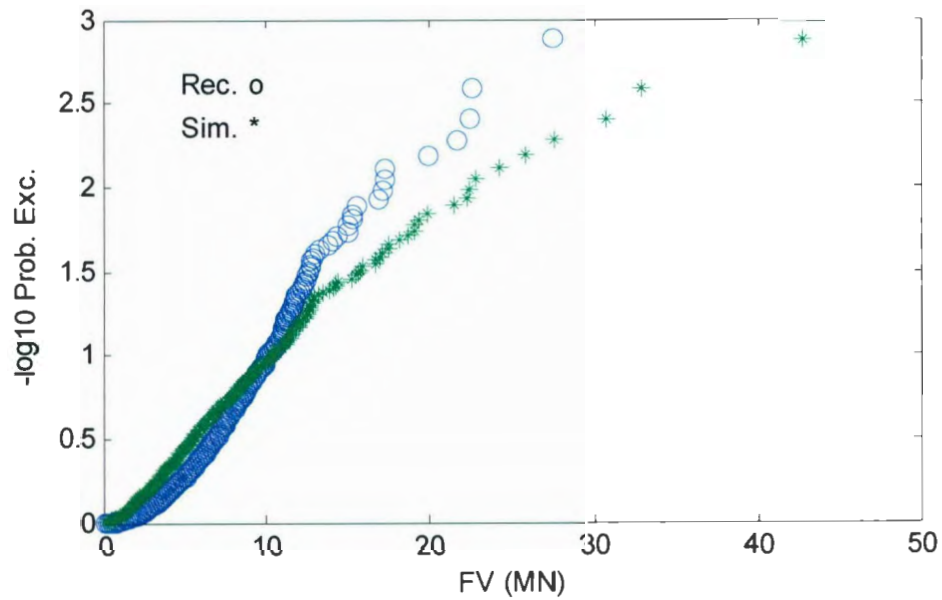
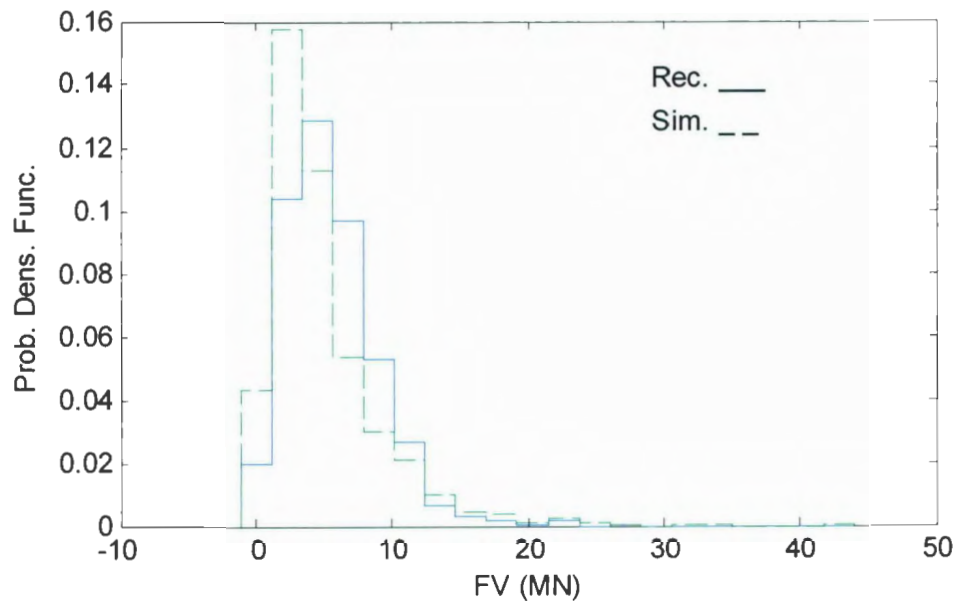


Figure B1: Histogram and exceedance probabilities of individual (parent) rams. This simulation utilized a flexural strength of 0.7MPa with a standard deviation of 0.2MPa.

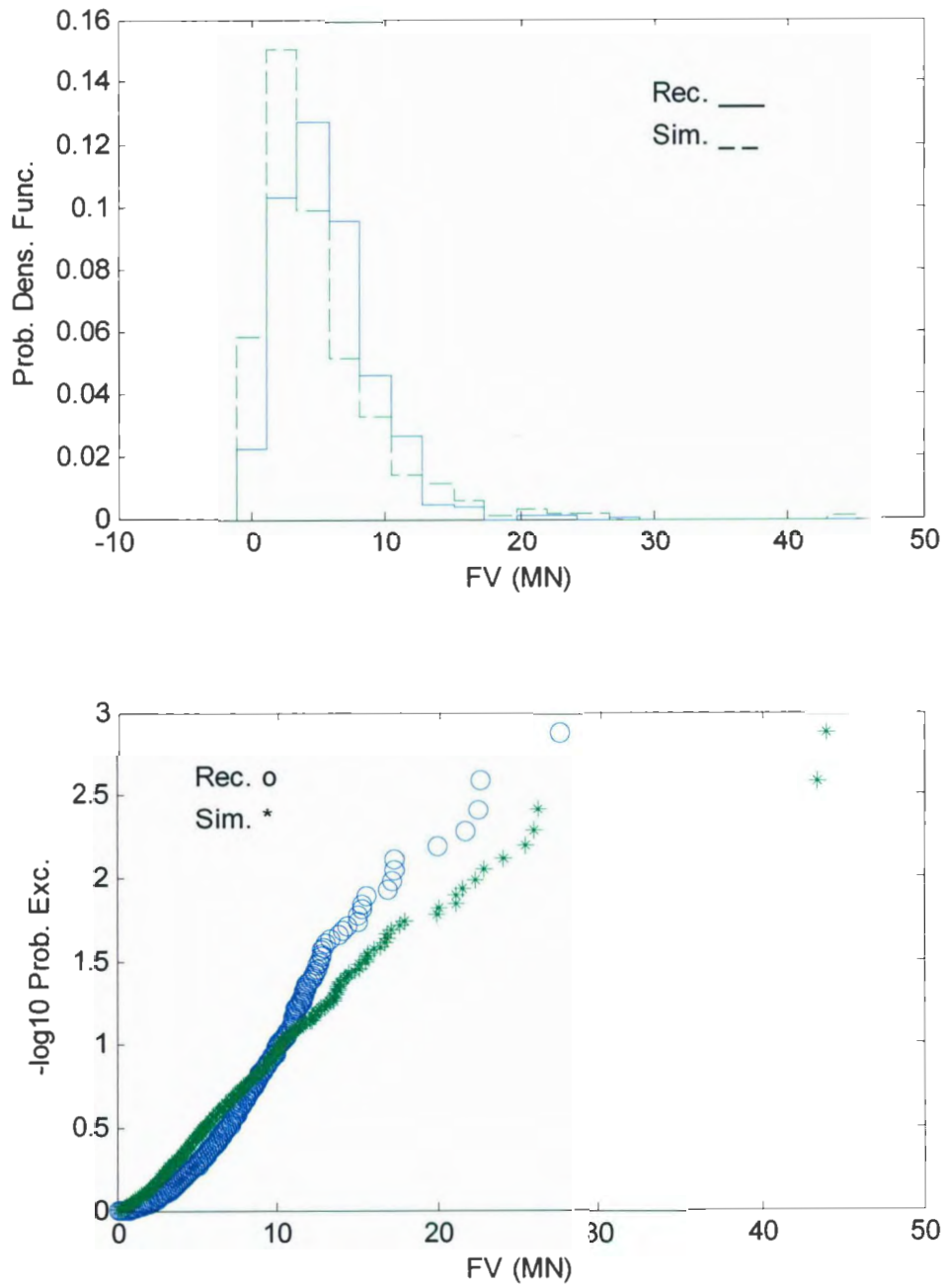


Figure B2: Histogram and exceedance probabilities of individual (parent) rams. This simulation utilized a flexural strength of 0.6MPa with a standard deviation of 0.2MPa.

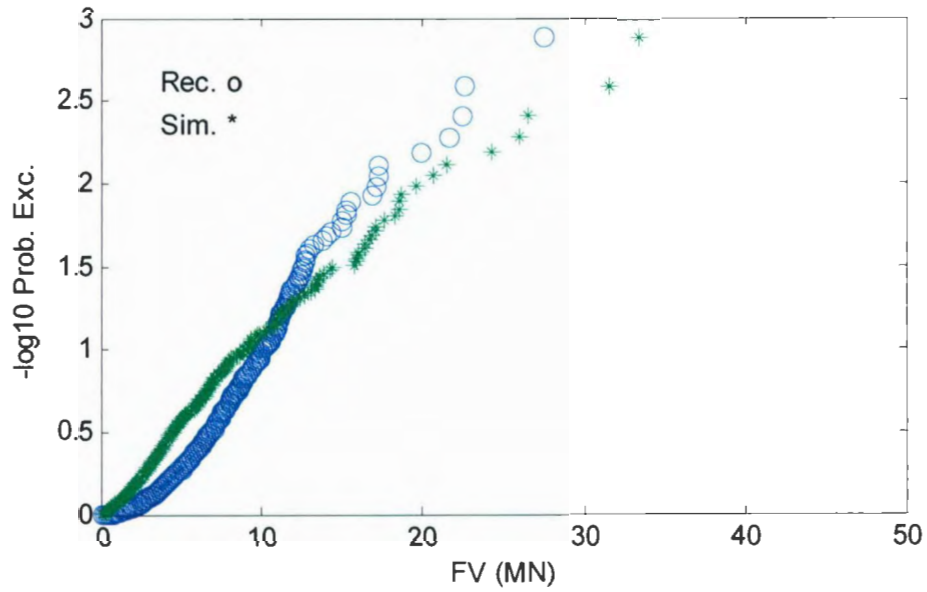
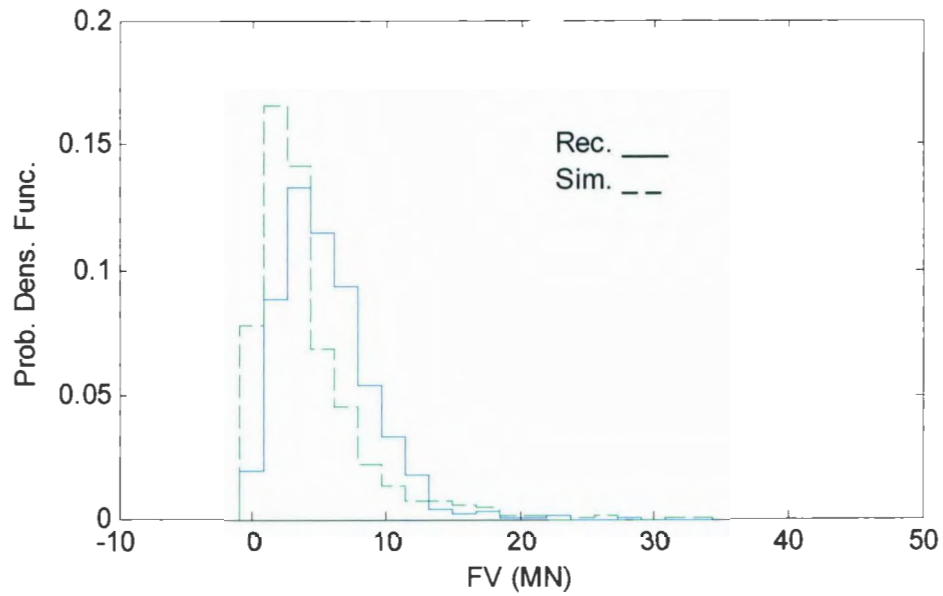


Figure B3: Histogram and exceedance probabilities of individual (parent) rams. This simulation utilized a flexural strength of 0.5MPa with a standard deviation of 0.2MPa.

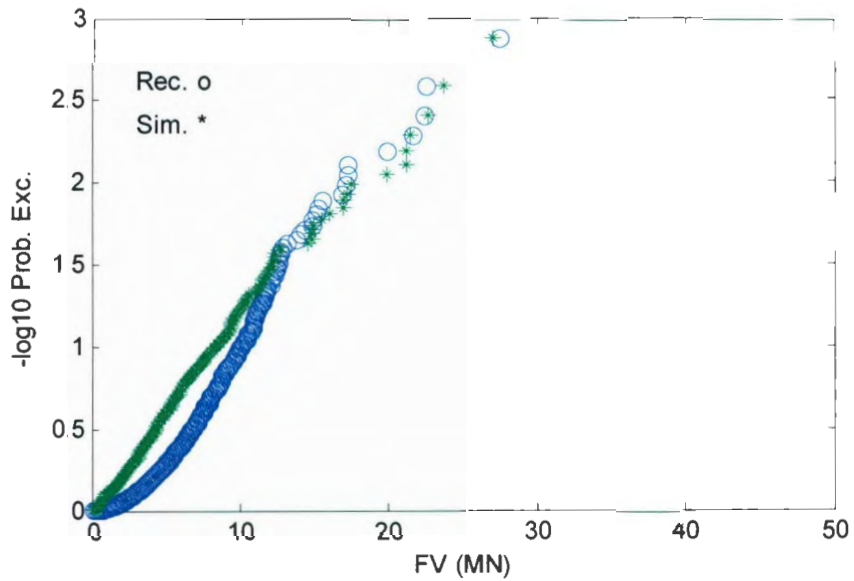
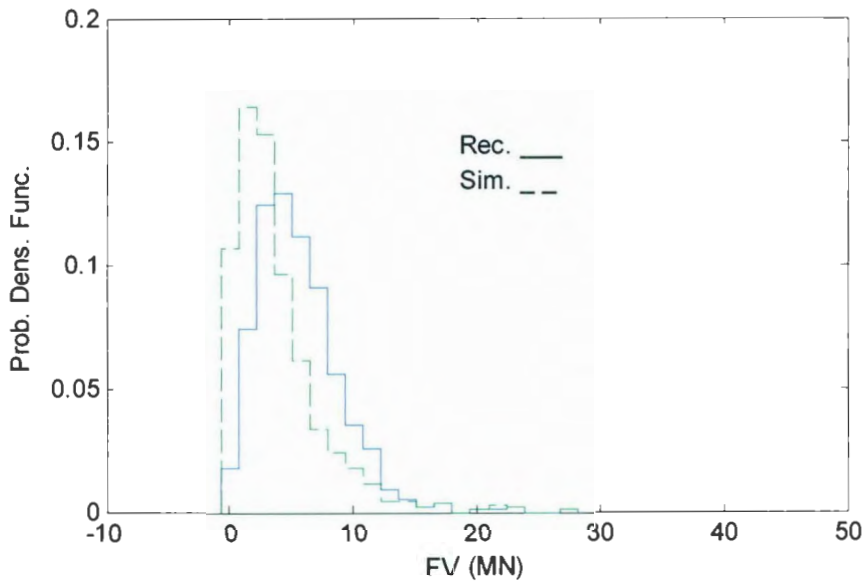


Figure B4: Histogram and exceedance probabilities of individual (parent) rams. This simulation utilized a flexural strength of 0.4MPa with a standard deviation of 0.2MPa.

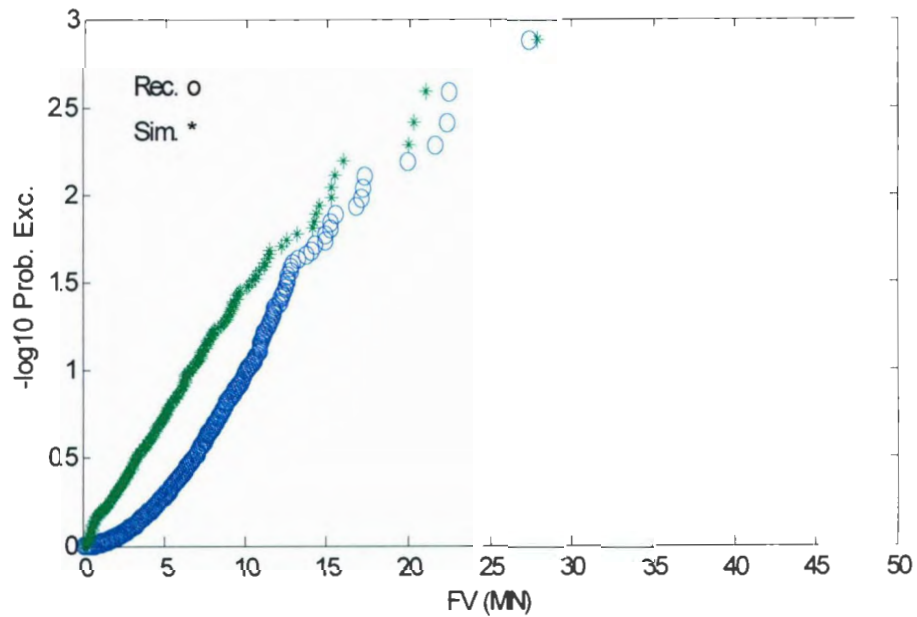
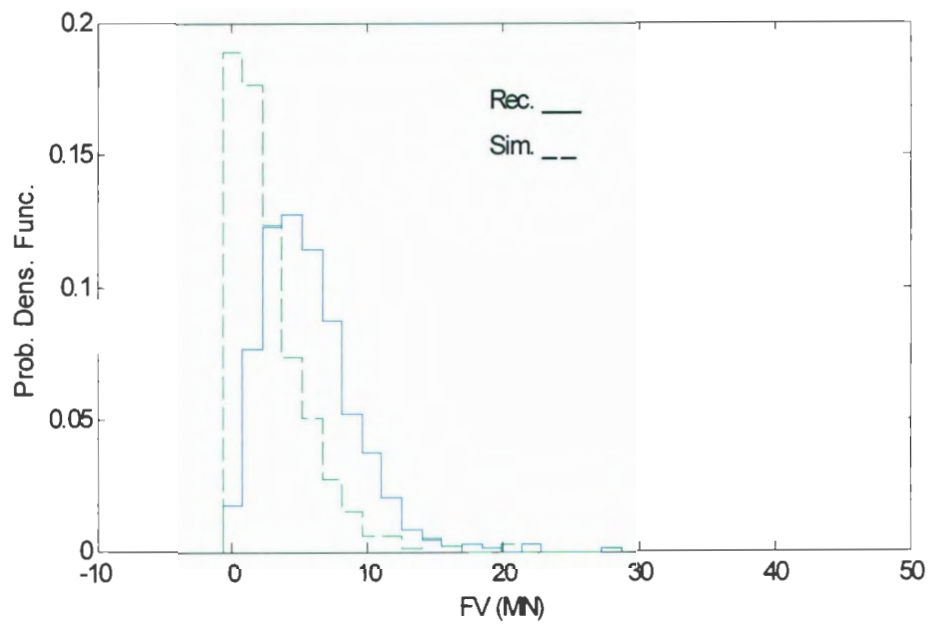


Figure B5: Histogram and exceedance probabilities of individual (parent) rams. This simulation utilized a flexural strength of 0.3MPa with a standard deviation of 0.2MPa.

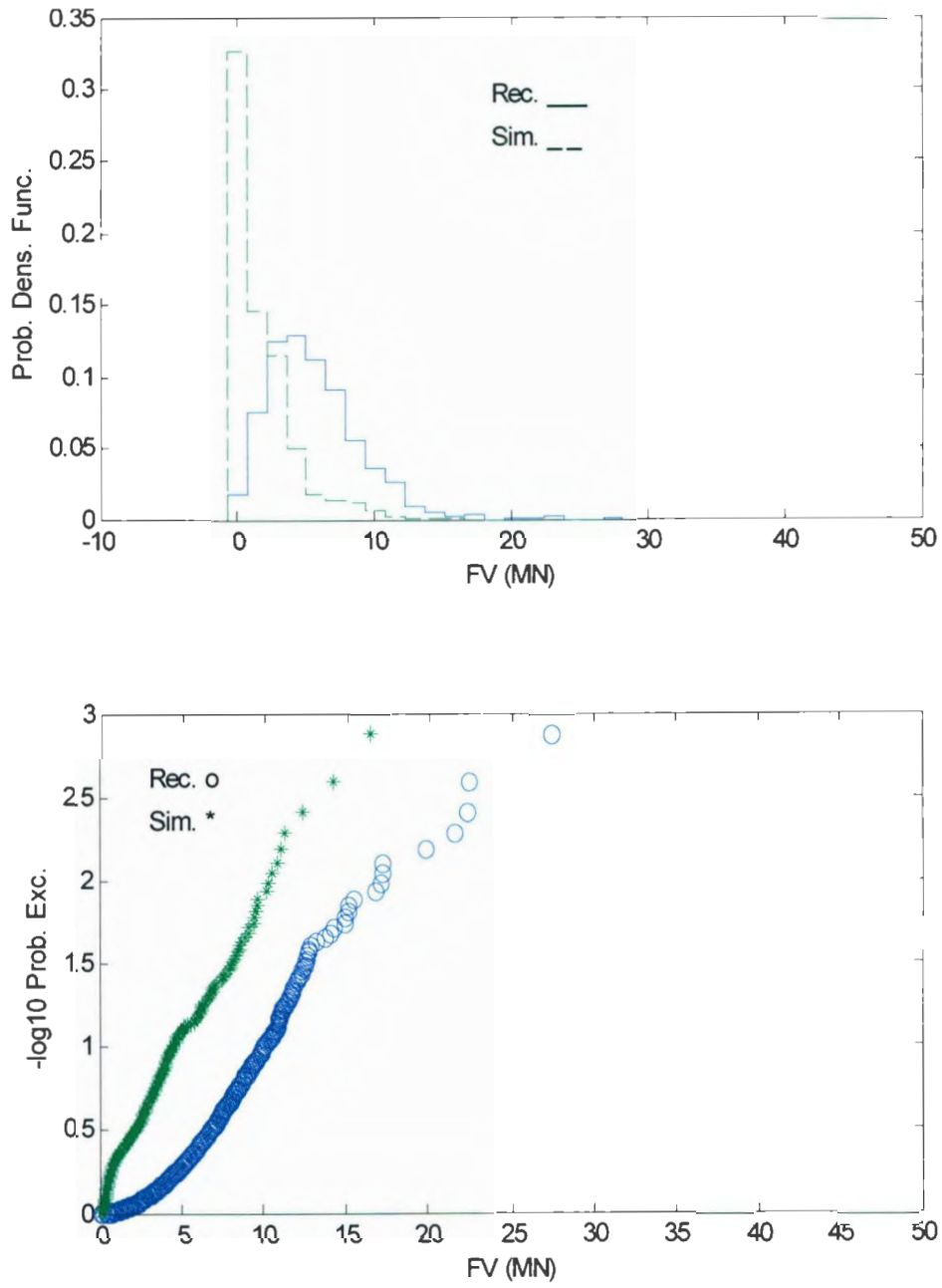


Figure B6: Histogram and exceedance probabilities of individual (parent) rams. This simulation utilized a flexural strength of 0.2MPa with a standard deviation of 0.2MPa.



